12-13-2021

Protein interactions with heme are vital for pathogenic bacteria, particularly in the utilization of heme as an iron source

Kristin V. Lyles
Georgia State University

Protein Interactions with Heme are Vital for Pathogenic Bacteria, Particularly in the Utilization of Heme as an Iron Source

by

Kristin V. Lyles

Under the Direction of Zehava Eichenbaum, PhD

A Dissertation Submitted in Partial Fulfillment of the Requirements for the Degree of

Doctor of Philosophy

in the College of Arts and Sciences

Georgia State University

2021

ABSTRACT

Iron is an essential nutrient for many pathogenic bacteria, and the most abundant source of the metal in the host is heme. Heme is often degraded by a heme oxygenase, and the first such enzyme (HO-1) was discovered in mammals. Many bacteria have homologous enzymes that allow them to leverage on the host heme pool during infection. Still, other bacteria that can degrade heme do not code for HO-1 like proteins. In Chapter 1, I conducted a comprehensive review of heme degrading enzymes in bacteria, describing four distinct families and focusing on structural and functional properties. In Chapter 2, I described the biochemical and genetic characterization of HupZ, a putative heme degrading protein from Group A Streptococcus (GAS, or Streptococcus pyogenes). I demonstrated that HupZ binds heme b without an axial ligand; therefore, the iron is not coordinated. HupZ also accommodates heme c, in which an external histidine residue coordinates the iron. *In vitro* studies showed that in the presence of a reducing partner, HupZ breakdowns heme c and heme b, but it requires an exogenous imidazole group to coordinate the iron. A knockout *hupZ* mutant exhibited reduced growth on heme iron and increased sensitivity to heme. Additionally, the expression of HupZ in *Lactococcus lactis* allowed for increased utilization of hemoglobin as the sole iron source. Together, the data demonstrate that HupZ is a unique heme binding and degrading protein that promotes heme metabolism and tolerance in GAS. In Chapter 3, I used structural modeling and prediction to examine the function of two heme-binding proteins from GAS. I used comparative modeling to map the binding region of an inhibitory monoclonal antibody to the heme capturing protein, Shr, and iterative threading to predict the structure of SiaF, a novel energy coupling factor transporter that imports heme. Altogether my work advances the

understanding of heme binding and degradation in GAS and related bacterial pathogens.

INDEX WORDS: Heme, Heme binding, Heme oxygenase, Heme degradation, Hemoglobin, Iron, *Streptococcus pyogenes*, *Lactococcus lactis*, HupZ, HupX, Shr, SiaF, Protein modeling, Structural biology, Moddler, Itasser

Protein Interactions with Heme is Vital for Pathogenic Bacteria, Particularly in the Utilization of Heme as an Iron Source

by

Kristin V. Lyles

Committee Chair: Zehava Eichenbaum

Committee: Irene Weber

Kuk-Jeong Chin

Eric Gilbert

Electronic Version Approved:

Office of Graduate Services

College of Arts and Sciences

Georgia State University

December 2021

DEDICATION

To my parents and my first teachers, Tim and Gayle VanMouwerik, for instilling in me a since of wonder and desire to learn. To my sister, Heather VanMouwerik, for her guidance and support, and to her daughter, Evelyn Joy. I have not known you for a full year, but you have brought such happiness; I cannot wait to see how far you go. Most importantly, to my loving husband, Grayson Lyles, and his continued support.

ACKNOWLEDGEMENTS

I would like to acknowledge Dr. Eichenbaum for her guidance and council during the complication of both my master's and PhD. She has shaped me as a scientist, and I will forever hear her voice when I am working on the bench and in my writing. I would like to acknowledge the work and support from all my committee members, as well as both the faculty and staff of the Biology department. So many of you have touched my life and I am grateful to have known you.

Special thanks to past and present members of the Eichenbaum lab, with specific thanks to Drs. Ankita Sachla, Nila Chatterjee, and Fahmina Akhter. As well as Edroyal Womack, Jr. and Kolby Grey.

I would like to acknowledge Grayson Lyles and his willingness to take my napkin scribbles and generate electronic versions (*i.e.*, Figure 1).

Lastly, I would like acknowledge funding through the Georgia State University Molecular Basis of Disease Fellowship.

TABLE OF CONTENTS

LIST OF TABLES

LIST OF FIGURES

1 INTRODUCTION

Iron plays a vital role in cell physiology. It exists in two primary states in aqueous solutions, ferric iron with a 3+ charge and ferrous iron with a 2+ charge. Cells utilize the redox potential of iron for many ligand binding and enzymatic conversions, with some iron-binding proteins even using high-valent 4+ or 5+ ions during catalysis [1]. The ability of iron to switch between these two states allows red blood cells to bind either oxygen or carbon monoxide and provides for the generation of ATP through the electron transport system. This rich coordination chemistry also has several drawbacks. First, ferric iron is insoluble and readily undergoes hydrolysis in water [1]. It precipitates as ferric hydroxides that decrease the pH of the solutions by the concomitant deprotonation of water. Ferrous iron is soluble under physiological conditions, but it is well established that free forms of this ion promote the formation of reactive oxygen species (ROS). Ferrous iron mixed with hydrogen peroxides is a strong oxidizing solution due to the hydroxyl radical generation described by Haber and Weiss [2].

Most bacteria incorporate iron into essential enzymes for the growth and survival, many of which are analogous to mammalian proteins. In pathogenic bacteria, some of these iron-containing proteins also serve as virulence factors. For example, pyogenic staphylococci, gonococci, and *Helicobacter pylori* produce large quantities of the iron-binding protein, catalase, limiting the oxygen-dependent killing capacities of neutrophils [3]. Iron-sulfur clusters serve as prosthetic groups for bacterial transcriptional regulators, such as the fumarate and nitrate reduction (FNR) regulatory protein [4, 5]. Apo-FNR is constitutively expressed in *E. coli*, but it only activates through the binding of an iron-sulfur cluster. When oxygen levels are low, holo-FNR

dimerizes and binds to DNA and leads to the upregulation of 125 genes used in anaerobic respiration. However, the iron-sulfur cluster is readily oxidated in response to oxygen exposure, causing it to release the DNA.

Due to iron's insolubility and high reactivity, it is highly sequestered in the extracellular and cellular compartments of the host, bound to proteins. Heme is the most abundant form of iron in the body, and two-thirds of the heme is bound to hemoglobin [6]. Excess heme and hemoglobin in the serum are removed from the blood by the glycoproteins hemopexin and haptoglobin, respectively. These proteins attenuate the adverse biochemical and physiological effects of extracellular heme and hemoglobin and promote clearance [7]. Iron ions in the serum and secretion are bound to transferrin and lactoferrin, which are kept at only 30% saturation and quickly remove any free iron. Under normal physiological conditions, iron in tissues is also bound to proteins, and the excess is stored in ferritin. These proteins ensure that free iron levels in the serum, secretion, and tissues are extremely low. During infection, nutritional immunity further limits the bioavailable of iron and has been explored in several recent reviews [8, 9]. Briefly, nutritional immunity inhibits dietary uptake of iron and its exportation into circulation, increases clearance by hemopexin and haptoglobin in the serum, and releases apo-lactoferrin into infection sites. These responses therefore put iron at the interface of host-pathogen interactions. Additionally, iron overload results in increased susceptibility to bacterial infection, underscoring how iron restriction works as a defense mechanism [6, 8]. Pathogens, including Group A Streptococcus (GAS, or *Streptococcus pyogenes*), have multiple ways to obtain heme from the host, transport it into the cell and degreed it to release the iron.

GAS is a Gram-positive, cocci bacteria of the Firmicute phylum. GAS causes a range of infections that affect the upper respiratory system and the skin. It is most well known for being the cause of pharyngitis, or Strep throat, a common illness in school-age children and people living in dormitories. GAS can also cause invasive diseases such as necrotizing fasciitis, or the flesh-eating disease, and Streptococcal toxic shock syndrome, which 23 -81% of the time results in death within seven days [10]. Cross reactive epitopes shared by GAS and the host leads to an autoimmune reaction in susceptible individuals that results in rheumatic fever and rheumatic heart disease, the primary form of heart disease for children in developing countries [11]. The number of invasive GAS infections is rising and has more than doubled between 1997 and 2019 in the United States [12]. While most of these infections were survivable, it is still a burden to our health care system, and it can level patients maimed and with lasting health issues. What is most alarming is that 30% of these infections were resistant to tetracycline, while 25% were resistant to macrolides. GAS is still susceptible to beta-lactams; however, many people have penicillin allergies. Any antibiotic resistance can be a problem in co-infections since it limits the pool of available antibiotics available for treatment, and there is not currently a vaccine.

GAS can utilize several iron sources, but its preferred source is heme attached to hemoglobin [13]. GAS can lyse blood cells by β-hemolysis, which releases heme and hemoglobin, but it then needs to quickly sequester the heme from host hemoproteins and deliver it through its thick cell wall to the membrane transporters. Two known operons encode iron acquisition and import proteins, the *sia,* and the *hupYZ* operons. Shr, the first gene of the *sia* operon, extends past the cell wall and directly interacts with hemoglobin to remove the heme (Fig. 1) [14]. It binds heme through Near transporter

domains (NEAT), a common heme-binding motif found in heme scavenging proteins of several pathogenic Firmicutes, including *Staphylococcus aureus* [15]. Shr has two NEAT domains. The first, NEAT1, can pass heme to either NEAT2 or the NEAT-like domain of Shp [16]. However, NEAT2 can only give heme back to NEAT1, and could function in heme storage when excess heme is available. From Shp, the heme is transported across the cell membrane by the traditional ABC transporter, SiaABC (sometimes referred to as HtsABC) [17, 18].

Interestingly, the last three genes of the *sia* operon, *siaFGH*, code for a novel energy coupling factor (ECF) transporter that also transports heme [19]. This type of transport was only discovered ten years again and is associated with vitamin import. SiaFGH is the first heme ECF system to be described in bacteria. However, similar transporters have subsequently been discovered in *Lactobacillus sakei* and *Staphylococcus lugdunensis*, suggesting a conserved mechanism from heme import among Firmicutes [20, 21]. The first gene in the *hupYZ* operon, *hupY*, also binds heme and deletion of this gene results in a decrease in intracellular iron and reduced ability to colonize in a mouse vaginal colonization model [22].

Once the heme has been transported into the cell, it is degraded to release the iron. While heme degrading enzymes have been described in bacteria, it is not known how GAS and any other *Streptococcal* species release heme. In the Canonical pathway, the heme ring is degraded via oxidation, and ferrous iron is released with equal amounts of biliverdin and carbon monoxide [6]. The first chapter of this dissertation will provide an in-depth review of the mechanize of heme degradation utilized by pathogenic bacteria and will give a structural analysis of the proteins involved in this process. The second chapter will discuss the streptococcal protein, HupZ, as we further elucidate its role as

either a heme storage protein or as a novel heme degrading enzyme in GAS. The third chapter of this dissertation will focus on the application of structural modeling to predict heme-binding in proteins by focusing on the heme capturing protein, Shr, and the S component of the novel ECF transporter, SiaFGH.

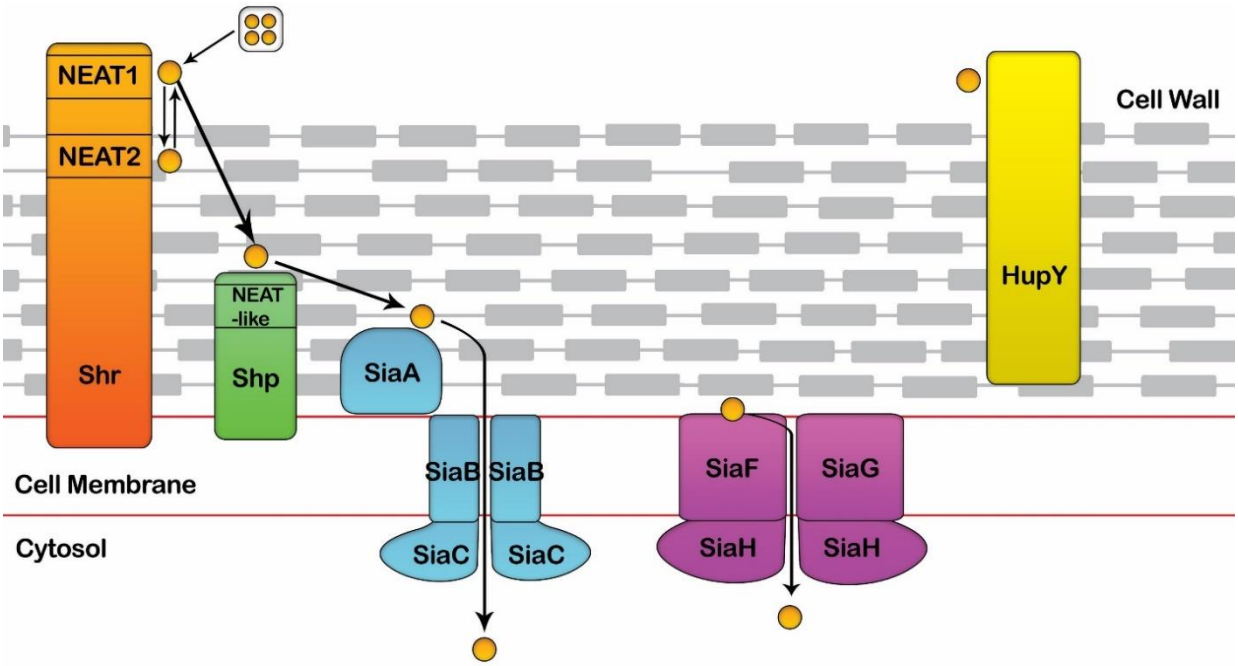

Figure 1 Cell envelope heme binding and uptake

(From left to right) Shr extends past the cell wall and interacts directly with hemoglobin to extract the heme. Heme is bound to the NEAT1 domain and can be passed to either the NEAT2 domain (for storage when heme levels are high) or to the NEAT-like domain of Shp. The heme is then transported through the cell membrane by the traditional ABC transporter, SiaABC. SiaFGH is an energy coupling factor (ECF) transported that also transports heme into the cell. HupY binds extracellular heme and is important for optimal growth on heme iron and for mucosal colonization.

2 CHAPTER 1. FROM HOST HEME TO IRON: THE EXPANDING SPECTRUM OF HEME DEGRADING ENZYMES USED BY PATHOGENIC BACTERIA

Previously published in Frontiers in Cellular and Infection Microbiology, 2018 [6].

2.1 Abstract

Iron is an essential nutrient for many bacteria. Since the metal is highly sequestered in host tissues, bound predominantly to heme, pathogenic bacteria often take advantage of heme uptake and degradation mechanisms to acquire iron during infection. The most common mechanism of releasing iron from heme is through oxidative degradation by heme oxygenases (HOs). In addition, an increasing number of proteins that belong to two distinct structural families have been implicated in aerobic heme catabolism. Finally, an enzyme that degrades heme anaerobically was recently uncovered, further expanding the mechanisms for bacterial heme degradation. In this analysis, we cover the spectrum and recent advances in heme degradation by infectious bacteria. We briefly explain heme oxidation by the two groups of recognized HOs to ground readers before focusing on two new types of proteins that are reported to be involved in utilization of heme iron. We discuss the structure and enzymatic function of proteins representing these groups, their biological context, and how they are regulated to provide a more complete look at their cellular role.

2.2 Introduction

In the late 1960s, Tenhunen and colleagues isolated the first heme oxygenase, HO-1 [23, 24]. While the enzyme was discovered in rats, HO-1 is highly conserved in mammals. The discovery of HO-1 provided valuable insights into the pathway that

reduces hemoglobin to bile [25]. Previous to this discovery, research showed that heme is cleaved to generate the linear tetrapyrrole biliverdin, which is subsequently reduced to bilirubin by biliverdin reductase. Yet, the mechanism by which heme was converted to biliverdin was not understood. Almost 30 years after discovering HO-1, the first prokaryotic HO, HmuO, was described in the Gram-positive Corynebacterium [26, 27]. Schmitt and colleagues screened a genomic library of *Corynebacterium diphtheriae* in *Corynebacterium ulcerans* mutants that were unable to grow in medium containing heme or hemoglobin as iron sources. The clone selected based on its ability to restore growth carried a gene (*hmuO*) with high homology to HO-1. Biochemical characterization revealed that, in the presence of a redox partner, HmuO catalyzes *in vitro* the oxidative cleavage of heme to produce biliverdin IX*α* [27, 28]. Two more bacterial HOs, HO-1 and HemO, were then cloned from *Synechocystis spp. PCC 6803* of the Cyanobacteria phylum*,* and the Gram-negative Proteobacterium, *Neisseria meningitides* respectively [29, 30]. Both HOs also share overall structural and mechanical similarities with the mammalian HO-1. The discovery of bacterial enzymes that are comparable to the mammalian counterparts promoted the initial notion that heme degradation represents an evolutionarily conserved mechanism. The mechanism these bacterial and mammalian HOs use to cleave the heme ring is referred to as "canonical heme oxidation" [31]. The discovery of IsdG and IsdI, two paralogous HOs from *Staphylococcus aureus*, and MhuD, a similar enzyme from *Mycobacterium tuberculosis,* gave rise to the second family of HOs due to their unique structure and novel mechanism for cleaving the protoporphyrin ring [32-34]. These enzymes demonstrated that oxidative heme catabolism could be achieved by more than one class of bacterial enzymes.

Since the discovery of HmuO, heme degradation in bacteria has become an active research area. Currently HOs are divided into the canonical HOs, which share structure and mechanistic similarities to HO-1 and the IsdG group [31]. Many potential HOs have also been identified based on their ability to carry out aerobic heme degradation *in vitro*. However, the acceptance of these proteins as HOs has met with some skepticism over the reaction mechanism and whether these proteins catalyze ring opening *in vivo* [35]. Non-enzymatic degradation of heme to verdoheme can be achieved by the addition of hydrogen peroxide (H_2O_2) to the solution (known as coupled oxidation). Coupled oxidation can take place in the presence of molecular oxygen (O_2) and a reducing agent that converts the heme iron to ferrous iron (Fe^{+2}) and H_2O_2. Various hemoproteins (e.g. myoglobin) and cytochrome mutants, in which the axial ligand was removed or replaced with a weaker ligand, readily exhibit this reaction [36]. While oxidative cleavage by a HO or breakdown by coupled oxidation is achieved by two separate mechanisms, they cannot be discriminated based on their products alone as they both yield CO and verdoheme (which is hydrolyzed to biliverdin under acidic or alkali conditions). Because of this complexity and since proteins that exhibit heme degradation *in vitro* (in the presence of a reductant) may have another function under physiological conditions, it was suggested that a comprehensive approach that combines genetics, mechanistic enzymology, and metabolite profiling is necessary for the characterization these proteins before terming them HOs [35]. Such extensive studies are not yet available for all cases but in this review, we attempt to compel what information exists. We briefly explain the HO-1 and the IsdG-like HOs before focusing on two new types of bacterial proteins that are reported to be involved in iron gain from heme. We discuss the structure and enzymatic function of these proteins, the biological context, and regulation mode. For

this paper, we reviewed the published literature as well as structural information. Protein structures were generated by downloading the Protein Data Bank file into PyMol (Table 1) and sequence comparisons were generated through NIH Protein BLAST.

Lastly, many bacteria degrade heme to obtain the iron. Here we focus on infectious bacteria, where heme catabolism is particularly important since it allows pathogens to leverage on the host heme pools. Nevertheless, it is important to note that non-pathogenic bacteria also use HOs and that these enzymes can be involved in additional functions. For example, in the photosynthetic Cyanobacteria, HO-1 catalyzes the first step in the production of phycocyanobilin, the tetrapyrrole chromophore the bacteria use to harvest solar energy [29].

2.3 The Structure and Function of Heme Degrading Enzymes

2.3.1 Canonical Heme Oxygenases

The first discovered group of HOs are usually referred to as canonical HOs, and include mammalian-HO-1, HmuO, and PigA/HemO. They are *α-only proteins and typically contain nine to ten helixes*. Their catalytic sites are highly conserved, especially the proximal α-helix [37]. Comparative studies between apo- and holo-HO-1 and HmuO show that heme binding induces a conformational change where the proximal α-helix twists in on itself, tightening the helix and shortening it. This results in the proximal α-helix moving towards the heme molecule. Concurrently, the distal α-helix swings towards the heme, causing the proximal and distal α-helix to open and close around the heme-binding pocket.

This group of HOs degrade heme to *α*-biliverdin (a linear tetrapyrrole), CO and free ferrous iron (Fe^{+2}) by three successive oxygenation steps and consumes three O_2 and seven electrons (Fig. 2a). This mechanism has been extensively reviewed in several

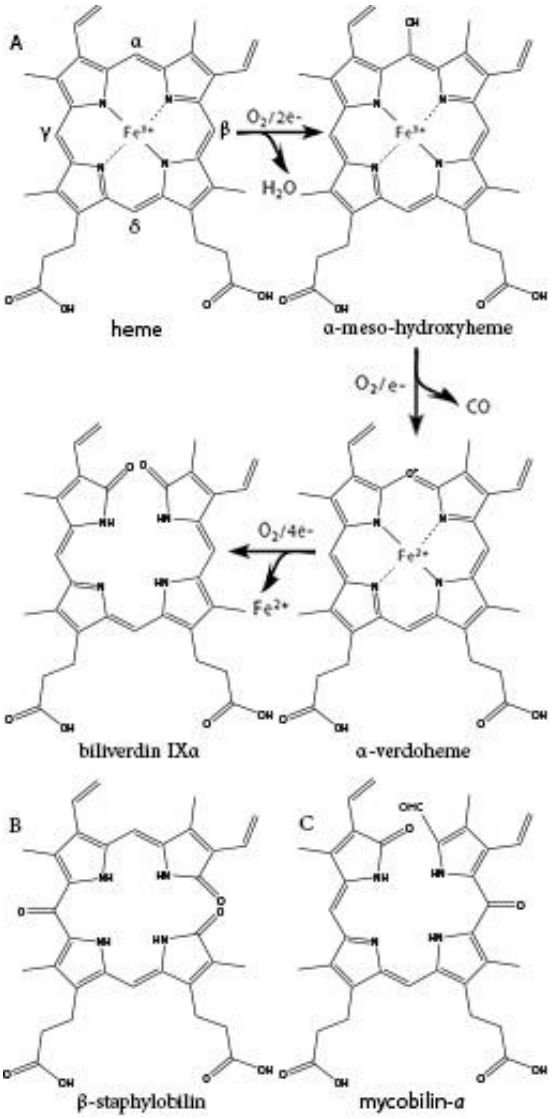

Figure 2 The three oxidative steps of canonical heme oxidation and the chemical structure of staphylobilin and mycobilin

A The three oxidative steps of canonical heme oxidation. In the first step heme is oxidized to ferric-hydroperoxide, then it is self-hydroxylated to α-meso-hydroxyheme. Next it is oxidized to α-verdoheme, which is ultimately oxidized to α-biliverdin. **B** One of the two isomers of staphylobilin produced by IsdG/I. **C** One of the two isomers of mycobilin produced by MhuD.

articles [31, 35]. Briefly, the reaction is initiated by the reduction of the heme ferric iron (Fe^{+3}) and O_2 binding. The coordinated oxygen (Fe^{+2}-O_2) is then reduced to peroxide (Fe^{+3}-OOH), a reactive species that hydroxylates the heme on the *α*-meso carbon. In the second step, the α-meso-hydroxyheme is oxidized to α-verdoheme while releasing CO. In the last step, the verdoheme ring is cleaved, generating Fe^{+3}-biliverdin complex that is reduced to release the iron (Fe^{+2}). This differs from coupled oxidation in the first step, were peroxide from the solvent (H_2O_2) instead of coordinated peroxide (Fe^{+3}-OOH) reacts with the heme iron to form the meso-hydroxyheme (which in turn progress to yield verdoheme). Hence, unlike HO catalysis, coupled oxidation is inhibited by the H_2O_2 scavenging enzyme, catalase.

Regioselectivity is the preference of a specific chemical bond over other possible bonds during a reaction. For this group of HOs the regioselectivity is for the α-meso carbon over the β-, γ-, or δ-meso carbons. Regioselectivity is controlled during the hydroxylation step due to steric hindrance of the distal helix interacting with the

protoporphyrin ring and allowing ring opening only at the α-meso carbon (Fig. 2a) [38]. The distal helix also bends, bringing the reactive iron dioxygen species closer to the α-meso carbon. The interactions between the distal helix and the protoporphyrin ring are stabilized through an extensive hydrogen bond network that is supplied by water molecules. This network also serves as the proton relay network required for oxygen activation [38, 39].

While the regioselectivity of the α-meso carbon is a defining characteristic of this group of bacterial HOs, a notable exception exists in PigA/HemO. Interestingly, PigA/HemO produces a mixed product of β- and δ-biliverdin in a 3:7 ratio [40]. A structure study of heme bound PigA/HemO shows that the heme is rotated about 100° in the binding pocket as compared to HO-1 and HmuO (Fig. 3a). This heme rotation is believed to result in the favoring of the δ-meso carbon over the α-meso carbon in PigA/HemO during the hydroxylation step [40, 41]. Mutagenic analysis of HO-1 and HmuO show that mutations to the amino acids that interact directly with the propionates or through solvent interactions are important for proper placement of the heme in the binding site [39]. In PigA/HemO, substituting Lys34 and/or Lys132 with alanine residues allows the production of α-biliverdin by the mutant enzymes in addition to β- and δ-biliverdin [41]. It was suggested that these residues interact with the propionate of the rotated heme molecule and that when the interactions are lost, it releases the ring rotation allowing the positioning the of α-meso carbon at the oxidation site. In addition, the ratio of β- and δ-biliverdin in PigA/HemO is greatly influenced by the amino acid identity at position 189, which is occupied by phenylalanine. A F189W mutant was found to produce mostly β-biliverdin (~90%) during heme catalysis. These

observations suggest that steric interactions bewteen the amino acid residue at position 189 with the heme impact the enzyme's topology and hence the reaction regiospecifificy.

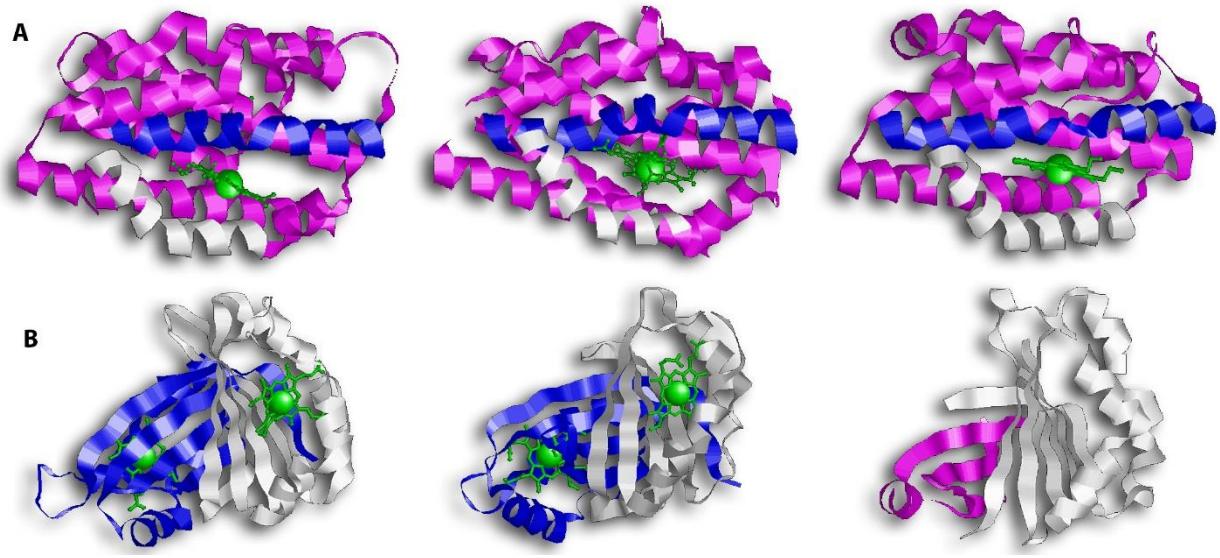

Figure 3 Overall structure of canonical and IsdG-like heme oxygenases

Line A from left to right: HO-1, HmuO, and PigA. This family of enzymes are commonly referred to as the canonical HOs. They are α-only proteins, and the proximal helix is in white, and the distal helix is in blue. These helixes take an open conformation when the binding pocket is empty but tighten and close around the heme molecule. The orange arrows point to the propionate groups on the heme. Note how the propionate groups in PigA are rotated compared to HO-1 and HmuO. **Line B** from left to right: IsdG, MhuD, Isd-LmHde. These enzymes represent the second group of HOs, the IsdG-like HOs. This group consists of α/β proteins that dimerize across their β-sheets. Both IsdG and MhuD have been colored so that one monomer is in white and the second monomer is in blue. The Isd-LmHde structure has been colored so that the N-terminal is in magenta and the C-terminal is in white.

2.3.2 The IsdG Family of Heme Oxygenases

The second group of bacterial HOs are commonly referred to as both non-canonical and IsdG-like HOs [31]. The founder of this group, IsdG, and its paralog, IsdI (64% sequence identity and 79% sequence similarity), were discovered in *S. aureus,* and degrade heme to staphylobilin and formaldehyde instead of biliverdin and CO (Fig. 2b) [32, 42, 43]. Following the discovery of IsdG/I, MhuD was discovered in *M. tuberculosis*. During heme degradation, MhuD retains its meso-carbon as an aldehyde

and generates mycobilin as its final product (Fig. 2c) [34]. MhuD shares 24% sequence identity and 46% sequence similarity with IsdG. Both of these enzymes are α+β class of protein and are part of the dimeric α- and β-barrel superfamily (Fig. 3b). MhuD and IsdG/I contain a ferredoxin-like fold, consisting of three α-helices and four β-strands arranged in a βαββαβ pattern, in their ABM domain (PF03992) (Fig. 3b). These enzymes also have similar active site structures. In IsdG, enzymatic activity is supplied by the catalytic triad Asn7, Trp67, and His77 [44]. His77 serves as the axial ligand, Trp67 induces heme ruffling, and Asn7, which is critical for catalytic activity, acts to stabilize the reaction intermediates and contributes to heme distortion. Mutagenesis of key residues in MhuD, showed that its heme ligand is a conserved histidine residue (His75) and that a mutation of Asn7 to alanine resulted in decreased enzymatic activity [34].

Advancements in time-resolved *in proteo* mass spectrometry have allowed for the characterization of the heme-derived species formed during IsdG mediated heme degradation [45]. Using this process, Streit and colleagues observed the production of an intermediate species with the same molecular weight as mycobilin (a formyloxobilin with α regiospecificity) (Fig. 2c). Further analysis revealed this intermediate consists of mixed β/δ-formyloxobilin isomers which is consistent with the reported production of both β- and δ-staphylobilin by IsdG [42]. Overall, the data suggests that in the IsdG reaction, an initial rapid conversion of heme to meso-hydroxyheme is followed by the formation of formyloxobilin, which resolves into staphylobilin by releasing CH_2O. More research is needed to understand why MhuD does not release formaldehyde from its formyloxobilin product. Interestingly, while a non-catalytic conversion of formyloxobilin to staphylobilin occurs when the product is extracted from the enzyme

under aerobic conditions, *in proteo* MS analysis revealed that IsdG converts only a fraction of the produced formyloxobilins to staphylobilins [45]. Hence, it seems possible that the remained formyloxobilin population might have a biological function.

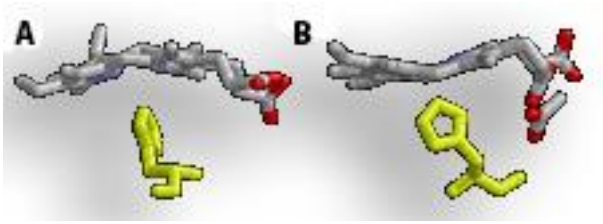

Figure 4 Alternatice heme ruffling in IsdG and MhuD

A represents the heme ruffling in IsdG and **B** represents the heme ruffling in MhuD. Notice in **A**, how the IsdG bends the heme so that the β- and δ-meso carbons are pushed away from the histidine, causing the α-meso carbon to move toward the ligand. In **B**, MhuD bends the heme so that the β- and δ-meso carbons are closer to the histidine ligand.

The difference in regioselectivity of staphylobilin and mycobilin may be explained by a 90° in-plane rotation of the heme in the catalytic site which results in alternative forms of heme ruffling (Fig. 4). Heme ruffling occurs when steric forces from the protein cause the usually planar heme molecule to bend. In IsdG/I, this results in the β- and δ-meso carbons being pushed towards the distal ligand [46, 47]. This is distinct from the MhuD-induced heme ruffling, which leads to the α- and γ-meso carbons being exposed to reactive iron-dioxygen species [48]. However, since the final product for MhuD are all α-formyloxobilins, other interactions must also be important for its regiospecificity. This differs from HmuO catalyzed heme oxidation, where water molecules associated with the HO push the α-meso carbon towards the reactive iron dioxygen species.

In addition to a putative *isdG* ortholog, the food-born pathogen *L. monocytogenes* codes for a second protein, Isd-LmHde, which shares structurally similarity with IsdG (Fig. 3b) [49]. Isd-LmHde is a monomer, and the full-length protein forms a β-barrel that is highly similar to the dimmers formed by IsdG/I and MhuD. The C-terminal region of Isd-LmHde shares 58% sequence similarity and 26% sequence identity with the IsdG monomer, but Isd-LmHde has an additional domain at

the protein amino terminus. The N-terminal domain of Isd-LmHde consists of a pseudo-ferredoxin-like fold, arranged βαβββ, while the C-terminal domain of the enzyme has of the same ferredoxin-like fold found in the IsdG-like HOs (βαββαaβ). Interestingly, an isolated C-terminal fragment of Isd-LmHde forms a homodimer in solution similar to the IsdG protein [49]. Both the full-length protein and isolated C-terminal domain of Isd-LmHde degrade heme *in vitro* (in the presence of catalase, favoring enzymatic degradation). However, activity by the truncated enzyme is significantly reduced compared to the full-length protein, demonstrating that both protein regions in Isd-LmHde are necessary for full function.

2.3.3 Enzymes with HemS Motifs

This group consists of heme-binding and degrading proteins, intracellular heme shuttling proteins, and possibly have other functions. We discuss these proteins together due to overall structural similarity. The group's founder member, HemS, is associated with the heme-specific transport system in *Yersinia enterocolitica* [50]. HemS alleviates heme toxicity in *Escherichia coli* and is required for *Y. enterocolitica* to utilize heme as an iron source [51, 52]. It also contains tandem repeats of a domain termed the HemS motif (PF05171). This motif is also found in the heme shuttling protein PhuS of *Pseudomonas aeruginosa,* and, in HmuS from the related *Y. pseudotuberculosis* and ChuS from *E. coli* O157:H7, both of which degrade heme *in vitro*.

HemS and ChuS function as monomers; while PhuS crystalized as a dimer, the monomeric form is more stable and the dominant form in solution (Fig. 5) [53-56]. HemS shares 35% sequence identity and 51% similarity to PhuS, and 34% sequence identity and 49% similarity to ChuS. Looking at the structure, ChuS consists of ten α-

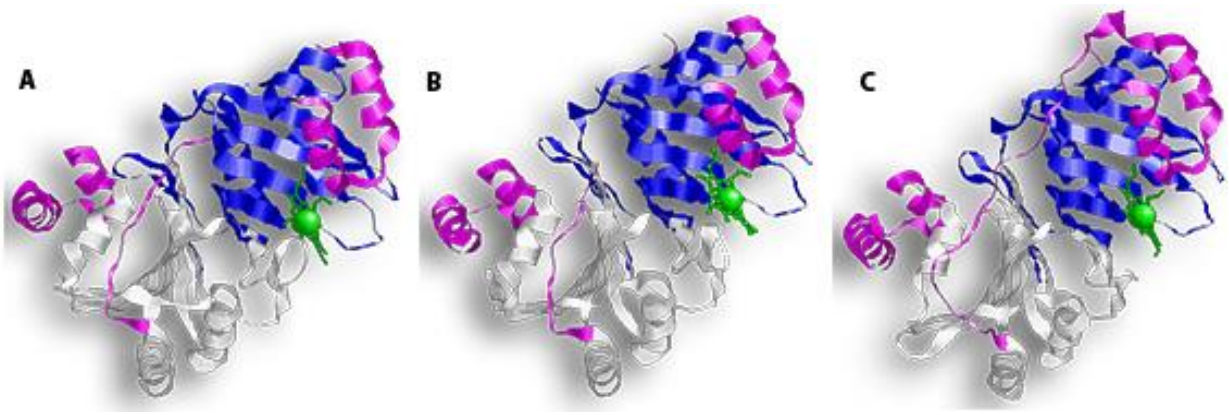

Figure 5 Overall structure of proteins with HemS motifs

A represents ChuS, **B** represents HemS, and **C** represents PhuS. In all representations the N-terminal HemS domain is in white and the C-terminal HemS domain is in blue. Looking at the structure, ChuS consists of a mix of α-helices and β-strands arranged so that the β-sheets form the core of the enzyme and are flanked by three α-helices on one side and two on the other side. This configuration is conserved in the structure of HemS, although HemS is symmetrical, with three α-helices on each side.

helices and eighteen β-strands arranged so that two β-sheets of nine antiparallel β-strands form the core of the enzyme. The core is flanked asymmetrically by three α-helices arranged in an α-loop-α-loop-α motif on the C-terminal side and a pair of parallel α-helices on the N-terminal. This configuration is conserved in the structure of HemS, although HemS is symmetrical, with three α-helices arranged in an α-loop-α-loop-α on each side. For ChuS the carboxy and amino termini share limited primary sequence homology, but they represent structural duplication in its tertiary structure [57]. The two halves appear to be associated across a central β-sheet, with key residues being conserved between both halves (i.e. Arg29/209, Phe127/304, and Tyr138/315). In the crystalized form, the PhuS dimers align across the β-sheets, forming a structure highly similar to ChuS. The C-terminal side of PhuS consists of three α-helices arranged in an α-loop-α-loop-α motif and a pair of parallel α-helices on the N-terminal side (Fig. 5c).

The binding pocket in PhuS and HemS is more open than in ChuS, with the C-terminal α-helices are closer to the binding site [54, 58]. This supports studies showing that PhuS acts *in vivo* as an intracellular heme transport protein [59]. PhuS shuttles heme to PigA/HemO, a HO in *P. aeruginosa* [60]. Upon binding heme, the C-terminal domain of PhuS rearranges to facilitate PhuS and PigA/HemO interactions, and heme transfer [61]. Heme-induced conformational changes were also reported for HemS, which alters between an apo-form that is open to a closed, heme-bound state [51].

The heme binding residues for these proteins are located on their α7 helix with a conserved histidine acting as the iron axial ligand (His196 for HemS, His193 for ChuS, and His209 for PhuS) [53-55]. Studies of a PhuS H209A mutant revealed that it can alternatively bind heme using His212 and that His210 helped stabilize these interactions [62]. Further analysis showed that the H209A mutant could still form a complex with the PigA/HemO, although to a less extend than the wild type protein. In comparison, while H212A and H210A mutants bound heme, they lost the ability to interact with PigA/HemO. Therefore, the current model suggests His209 and His212 of holo-PhuS act as a ligand switch for PigA/HemO [53, 62].

ChuS completes several cycles of aerobic heme degradation *in vitro* when either ascorbic acid or cytochrome P450 reductase (CPR)/NADPH are used as electron sources [55, 57]. Interestingly, both the N-terminal and the C-terminal halves of ChuS are tandem repeats that retained enzymatic activity, but the activity of the isolated domains varies depending on which reductant is used in the reaction [57]. Catalase was found to inhibit this reaction in a concentration dependent manner, indicating that H_2O_2 is required for activity. While the exact mechanism is not fully understood, UV/Visual stop flow spectroscopy, NMR spectroscopy, and EPR analysis have provided insights into the

reaction intermediates and products [63]. Ouellet and colleges suggest that the first intermediate, α-meso hydroxyheme generated by H_2O_2 attack of ChuS-bound heme, is a short-lived intermediate that progresses to ferric verdoheme. A subsequent ring cleavage releases Fe^{+3}, hematic acid (a monopyrrole moiety) and a tripyrrole product (containing both vinyl groups and one propionate). The tetrapyrrole ring cleavage in this reaction is different from simple hydrolysis of verdoheme, which produces a mixture of the four biliverdin isomers. This reaction also takes place in the presence of ascorbate or CPR/NADPH without externally added H_2O_2. The enzyme accelerates the production of H_2O_2 by ascorbate, suggesting that ChuS promotes H_2O_2-coupled heme degradation. The *chuS* gene is associated with heme-uptake machinery and is regulated due to iron availability, implying a function in supplying the bacteria with heme iron. The ability to release iron from heme under a relatively mild peroxide concentration, and the absence of known HOs in *E. coli* that degrade heme under aerobic conditions, are consistent with this proposal. Nevertheless, genetic analysis and addition biochemical characterization are required to test this hypothesis, and the possibility that ChuS serves alternative roles (e.g. protection from oxidative stress).

An ortholog of HemS from *Bartonella henselae's* was tested for heme degradation *in vivo* using the *E. coli* strain FB8.27 [64]. This strain is engineered to take up heme, but it cannot release the iron from the porphyrin ring due to inactivation of the enzymes *efeB* and *yfeX*. Therefore FB8.27 cannot grow using externally added heme as the sole source of iron. A recombinant *B. henselae* HemS protein restored growth of FB8.27 using heme iron, suggesting that HemS promotes the release of iron from heme *in vivo*. Currently the degradation products have not been characterized, and while it degrades heme in the presence of ascorbate or CPR/NADPH, HemS's sensitivity to

catalase has not been investigated [64]. Interestingly, a reduction of *hemS* gene expression does not impact growth, although it did increase the bacterial sensitivity to H_2O_2, implicating this enzyme in oxidative stress protection.

HmuS, a close HemS ortholog from *Y. pseudotuberculosis*, degrades heme to mixed biliverdin β- and δ-isomers *in vitro* [65]. Heme degradation using either ascorbate or ferredoxin/NADPH both with and without catalase produced biliverdin while consuming molecular oxygen and releasing CO. The spectral readings of reactions performed with and without catalase remained the same. Although the reaction was slower with catalase, the heme was eventually converted to biliverdin. When HmuS was incubated with only H_2O_2, verdoheme accumulated as the final product. Heme degradation (but not binding) was abolished when the proposed axial ligand (His196) or a distal arginine (Arg102) was mutated to alanine. Together the data is consistent with enzymatic degradation of heme, but direct evidence that supports its function in heme catabolism *in vivo* is still missing.

In summary, evolution of the HemS family may reflect individual adaptation of different bacteria to their growth environment. While some proteins from this family (e.g. PhuS) serve in intracellular heme shuttling, others may contribute to protection from oxidative stress and/or iron supply (e.g. *B. henselae* HemS and ChuS). *In vitro*, many of the family members are reported to exhibit heme degradation activity, yet biliverdin was confirmed only with HmuS from *Y. pseudotuberculosis*. Non-enzymatic cleavage was not ruled out in all cases and at least with ChuS, heme cleavage by H_2O_2-driven reaction is suggested, albeit by a unique enzymatic mechanism that seems possible under physiological conditions. Hence more investigations, specifically with

whole bacteria, are required to gain a better understanding of the function of proteins from this family.

2.3.4 Enzymes with FMN-binding domains

The FMN binding-like superfamily is divided into the NADH FMN oxidoreductase-like subfamily and the pyridoxamine 5'-phosphate oxidase (PNPOx)-like subfamily (PF01243). Several proteins from the PNPOx-like subfamily bind and/or degrade heme *in vitro*. Based on this proliferation, Hu *et al*. 2011 recommend adding a third subfamily to the FMN superfamily that includes these heme-binding proteins [66]. HutZ (*Vibrio cholerae*), ChuZ (*Campylobacter jejuni*), HugZ (*Helicobacter pylori*), and HupZ (*S. pyogenes*) are examples of heme-binding proteins with PNPOx-like domains that could belong to this third subfamily. While they all contain FMN-like binding domain, neither HupZ nor HutZ bound FMN *in vitro* (HupZ data not published) [67].

All four of these enzymes crystallized as dimers, and size-exclusion assays for HugZ, ChuZ, and HutZ confirmed that they purify as dimers [66, 68, 69]. Looking at their genetic sequence, the C-terminal regions are more conserved than the N-terminal region. HugZ and ChuZ have the highest level of similarity (54% sequence identity and 68% sequence similarity). Their N-terminal regions contain a simple α/β-type domain arranged in a three-stranded anti-parallel β-sheet, stacked against two α-helices in HugZ and three α-helices in ChuZ (Fig. 6a). Their C-terminal regions contain the PNPOx-like domain and consist of eight anti-parallel β-stands and four α-helices. In ChuZ, the β-barrel takes on a distorted form with β10 and β11 extending out on one end of the barrel. HutZ and HupZ are smaller than HugZ and ChuZ, and share more similarity to the C-terminal region of HugZ and ChuZ than the N-terminal region (Fig. 6b). In HutZ and HupZ, the antiparallel split-barrels are formed by six β-strands and

helices α1 and α2 block the open ends of the β-barrel. HutZ has two more α-helices that are packed against the side of the β-barrel and HupZ, the smallest of all, has only one additional α-helix.

Dimerization in these proteins occurs across their β-sheets with one monomer packed at about 90° from the second monomer. Crystal structures of holo-HugZ and ChuZ show that the heme-binding pocket lies near the dimerized β-sheets and that heme binding is stabilized through interactions with residues from both monomers (Fig. 6a). In ChuZ, the heme is bound between neighboring dimers using hydrophobic interactions between the protoporphyrin ring and the side-chains of His9 and His14 on different dimers [68]. The heme molecule binds with the propionic groups pointed toward the center of the dimer (Fig. 6a). This is distinctive from canonical HOs where the propionic group is parallel to the enzyme (Fig. 3a). Site directed mutagenesis of HugZ confirmed that His245 is involved in heme iron coordination and Arg166 interacts with the carboxylate group of the propionates [66]. In ChuZ, His245 is also involved in heme iron coordination but Arg166 is not conserved and instead Lys166 interacts with the carboxylate group [68]. Currently only apo-crystal structures exist for HutZ and HupZ, but analyses using single site substitution mutagenesis of HutZ have shown that His63 and Arg92 (corresponding to His245 and Arg166 in HugZ) interact with the propionate due to shifts in heme-bound spectra [67]. HupZ, however, lacks His245 and contains a glycine instead of Arg166, making it difficult to determine the heme coordinating residues based on sequence analysis alone [70]. Interestingly, ChuZ crystallized not only with the expected heme binding site, but with an additional surface bound heme molecule [68]. If ChuZ can also bind heme via the surface pocket *in vivo*, it may serve as a mechanism for preventing heme toxicity.

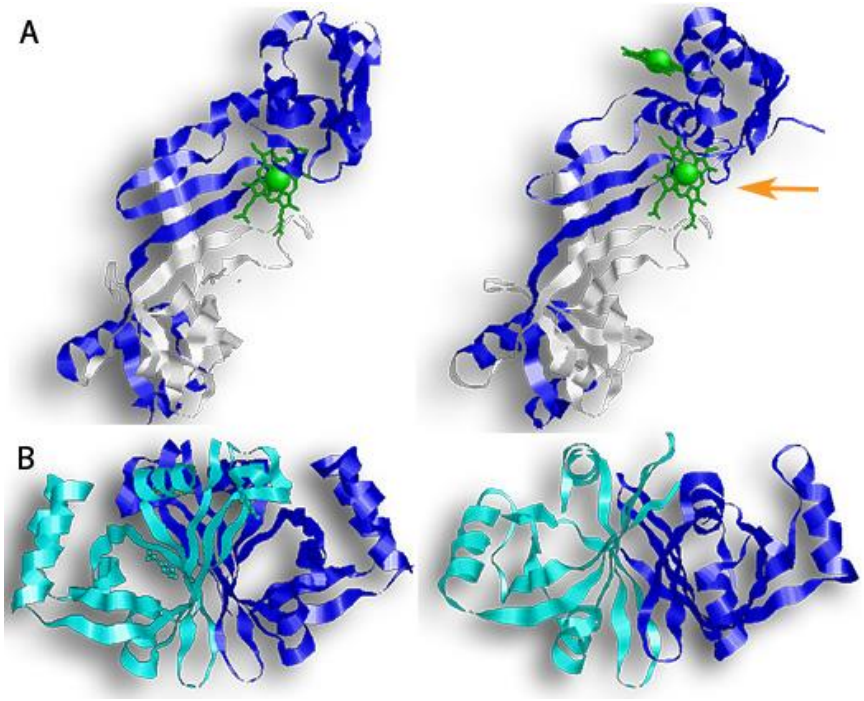

Figure 6 Enzymes with FMN binding domains

Proteins from the PNPOx-like subfamily contain a β-barrel with a Greek key topology (a protein structure consisting of four antiparallel strands connected by three hairpin loops that is named for a common pattern in Grecian decoration). The pictured enzymes also contain FMN-binding domains, although neither HutZ or HupZ can bind FMN. **Line A** (from left to right) a monomer of HugZ and a monomer of ChuZ. In both representations, the PNPOx domain is in white. In ChuZ, the canonical heme binding pocket is indicated by the orange arrow. **Line B** (from left to right) HutZ and HupZ. In both representations one monomer is colored blue and the other monomer is colored teal.

While all four proteins bind heme and mediate heme degradation *in vitro*, their physiological role is still under debate. A recent biophysical analysis of HutZ demonstrated that in the presence of exogenically added H_2O_2, heme is degraded to verdoheme (possibly β- or δ-isomer) and CO [69]. In the presence of ascorbate, the HutZ reaction is suggested to produces ferric biliverdin based on the appearance of broad featureless absorption in the visible region but this reaction is inhibited by catalase, which suggests coupled oxidation over enzymatic activity [71]. The *hutZ* gene is encoded by the iron-regulated *hutWXZ* operon that is divergently expressed from a

heme import system in *V. cholera*. This operon compliments the growth of *hmuO* mutants in *Cyanobacteria* on heme iron, although complementation requires an intact *hutZ* gene (but not *hutW* or *X*). In addition, a *V. cholera* mutant that lost *hutZ* could not efficiently use heme as a source of iron. Since the *hutZ* mutant is not more sensitive to heme toxicity, it's phenotype is likely related to a defect in acquisition of heme iron [71]. I*n vivo* studies implicate HutZ in heme catabolism, but more research is required.

In vitro degradation of heme by HugZ, ChuZ, and HupZ was observed in the presence of catalase [70, 72, 73]. All three proteins degrade heme to produce CO and a chromophore that absorbs at 660 nm (in the presence of ascorbate or CPR/NADH). HPLC chromatography has confirmed that HugZ produce δ-biliverdin [72]. While the chromophore produced by the ChuZ and HupZ reactions were not identified, the stability of HupZ's chromophore under acidic conditions suggests it is not verdoheme [70]. The iron-regulated expression of all three enzymes is consistent with a role in iron acquisition. Genetic studies are available only for *chuZ* where inactivation of this gene impaired the ability of *C. jejuni* to use heme or hemoglobin as a source of iron. Notably, the loss of *chuZ* had no impact on the bacterial sensitivity to oxidative stress [73]. In summary, similarly to the proteins with HemS domains, heme-binding proteins from the PNPOx-like subfamily might have evolved to play separate roles in different bacterial species, and more comprehensive investigations are required to describe the reaction catalyzed by these proteins and to determine their role in bacterial physiology.

2.3.5 The genetic link to iron metabolism in pathogenic bacteria

Bacteria tightly regulate iron levels to prevent overload and the resulting oxidative stress. Accordingly, expression of genes involved in heme catabolism are often repressed by iron and activated by heme, sometimes in competing manners. Here we

discuss several examples of metal-dependent transcriptional regulation, as well as heme regulation by a two component system and a post-translational modification.

Many enzymes, including *isdG* and *isdI*, are regulated by the Ferric Uptake Regulator, or Fur [74, 75]. The *isdG* gene is part of a chromosomal locus that encodes a key heme uptake pathway and it is the terminal gene of the *isdCDEF/srtB/isdG* operon. This operon also encodes a membrane heme transporter (*isdCDEF*) and a dedicated heme import sortase (*srtB*) [76]. Transcription of this operon is derived from the *isdC* promoter, divergently from the heme-receptor genes *isdA* and *isdB*. The *isdI* gene is the second gene in a bicistronic operon located elsewhere in the genome [76]. The promoters controlling the expression of *isdG* and *isdI* each contain a Fur box. In the wild type strain, IsdG and IsdI levels increase when medium iron levels are decreased, however the enzymes levels remain stationary in a null *fur* mutant [76]. This Shows that expression is repressed in the presence of iron, although IsdG is also stabilized in the presence of heme (discussed below). Of note, *isdG* and *isdI* double knock-out mutants still exhibit growth with heme as the only iron source, suggesting *S. aureus* contains a third heme degrading mechanism [76].

Similarly, to *S. aureus*, *P. aeruginosa* also encodes two HOs, PigA/HemO and BphO; however, only PigA/HemO is involved in iron metabolism. The *pigA/hemO* gene, which is part of a Fur regulated gene cluster, is required for efficient use of heme iron by *P. aeruginosa* and can complement the phenotype of *hemO* mutants in *N. meningitidis* [77]. The second HO, BphO catalyzes the production of biliverdin used for the assembling the photoreceptor phytochrome, BphP [78]. BphO is transcribed upstream from BphP in a bicistronic operon that is regulated by cell density and expressed independently of the iron status. PhuS, however, only transfers heme to PigA/HemO. In

addition to studies demonstrating heme transfer from holo-PhuS to PigA/HemO, ^{13}C-heme isotopic labeling studies showed that a □*phuS* mutant degrades externally provided heme using both of its HOs, PigA/HemO and BphO [79]. Since the wild type strain uses only PigA/HemO to degrade externally provided heme, these experiments support the role of PhuS as intracellular heme chaperon that shuttles the heme specifically to PigA/HemO. Interestingly, these studies also implicated PhuS as a modulator of heme uptake since the mutant strain demonstrated altered expression of the heme uptake machinery.

The expression of the *chuZ* gene, an enzyme with a PNPOx-like domain found in *C. jejuni,* is also regulated by Fur. The *chuZ* gene, is located directly upstream of the *chuABCD* genes, which together code for a heme ABC transporter [73]. Mutants that lack either *chuZ* or *chuA* are unable to utilize heme as an iron source, but mutants that lack *chuB*, *chuC*, or *chuD* are only partly affected, suggesting an additional heme uptake system. Two fur boxes lie in between *chuZ* and *chuA*. Using transcriptional fusions and competitive EMSA assays, Ridley and colleagues demonstrated that both promoters are expressed in an iron-dependent manner and bind to Fur protein *in vitro* [73].

The Diphtheria Toxin Repressor (DtxR) is mechanistically similar to Fur and controls the expression of genes involved in metal homeostasis and pathogenesis of many Gram-positive bacteria [80, 81]. The transcription of *hmuO* from *C. diphtheriae* is repressed in the presence of iron by DtxR (and activated by heme, as will be described below) [82]. EMSA and DNase I footprinting experiments showed that DtxR binds in a metal-dependent manner in the promoter region of *hmuO* in *C. diphtheriae* [82]. The expression of *hmuO* in *C. ulcerans* appears to be controlled differently [28]. Although the *hmuO* promoter in *C. ulcerans* contains a putative DtxR like box, promoter fusion

studies revealed that it is only weakly repressed by iron. The basal expression of *hmuO* grown in the absence of heme is significantly higher in *C. ulcerans* than in *C. diphtheriae*, although the mechanism is unclear. A null *hmuO C. ulcerans* mutant cannot survive with heme as the only iron source while the phenotype of *C. diphtheriae* mutants vary, exhibiting moderate to no growth attenuation depending on the strain [28]. Together these observations suggest that *hmuO* is important for the extraction of iron from heme in *C. ulcerans* and in some strains of *C. diphtheriae*, and that *C. diphtheriae* likely encodes additional factor(s) that allow the use of heme iron.

A DtxR-like protein named MtsR regulates the transcription of *hupZ*, a recently described enzyme in *S. pyogenes* [70, 83]. MtsR binds to DNA in the presence of either iron or manganese. It was first recognized as the repressor of the *sia* operon (*shr/shp/siaABCDEFG*) which encodes a central heme import pathway and of the *mtsABC* metal transporter [70, 84]. Global transcription analysis of null *mtsR* mutants established MtsR as a global regulator that controls the expression of many *S. pyogenes* genes, including iron and heme uptake, metal homeostasis and important virulence factors [85]. A two-gene cluster encoding a putative surface receptor and a cytoplasmic enzyme, later named HupZ, was identified in the MtsR regulon [70]. The *in vitro* activity of HupZ and its repression by MtsR implicate this enzyme in the utilization of heme as an iron source, but this role has yet to be established *in vivo*.

The expression of some heme associated genes is dependent on heme availability. The heme dependent-regulation of *hmuO* from *C. diphtheriae* is the first case where bacteria were shown to use two component systems to modulate the expression of HOs. Out of the eleven two component systems encoded by *C. diphtheriae*, two (ChrAS and HrrAS) modulate heme homeostasis. Both regulatory systems activate the *hmuO*

promoter in the presence of heme, but the ChrAS system is the dominant one [86, 87]. ChrAS also activates the transcription of *hrtAB*, an ABC transporter that functions in heme detoxification. While ChrAS and HrtAB both repress *hemA*, a heme biosynthesis gene. Fluorescence staining experiments demonstrated that the sensor kinase, ChrS, autophosphorylates then phosphorylates ChrA, the response regulator [88]. A conserved aspartate residue in ChrA (Asp50) was implicated as the phosphorylation site and shown to be important for ChrA binding to *hmuO* promoter. DNase I footprint experiments identified two 10-bp segments (designated as S2ho and S3ho) that protected by ChrA and are conserved in other ChrA regulated promoters. S3ho partially overlaps the DtxR binding box, suggesting that ChrA and DtxR compete for binding during growth in the presence of heme and iron. Mutagenesis and promoter fusion experiments confirm the importance of the both S2ho and S3ho in the regulated expression of *hmuO* [88].

Heme availability also regulates IsdG, but via a post-translational modification [76, 89]. As was previously mentioned, IsdG is the terminal gene of the *isd* operon. While the entire operon is repressed by Fur in the presence of iron, only the concentration of IsdG is enhanced in the presence of heme. A pulse-chase and immunoprecipitation study of IsdG (expressed from a constitutive promoter) found that the half-life of IsdG increased 2.5 fold in medium containing heme, suggesting that heme stabilizes the protein [76]. The stability of a catalytically inactive IsdG was similarly increased by heme, indicating that it is the heme and not the reaction product (staphylobilin) that facilitates stability. Analysis of a collection of chimeric proteins consisting of different IsdI and IsdG segments implicated an internal, β-strands containing, fragment in IsdG degradation. Further investigations identified a flexible

loop near the heme-binding site that is required (but not sufficient) for proteolysis in the absence of heme [89]. It was hypothesized that the differential regulation of IsdG/I allows *S. aureus* to specifically adjust the expression of its HOs to the different host environment. Interestingly, while both enzymes are required for full pathogenesis, *isdG* mutants are more impaired in heart and kidney colonization models in comparison to *isdI* mutants [76].

2.4 Future Direction

Advances in the fields of biochemistry and bioinformatics are improving the understanding of bacterial heme degradation. There is, however, still more to learn about these enzymes, such as why MhuD retains an aldehyde while IsdG does not and whether proteins with HemS or PNPOx domains degrade heme or protect from oxidative stress *in vivo*. Additionally, several species of bacteria lack proteins with homology to reported heme degrading enzymes and several enzymes were discovered that do not use oxidation to open the heme ring. One such protein is the recently discovered ChuW, a radical S-adenosylmethionine methyltransferase from *E. coli* O157-H7, which appears to degrade heme use a primary carbon radical to initiate a methyl transfer instead of binding O_2 [90]. In *E. coli* K12 the enzymes YfeX and EfeB also liberate iron from heme without breaking the protoporphyrin ring [91].

More research is needed to understand the mechanism for many of these proteins and would allow better understanding of their cellular role. Oxidative heme degradation requires an electron supply in addition to molecular oxygen and the electron donor for most bacterial HOs are unknown. Mammalian HOs use CPR and in the absence of a known physiological electron donor, *in vitro* heme degradation is achieved using CPR or an alternative reducing agent (e.g. trolox or ascorbate). Often, different reducing agents

produce different degradation kinetics and can halt the reaction at different stages, therefore they give a limited view of the *in vivo* reaction. In *P. aeruginosa*, the NADPH-dependent ferredoxin reductase, Fpr, was implicated as the physiological electron donor for PigA/HemO due to its ability to sustain catalytic activity during *in vitro* studies [92]. The two likely reductase partners for the Staphylococcal HOs are IruO (a pyridine nucleotide-disulfide oxidoreductase) and NtrA (a nitroreductase) [93]. Severe defects in heme usage are exhibited by an *iruO ntrA* double mutant (but not with either of the single gene mutants) implicated these enzymes in the process of heme catabolism. The search for native electron donors for bacterial HOs is important to develop the understanding of heme catalysis at the molecular level. New advances in our ability to monitor heme degradations as they are carried out in the cell are likely to enhance this important area of bacterial physiology.

Understanding the downstream effects of heme degradation products, such as biliverdin, staphylobilin, and CO is another area of research that could be expanded. In mammals, biliverdin is released from HO-1 and reduced to bilirubin by the action of biliverdin reductase. In bacteria, the destiny of the bilin produced during heme catalysis and its role in the cell physiology remains largely unknown. A recent mouse study showed that over expression of the *E. coli* ChuS leads to attenuation of the innate immune system [94]. This immunomodulation was achieved by decreasing the expression of the pro-inflammatory cytokine, IL-12 p40, and increasing expression of the anti-inflammatory cytokine, IL-10. Researchers speculated that cross-talk between mammalian HO-1 and enteric bacteria HOs might be a key component of maintaining healthy intestinal microbiota, making it an important area for farther study.

Since heme iron is used by many pathogenic bacteria, targeting heme uptake and degradation provides attractive targets for therapeutic inhibition. A direct role between HOs and virulence was established in only a few cases. Mice challenged with mutant *S. aureus* that lacked either *isdG, isdI,* or both genes, showed decreased bacterial loads in heart and kidney tissues compared to WT indicating that they are necessary for full pathogeneses [76]. Deleting the *hemO* gene in *Leptosria interorgans*, which is required for growth on hemoglobin iron, resulted in a 50% increase of survival rate of infected hamsters [95]. A better understanding of HOs function and the mechanisms that facilitate heme degradation during infection may lay the ground for new therapeutic designs.

Conclusion In many pathogenic bacteria, heme catabolism is carried out by HOs similar to either HO-1 or IsdG. Other bacteria encode enzymes that bind and degrade heme *in vitro*. These proteins fall into two families based on structure: enzymes that contain HemS motif and those with PNPOx domains. Proteins from these families are regulated by iron, support bacterial growth on heme iron, and/or aid in tolerance of heme and oxidative stress. It seems possible that proteins from these families might have evolved to serve separate functions in different bacteria. Already, PhuS was shown *in vivo* to shuttle heme to the HO, PigA/HemO. While *in vitro* degradation and additional investigations link proteins from these families to iron/heme metabolism, more work is required to determine their physiological role. Genetic studies suggest that even in bacteria with recognized HOs there are additional (likely non-homologous) enzymes that aid in heme degradation. This redundancy emphasizes the importance of this mechanism for bacterial physiology. For 50 years, this area has challenged both researchers and technology. While much has been learned about how pathogenic

bacteria obtain iron, the complexity and diverse strategies employed by the bacteria could easily fascinate researchers for many more years.

2.5 Conclusion

In many pathogenic bacteria, heme catabolism is carried out by HOs similar to either HO-1 or IsdG. Other bacteria encode enzymes that bind and degrade heme *in vitro*. These proteins fall into two families based on structure: enzymes that contain HemS motif and those with PNPOx domains. Proteins from these families are regulated by iron, support bacterial growth on heme iron, and/or aid in tolerance of heme and oxidative stress. It seems possible that proteins from these families might have evolved to serve separate functions in different bacteria. Already, PhuS was shown *in vivo* to shuttle heme to the HO, PigA/HemO. While *in vitro* degradation and additional investigations link proteins from these families to iron/heme metabolism, more work is required to determine their physiological role. Genetic studies suggest that even in bacteria with recognized HOs there are additional (likely non-homologous) enzymes that aid in heme degradation. This redundancy emphasizes the importance of this mechanism for bacterial physiology. For 50 years, this area has challenged both researchers and technology. While much has been learned about how pathogenic bacteria obtain iron, the complexity and diverse strategies employed by the bacteria could easily fascinate researchers for many more years.

Table 1 Proteins and their corresponding Protein Data Bank Identity (PDB) used for bioinformatical analysis

Protein	PDB	Protein	PDB
HO-1	1N3U	ChuS	4CDP
HmuO	3I8R	PhuS	4MF9
PigA	1SK7	HemS	2J0P
HemO	1p3T	HugZ	3GAS
IsdG	1XBW	HutZ	3TGV
MhuD	4NL5	HupZ	5ESC
HmoB	4FVC	ChuZ	3SWJ
Isd-LmHde	4KIA		

3 CHAPTER 2. HUPZ, HEME SHUTTLING PROTEIN OR UNIQUE HEME DEGRADING ENZYME

3.1 Abstract

Group A Streptococcus (GAS) is a common human pathogen that can cause highly invasive infections. Heme-iron from hemoglobin is the preferred host source of iron for the b-hemolytic GAS. Yet, it is not understood how GAS releases the iron from the pyrrole ring. We previously described GAS HupZ protein, which shares homology with a family of heme binding and degrading proteins such as HugZ and ChuZ. A recombinant HupZ-His_6 protein binds and degrades heme *in vitro,* but the His_6 tag was recently implicated in heme iron coordination and degradation. In this paper, we tested three new recombinant versions of HupZ, demonstrating that HupZ binds heme in the absence of a His_6 tag and that the heme-bound UV/Vis spectra lacked the α and β Q bands present in spectra of proteins containing axial heme ligands. HupZ readily accepted exogenous histidine residues to serve as its axial heme ligand, thereby coordinating the center iron and allowing for heme degradation in the presence of reducing partners. Importantly, HupZ bound and degraded a fragment of heme c (MP-11) using the histidine attached to heme c's proteinaceous region. Similar activity was recently reported for Pden_1323, a HugZ homolog from *Paracoccus denitrificans*. Inactivation of *hupZ* resulted in a small but significant reduction in GAS growth on hemoglobin iron and increased GAS sensitivity to heme toxicity. In addition, HupZ expression increased heme-iron use by *Lactococcus lactis*. Hence, the data suggest that HupZ is involved in heme metabolism. Still, additional studies are required to determine if HupZ functions in heme shuttling *in vivo* or if it is a novel enzyme that

excepts exogenous histidine residues from a partner protein or heme c to coordinate the central iron and degrade heme.

3.2 Introduction

Group A Streptococcus (GAS, or *Streptococcus pyogenes)* is an obligate human pathogen that frequently causes mild skin and throat infections. GAS can also produce invasive, systemic diseases, including Streptococcal toxic shock syndrome and necrotizing fasciitis, which have high mortality rates and may require amputation. In some cases, superficial GAS infections can cause harmful immune responses leading to post-streptococcal sequelae like glomerulonephritis and rheumatic fever, which is the primary cause of rheumatic heart disease in children in the developing world [96]. GAS also causes scarlet fever, which ran rampant in mid-19th to early 20th century Europe, killing 174 per 100,000 across all age groups and 419 per 100,000 in children under 5 in England [97]. While the global GAS burden of disease declined in the middle of the 20th century, in the late 1980s, there was a marked increase in invasive GAS infections in the United States and Europe with the emergence of more virulent strains, particularly the M1T1 strain [98]. Beginning in 2009, Vietnam, South Korea, China, and Hong Kong all reported dramatic increases in the rate of scarlet fever, with Hong Kong expiring a 10-fold increase in a single year and South Korea seeing a 40-fold increase from 2010 to 2015 [98]. Alarmingly, the scarlet fever outbreak in Asia and invasive GAS infections in the United States are increasingly resistant to tetracycline and macrolides, limiting available antibiotics for people with β-lactam allergies [12, 99]. The emergence of antibiotic resistance in GAS is of great concern since there is no vaccine.

There is very little free iron in the human body; most of it is sequestered by proteins that facilitate transport and storage and reduce iron-mediated toxicity. Ferric

iron is not soluble under physiological conditions. Transferrin quickly binds and transports ferric iron in serum, while lactoferrin fulfills this role in secretions. Most iron in the body is bound to a porphyrin ring, called heme, and two-thirds of the body heme is found in hemoglobin (i.e., heme b). The serum glycoproteins hemopexin and haptoglobin remove free heme and hemoglobin, respectively, to limit reactivity and promote clearance [7]. There are other types of heme in the body; for example, heme c is bound to cytochrome c and differs from heme b in that it is covalently bound to a proteinaceous region. For clarity, in this manuscript, we will use heme to refer to heme b. The innate immune system further limits free iron during infection by decreasing iron uptake and releasing extra hemopexin and haptoglobin into serum and lactoferrin at the infection site (for detailed reviews, see [8, 100]). Pathogenic bacteria, such as GAS, have evolved several mechanisms to overcome nutritional immunity and obtain heme from the host.

GAS lyses red blood cells by hemolysins, which releases heme and hemoglobin. The *sia* and *hupYZ* operons allow GAS to bind extracellular heme and transport it into the cell. The metalloregulator, MtsR, derepresses the expression of both operons during low iron conditions [83]. Shr, the first gene of the *sia* operon, extends past the cell wall and interacts directly with hemoglobin to bind heme [101]. Shr contributes to adherence and virulence and is protective in both active and passive vaccination models in mice [102, 103]. Recently, a monoclonal antibody to Shr that promotes phagocyte killing and increases mice survival from systemic GAS infection was reported, making Shr an exciting target for vaccination and therapeutics [104]. Heme bound to Shr is transferred to Shp, the second gene of the *sia* operon. Shp forms a protein complex with SiaA, the binding protein of the ABC transporter, SiaABC, encoded by the third through the fifth

genes [18, 101]. The last three *sia* genes (*siaFGH*) encode a novel heme importer, belonging to the new family of energy-coupling factor (ECF) transporters [19]. HupY is a heme receptor that aids in the growth on hemoglobin iron and contributes to mucosal colonization [22]. Once heme is imported, the porphyrin ring is likely degraded in the cytoplasm to release the iron.

The first heme degrading enzyme and its isoform, Heme Oxygenase 1 and 2 (HO-1/2, also abbreviated as Hmox1/2), was identified in mammals [105]. Subsequently, homologs were identified in several bacterial species, such as HmuO of *Corynebacterium diptheriae*, HemO of *Neisseria menigitidis,* and HemO/PigA of *Pseudomonas aeruginosa* [77, 106, 107]. This class of enzyme degrades heme through a pathway typically referred to as Canonical heme degradation or HO-1-like. Degradation is carried out through three oxygenation steps that occur at the α-meso carbon and result in equal amounts of α-biliverdin, ferrous iron, and carbon monoxide (for detailed reviews, see [6, 31, 35]). The first non-canonical heme oxygenases, IsdG, and its homolog IsdI were identified in *Staphylococcus aureus* [32]. In IsdG/I reaction, either the β- or δ-meso carbons are attacked and released as formaldehyde instead of carbon monoxide, yielding a mixture of β- and δ-staphylobilin. MhuD is an IsdG homolog found in *Mycobacterium tuberculosis* that contains subtle differences in the heme-binding pocket [34]. These differences result in a 90° in-plane rotation of heme in the catalytic site, which might explain why MhuD reaction occurs at the α- and γ- meso carbons and why the meso carbon is retained as an aldehyde [48]. Some pathogenic bacteria utilize proteins from the flavin mononucleotide (FMN)-binding subfamily for heme binding or degradation. HugZ from *Helicobacter pylori* and ChuZ from *Campylobacter jejuni* are dimers that bind a heme molecule with each monomer [66,

68]. These enzymes also degrade heme, releasing δ-meso biliverdin and carbon monoxide.

HupZ is a small protein that is co-expressed with the heme receptor, HupY. ApoHupZ crystallized as a homodimer with a split β-barrel conformation shared by heme degrading enzymes from the FMN-binding subfamily [70]. HupZ purified with a His_6-tag binds and degraded heme *in vivo,* releasing CO, free iron, and an unidentified chromophore. Further investigation of the recombinant protein using EPR and resonance Raman spectroscopy indicated that a histidine residue coordinated the heme iron, yet site mutation of the only histidine residue in HupZ did not affect the spectra [108]. This suggests that the His_6-tag was facilitating heme binding and degradation that was observed by the HupZ-His_6 protein. Here, we investigate heme binding and degradation by HupZ expressed without a His_6 tag and used mutagenesis and heterologous expression to probe the protein's function *in vivo*. The data suggest that HupZ plays a role in heme use and tolerance in GAS and suggest that HupZ is a member of an emerging group of heme binding or degrading bacterial proteins.

3.3 Materials and Methods

3.3.1 Strains, media, and chemicals

A list of strains and plasmids can be found in Table 2. *E. coli* were grown at 37°C aerobically (225 rpm) in Luria-Bertani (LB) broth or agar, supplemented with appropriate antibiotics. Unless otherwise mentioned, GAS was grown statically in Todd Hewitt yeast broth (THYB, 5 ml media in 15 mL screw-top tubes, Thermo Scientific #33965) or agar (THYA) at 37°C. *L. lactis* was grown statically in GM17 at 30°C (10 ml media in 15ml screw-top tubes). Plasmid extractions were performed using Promega

Wizard Miniprep kit (PR-A7510) or Qiagen Midiprep kit. Genomic DNA was harvested with Invitrogen PureLink (K1820-01). Primers were ordered from Integrated DNA Technologies, and unless otherwise specified, chemicals were purchased from Sigma. The primers used in this study are listed in Table 3. Restriction enzymes were purchased from New England Bio. Cloning PCR was carried out with AccuTaq LA DNA Polymerase (Sigma D8045), and diagnostic PCRs used Taq DNA Polymerase (Thermo Scientific EP0401).

3.3.2 Plasmid construction.

Plasmid engineering was confirmed with restriction digest and PCR analyses.

3.3.2.1 Plasmids pKV111 and pKV117:

A *hupZ::cm*^{R} (chloramphenicol acetyltransferase) allele with flanking regions of chromosome homology was assembled in pUC19 using NEBuilder HiFi Assembly Kit (#E5520) generating plasmid pKV111. The chromosomal *hupZ* upstream region was cloned from GAS strain NZ131 using primers ZE844 and ZE845. The downstream was cloned using ZE842 and ZE843. The *cm*^{R} gene was amplified from pDC123 using primers ZE840 and ZE841. Clones were selected in *E. coli* using ampicillin (vector marker) and screened for resistance to chloramphenicol. The *hupZ::cm*^{R} allele was amplified from pKV111 with ZE876 and ZE787 primers, which also added flanking EcoRI sites for easy transfer of the fragment into the temperature-sensitive vector, pJRS700, generating pKV117. Transformations were selected on kanamycin and screened for resistance to chloramphenicol.

3.3.2.2 Plasmids pKV138 and pKV141:

The shuttle vector, pKV138, expressing *hupZ* under GAS r*ecA* promoter, was generated for complementation. The *hupZ* gene was amplified from NZ131 gDNA, digested with NotI and BamHI, and then ligated into pLC007. Clones were selected on spectinomycin after transformation into *E. coli*. To generate an empty vector (pKV141) control, plasmid pLC007 was cut with HindIII and self-ligated, then transformed into *E. coli* and selected by spectinomycin resistance.

3.3.2.3 Plasmids pKV105:

The vector, pKV105, expressing *hupZ* under the regulation of nisin, was used for heterologous expression in *Lactococcus lactis* (*L. lactis*). The gene was cloned from NZ131 strain using primers ZE685 and ZE686 that added an upstream EcoRI cut site and a downstream HindIII cut site. Both the insert and pNZ8008 were digested with EcoRI, and HindIII then ligated and electroporated into MC4100 *E. coli*, and colonies were selected for chloramphenicol resistance. Competent MG1363 *L. lactis* that already contained pXL14, which codes the nisin response regulator, were electroporated with either pKV105 or pNZ8008 (as a negative control). Colonies were selected for resistance to chloramphenicol and then confirmed for resistance to erythromycin.

3.3.2.4 Plasmids pKV102:

Plasmid pKV102 expressing HupZ with a C-terminal Strep-tag was purchased from Vector Builder. The HupZ sequence was placed in a pET bacterial protein expression vector that contains a T7 promoter and pBR322 origin of replication. It was introduced and propagated in BL21 *E. coli* with ampicillin.

3.3.2.5 Plasmids pKV130 and pKV135:

Maltose binding protein (MBP) fusions were generated with ligation independent cloning into either pET/His6/TEV or pET/MBP/TEV expression vector as previously described [109]. Both expression vectors were gifts from Dr. Scott Gradia (Addgene plasmid #29656 and #48311, respectively). The *hupZ* was cloned from NZ131 with primers ZE978 and ZE979 that added the following upstream sequence, 5'TACTTCCAATCCAATGCA3' and downstream 5'TTATCCACTTCAATGTTATTA3' to the insert. The purified PCR products were incubated with T4 DNA polymerase (Invitrogen 1800-5017), bovine serum albumin (BAS), dithiothreitol (DTT), dCTP, and T4 polymerase buffer. The vector, either pET/His6/TEV or pET/MBP/TEV, were linearized with SspI restriction enzyme, then incubated with T4 DNA polymerase, BSA, DTT, dGTP, and T4 polymerase buffer. The reactions were cleaned using ethanol precipitation and resuspended in 12 µl of diH_2O. One µl of the vector was incubated with 4 µl of insert for 30 minutes at room temperature, then 1 µl of 25 mM EDTA was added to the solution and allowed to sit for an additional 15 minutes. The complete reaction was then transformed into *E. coli* and selected for with kanamycin (pKV130) or ampicillin (pKV135 and pKV140).

3.3.3 Generation of GAS ΔhupZ::cmR mutant (M49Lyles)

We used insertion inactivation to knock out *hupZ* in the GAS M49 strain NZ131. Competent NZ131 was transformed with the temperature-sensitive pKV117 (harboring the *hupZ::cm^R* allele and flunking chromosomal region) and plated on THYA with kanamycin (the vector marker) at 30°C. Colonies were then passed three times in THYB with kanamycin at 37°C and were plated with either chloramphenicol or no antibiotic at 30°C. The resulting GAS clones harboring an integrated pKV117 were confirmed by

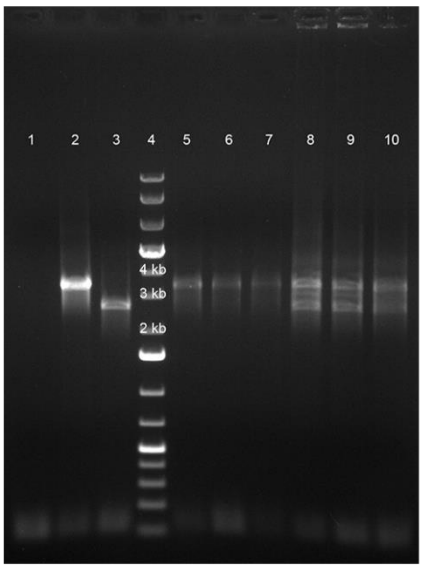

Figure 7 Schematic for the generation of ΔhupZ mutant

The *hupZ* gene in colonies isolated at different steps of the screen was examined by PCR (using primers ZE843 and 844) and run on a 0.8% agarose gel. Lanes 1 – 3 indicate controls and are (from left to right) negative control (no template DNA), *hupZ::cm*^{R} allele (pKV117, 3.1 kb), wt *hupZ* (WT gDNA, 2.5 kb). Plasmid integration would result in a merodiploid harboring the wt and mutant copy of *hupZ* (lanes 8 – 10). A second recombination event would result in either the *hupZ* band or the *hupZ::cm*^{R} band (lanes 5 – 7).

PCR. Daily, individual colonies were propagated at 37°C and screened through replica plating to ensure the loss of the vector marker and the maintenance (knockout mutant) or loss of the *cm*^{R} gene (wildtype rescue). The replacing of *hupZ* with *hupZ::cm*^{R} allele in M49Lyles or the regeneration of the wildtype *hupZ* allele in M49Rescue were confirmed with PCR (Fig. 7).

3.3.4 Hemoglobin iron use assays

GAS from glycerol stock was grown overnight with the appropriate antibiotics and used the next day to inoculate fresh media (without antibiotics), with or without 2.5 mM of the iron chelator dipyridyl (DP) and hemoglobin in a range of concentration. Hemoglobin was solubilized in 0.9% saline, diluted to the proper concentration with THYB, and filter-sterilized using a 0.45 uM filter unit. Growth media was made in batches and pre-incubated for one hour at 37°C before aliquoting 5 ml into screw-top tubes. Cultures with a starting OD_{600} of 0.01 were incubated at 37°C, and the OD_{600} was recorded after 20 hours of incubation.

L. lactis expressing HupZ (pKV117) or harboring an empty vector (pNZ8008) were assayed in a similar way, except that the assay was conducted in M17 with 0.5% Glucose (10 ml of media in 15 ml screw-top tubes). Nisin (1 ng per ml) was added to the

media after pre-incubation of the growth media to induce expression. Cultures were inoculated at OD_{600} of 0.0025 and incubated at 30°C for 20 hours.

3.3.5 Heme toxicity assays

Bacteria from an overnight culture were grown in fresh media containing heme in a range of concentrations. GAS was inoculated with a starting inoculum of OD_{600} of 0.01, and the OD_{600} was recorded after 20 hours of incubation. Like with the hemoglobin use assay, antibiotics were omitted from the growth medium in the experiments (2^{nd} overnight incubation) done with GAS.

3.3.6 Protein expression

E. coli harboring the appropriate plasmids were grown overnight from a glycerol stock, then diluted 1:100 in fresh LB media with antibiotics. The culture was grown at 37°C with 225 rpm until it reached an OD_{600} of 1, induced with 1 mM isopropyl β-D-1-tiogalactopyranosie (IPTG) and incubated overnight at 20°C with 180 rpm. The next day cells expressing the His_6-tag or MBP fusion cells were harvested by centrifugation then resuspended in 20 mM Tris (pH 8.0), 100 mM NaCl, and 0.1% Triton X-100. Strep-tag proteins were centrifuged and resuspended in 20 mM Tris/HCl, 500 mM NaCl. One EDTA-free protease inhibitor (Roche) was crushed, dissolved in deionized water, and added to all the resuspension directly before sonication. Cells were sonicated on ice using a Branson Sonifier 450 with an amplitude of 15% for 20 minutes with 10-second rest every 50 seconds. The cellular debris was pelleted by centrifugation at 20,000 x g for 30 minutes at 4°C. Then the lysate was further clarified by filtration with a 0.22 μM filter unit.

Protein was purified on an AKTA FPLC using either HisTrap HP, MBPTrap HP, or StrepTrap HP Sepharose column (Cytiva 17-5248-01, 28-9187-79, 28-9075-47). Buffers for the His_6-tag and MBP fusion proteins consisted of: a binding buffer (pH 7.4) containing 20 mM Tris-HCl, 200 mM NaCl, and 1 mM EDTA, and an elution buffer (the binding buffer containing 10 mM maltose). HupZ-Strep binding buffer (pH 8.0) contained 20 mM Tris/HCl, 500 mM NaCl, 1 mM EDTA, and the elution buffer was of similar composition with the addition of 2.5 mM desthiobiotin.

Protein purification was tested on either a 10 or 13% sodium dodecyl sulfate-polyacrylamide gel electrophoresis depending on the protein size (SDS-PAGE). Fractions of equal concentration and purity were combined, and the maltose or the desthiobiotin was removed by dialysis or buffer exchange (Amicon Ultra 15 filter Sigma). The buffer used for reconstitutions and degradations (*i.e., "*reaction buffer") consisted of 20 mM sodium phosphate and 500 mM NaCl (pH 7.4). To promote folding and solubility in the HupZ-Strep protein, 50 mM Arginine and 0.1% glycerol were added during dialysis. Protein was concentration was determined by Lowry (Thermo Scientific 23240).

3.3.7 HupZ reconstitutions with heme or MP-11

Hemin was dissolved in dimethyl sulfoxide and mixed with HupZ in a 2:1 ratio in a 20 mM potassium phosphate buffer with 500 mM sodium chloride. Microperoxidase (MP-11) sodium salt was dissolved in deionized water and then mixed with HupZ using the same ration. In both reactions, the reconstitution was incubated overnight a 4°C, and excess heme or MP-11 was removed by passing the solution through a PD10 desalting column (Cytiva 17-0851-01). When applicable, after reconstitution, 1.6 mM imidazole was added to the solution and allowed to rest for 5 minutes at room

temperature. For HupZ-Strep to remain soluble in the presence of hemin, its reconstitutions also included 50 mM arginine and 0.1% glycerol.

3.3.8 Heme and MP-11 degradations

Degradations were carried out in a total volume of 1 ml and contained 10 μM holo-HupZ, 20 μM bovine catalase, and an NADPH regeneration system consisting of 10 mM Glucose-6-phosphate, 1 U Glucose-6-phosphate dehydrogenase. The degradations were initiated with 10 mM sodium ascorbate or 10 μM ferredoxin with 100 μM nicotinamide adenine dinucleotide phosphate. The UV-Vis spectra was recorded every 15 minutes for the first hour and every hour after that for a total of five hours.

3.3.9 Structural alignment

The structural alignment was generated in Visual Molecular Dynamics (VMD) with the following Protein Data Bank (PDB) accession codes: HupZ 5ESC and pden_1323 6VNA [110]. One monomer of each protein was loaded into VMD as a new molecule and then aligned using the built-in MultiSeq analysis, which uses the STAMP or structural alignment of multiple proteins tool for aligned protein sequences based on a three-dimensional structure [111]. The resulting alignment had a Q value, which measures the structural conservation of 0.61, where Q=1 implies that the structures are identical and scores below 0.3 are not well aligned. The structure also had a root-mean-square deviation (RMSD) of 2.28 and a Percent Identity of 6.9%.

3.4 Results

3.4.1 Recombinant HupZ proteins expressed without a His_6 tag bind heme with 404 nm Soret

We previously showed that a recombinant HupZ protein containing a C-terminal fusion to His_6 tag binds and degrades heme *in vitro* [70]. Moreover, HupZ-His_6 crystallized as a homodimer with a split b-barrel conformation, a fold shared by FMN-binding heme degrading proteins described in several bacterial species. Still, additional and more detailed investigations revealed that this recombinant HupZ protein binds heme *in vitro* by its His_6 tag, leading to a higher-order oligomeric structure, heme stacking, and degradation [108]. These findings cast doubts about the function and the role of HupZ in heme metabolism. To reexamine heme binding by HupZ, we constructed a new recombinant C-terminal fusion replacing the His_6 with a Step-tag to facilitate purification. We expressed and purified the recombinant HupZ-Strep from *E. coli* (Fig. 8a), but the purified protein was not very stable and quickly precipitated out of solution, especially in the presence of heme. We attempted to increase stability by adding 1% glycerol and 30 – 50 mM arginine to the buffer [112, 113]. A buffer containing 1% glycerol and 30 mM arginine increased HupZ solubility and thus was used in heme titration experiments. Titration of HupZ-Strep with externally added heme revealed the formation of a growing UV-VIS absorption peak at 404 nm that is indicative of heme-binding (Fig. 8c). However, the heme bound form of HupZ-Strep exhibited a significant shift in absorption maxima compared to the holo HupZ-His_6, which has a 414 nm Soret peak (Fig. 8e). Additionally, unlike HupZ-His_6, the absorption spectrum of HupZ-Strep did not include the α and β bands between 500 and 600 nm, implying this recombinant protein binds heme without an axial heme ligand that coordinates the heme iron [114].

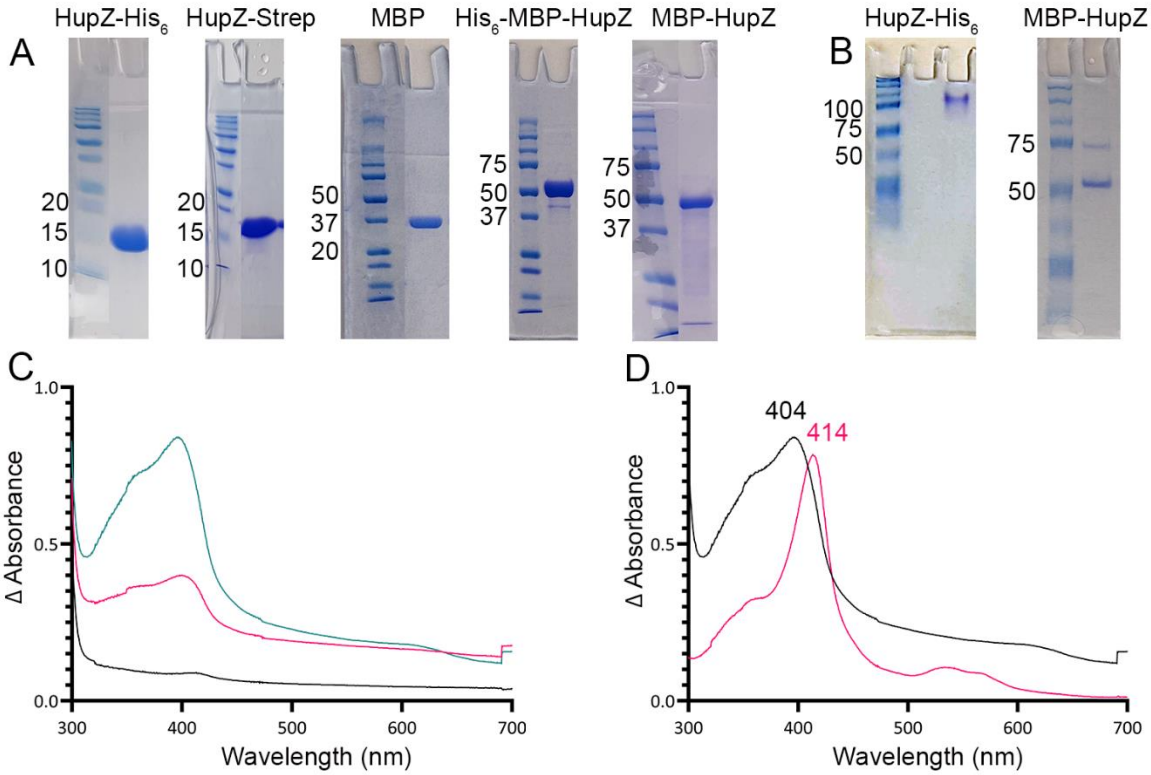

Figure 8 HupZ-strep binds heme but without iron coordination

Purified proteins used in this study (**A**, from left to right) HupZ-His_6 (18.5 kD), HupZ-Strep (18.7kD) were run on 13% acrylamide SDS gel. MBP-Empty (40.2 kD), His-MBP-HupZ (56.7), MBP-HupZ (56.5 kD), were run on a 10% acrylamide SDS. Native PAGE gels running 10 µM of HupZ-His_6 (**B**, left) and 10 µM of MBP/HupZ (right). 10 µM of HupZ-strep incubated (**C**) for 1 hour with 5 (pink) or 10 (teal) µM of heme. The blank contain reaction buffer with 1% glycerol, 30 mM Arg and a corresponding amount of heme. 10 µM HupZ-Strep (**D**, black) compared to 10 µM HupZ-His_6 (pink) incubated for 24 h, free heme was removed by PD-10 and the UV-Vis spectrum recorded. The blank for HupZ-His_6 contain only reaction buffer, while the blank for HupZ-Strep contain the reaction buffer, 1% glycerol, 30 mM Arg.

3.4.2 MBP-HupZ uses an exogenous histidine for iron coordination

Due to the remaining solubility problem, HupZ-Strep exhibited even in the presence of glycerol and arginine. We decided to replace the Strep-tag with a fusion to MBP, which often aids in protein solubility. The crystal structure of HupZ-His_6 indicates that the protein C-terminus is close to where the HupZ dimers form a β-barrel. To avoid the possibility that a C-terminal addition may interfere with HupZ function, we constructed and tested an N-terminal MBP-HupZ fusion. The MBP-HupZ protein was

readily expressed and purified (Fig. 8a), and unlike HupZ-Strep, this recombinant protein was stable and soluble. In addition, MBP-HupZ migrated as a monomer on native PAGE, unlike HupZ-His_6, which assembles into a high oligomeric state *in vitro* and migrates as a high molecular protein band in native gel (Fig. 8b). Heme titration experiments resulted in a UV-VIS spectrum similar to HupZ-Strep containing a 390 nm Soret peak and no α and β bands (Fig. 9a). The negative control, a purified MBP protein, bound only a negligible amount of heme, exhibiting a different absorption spectrum (Fig. 9b). Therefore, both HupZ-Strep and MBP-HupZ proteins bind heme, albeit without using an axial heme ligand. These findings suggest that heme binding is native to the HupZ protein and independent of the tag, the location of the fusion, or the multimeric state.

Histidine, along with tyrosine and, to a lesser extent, cysteine, are common residues in short amino acid sequences that bind heme and are specifically known to function as a heme axial ligand [115]. For histidine, the imidazole ring is the moiety that acts as a ligand toward iron and other transition metals. Since HupZ did not exhibit iron coordination in the absence of the His_6 tag, we tested if exogenous imidazole could react with the heme in HupZ by adding 1.6 mM of imidazole to the heme reconstitution after removal of unbound heme (Fig. 8c). After adding the imidazole, the spectra blue shifted, there was the formation of α and β bands, and the protein solution turned red (Fig. 9c insert). We also measured the UV-Vis spectrum for 10 μM of MBP after heme reconstitution and passage through a PD-10 column (Fig. 9d). Upon addition of 1.6 mM of imidazole, a low Soret appeared at 398 nm, but the Q bands were not generated, indicating the heme iron was uncoordinated. The UV-Vis spectra for 10 μM of heme did

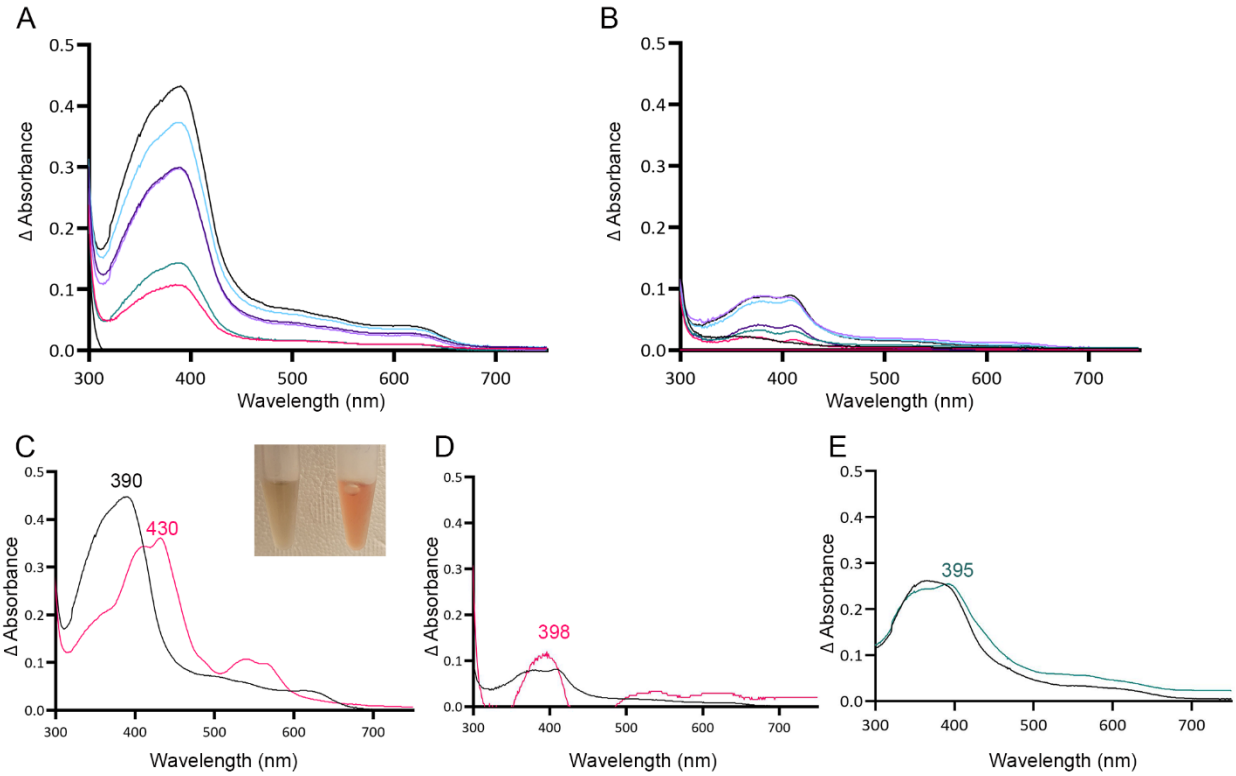

Figure 9 MBP-HupZ binds heme and uses exogenous histidine for iron coordination

UV-VIS absorption spectra of 10 µM MBP-HupZ incubated for 1 hour with 2-12 µM heme at 2 µM intervals (**A)** or MBP (**B)**. The blank contained reaction buffer and 2-12 10 µM µM heme. MBP-HupZ was incubated with 20 µM heme for 24 h, free heme was removed by PD-10 and the UV-Vis spectrum was determined before (**C,** black) or after the addition of 1.6 mM imidazole (pink). 10 µM MBP was incubated with 20 µM heme for 24 h, free heme was removed by PD-10 and the UV-VIS spectrum was determined before (**D,** black) or after the addition of 1.6 mM imidazole (pink). UV-VIS spectrum of 10 µM free heme with (**E**, black) or without (teal) imidazole. For **C** through **E** the blank only contained reaction buffer.

not change dramatically with the addition of 1.6 mM of imidazole (Fig. 9e). We also created and tested an amino-terminal His_6-MBP-HupZ fusion. Upon heme titration, the His_6-MBP-HupZ protein initially developed a spectrum similar to the MBP-HupZ construct (Fig. 10). However, the UV-Vis spectrum changed following overnight incubation at 4°C, with the Soret peak shifting to 416 nm and the formation of the α and β bands. These spectrum changes indicate heme iron coordination, likely by one of the residues in the His_6 tag upstream of MBP. Together, the data indicate that HupZ binds

heme without an axial heme ligand but can readily interact with an imidazole group to coordinate the iron.

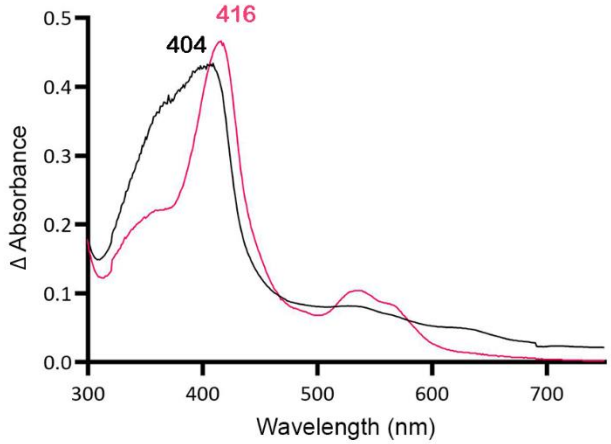

Figure 10 His6-MBP-HupZ initially binds heme without iron coordination, but becomes coordinated with longer incubation

10 μM MBP-HupZ was incubated with 20 μM heme for 24 h, free heme was removed by PD-10 and the UV-VIS spectrum was determined before (black) or after the addition of 1.6 mM imidazole (pink). The blank contained only the reaction buffer.

3.4.3 MBP-HupZ degrades heme in the presence of an exogenous histidine group

HupZ-His$_6$ degrades heme *in vitro*, releasing CO, free iron, and a chromophore. Since we found that the heme iron in MBP-HupZ can be coordinated by the externally added imidazole, we tested if holo-MBP-HupZ protein can also break down the heme under these conditions. Holo-HupZ was incubated with 1.6 mM imidazole, ferredoxin (as a reducing agent), NADPH, an NADPH regeneration system, and catalase (to control for non-enzymatic degradation of heme by hydrogen peroxide). The reaction was incubated at room temperature, and the change in the UV–Vis absorption spectrum was recorded at every 15 mins for the first hour and then hourly for six at room temperature and again after overnight incubation at 4°C. The Soret and the α and β bands decreased steadily during the incubation time, indicating heme degradation (Fig 11b. Still, the

MBP-HupZ reaction did not result in the formation of an absorption peak at 600-700 mm, which is typical for biliverdin or similar molecules. *In vitro* heme degradation by some heme oxygenases (e.g., HemO and HemO/PigA) can result in the formation of ferric biliverdin, which has no absorption properties, instead of biliverdin (which absorbs at the 600-700 mm range) [77, 107]. We treated the MBP-HupZ reaction with acid (to liberate the iron). As with HemO, the reaction acidification caused the reduction of the α and β bands and formed a chromophore, although at 660 nm, and not 680 nm as with HemO. Hence, holo-MBP-HupZ can degrade heme only when the heme iron is coordinated by an externally provided imidazole group. No significant spectral changes were observed in the absence of imidazole by (Fig. 11a), indicating that Holo-MBP-HupZ did not degrade the heme.

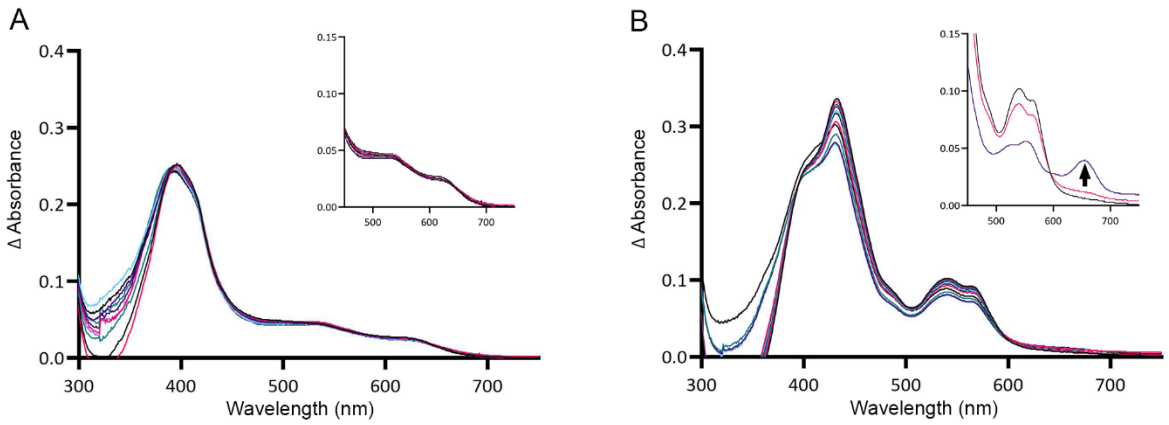

Figure 11 MBP-HupZ degrades heme b only in the presence of imidazole

10 μM holo-MBP-HupZ without imidazole (**A)** or 1.6 mM imidazole (**B)**, where incubated with 10 μM of Ferredoxin, NADPH, an NADPH regeneration system and catalase. After acidification of the MBP-HupZ reaction with imidazole, a peak at 660 nm formed (**insert**, purple). The blank contained with 10 μM of Ferredoxin, NADPH, an NADPH regeneration system, catalase, with or without 1.6 mM imidazole.

3.4.4 HupZ shares functional and structural similarities to heme c degrading enzyme Pden_1323

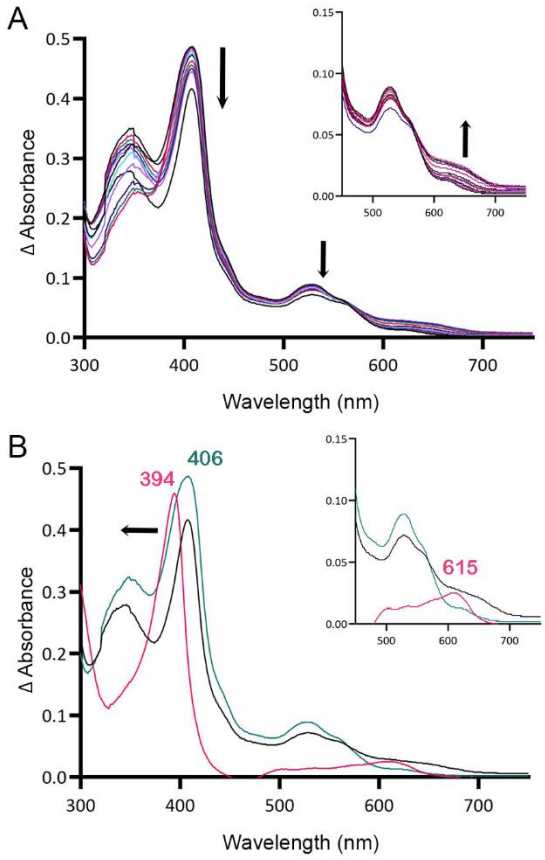

Figure 12 MBP-HupZ degrades heme c

10 μM MBP-HupZ in solution with 10 μM MBP, 10 μM of Ferredoxin, NADPH, an NADPH regeneration system, and catalase **(A)**. UV-VIS spectrum was monitored every 15 mins for the first hour, and hourly after that for a total of six hours. The zero minute of the same degradation (**B, teal)** and the six-hour time point (black). After acidification of the reaction (pink) the Soret shifted from 406 to 394 nm and a peak formed at 626 nm formed (**insert**, pink). The blank contained with 10 μM of Ferredoxin, an NADPH regeneration system, catalase, with or without 1.6 mM imidazole.

All of the heme-degrading proteins described up to date catalyze the breakdown of heme b, the type that is found in hemoglobin. The one exception is Pden_1323, from *P. denitrificans,* who belongs to the HugZ family. Pden_1323 lacks the C-terminal loop that contains the axial heme ligand (His245 in HugZ) but degrades heme c bound to a cytochrome fragment (MP11) containing the heme coordinated by a histidine residue. Since MBP-HupZ can degrade heme if the iron is coordinated by exogenous imidazole, we also tested if it could degrade heme c provided by MP11. MBP-HupZ bound MP11 with a 406 nm Soret and had α and β bands, indicating that the histidine in the proteinaceous section of MP11 could coordinate the heme iron (Fig. 12). MBP-HupZ bound to MP11 was then tested for degradation with ferredoxin, NADPH, and NADPH regeneration system (in the presence of catalase). It resulted in a progressive decrease in the Soret and the α and β bands (Fig. 6a). Like with

heme b, the HupZ reaction did not produce an absorption peak at the 600-700 mm. However, subsequent acidification of the solution led to the formation of a 615 nm chromophore (Fig. 12b). Together the data show that HupZ degrades heme c.

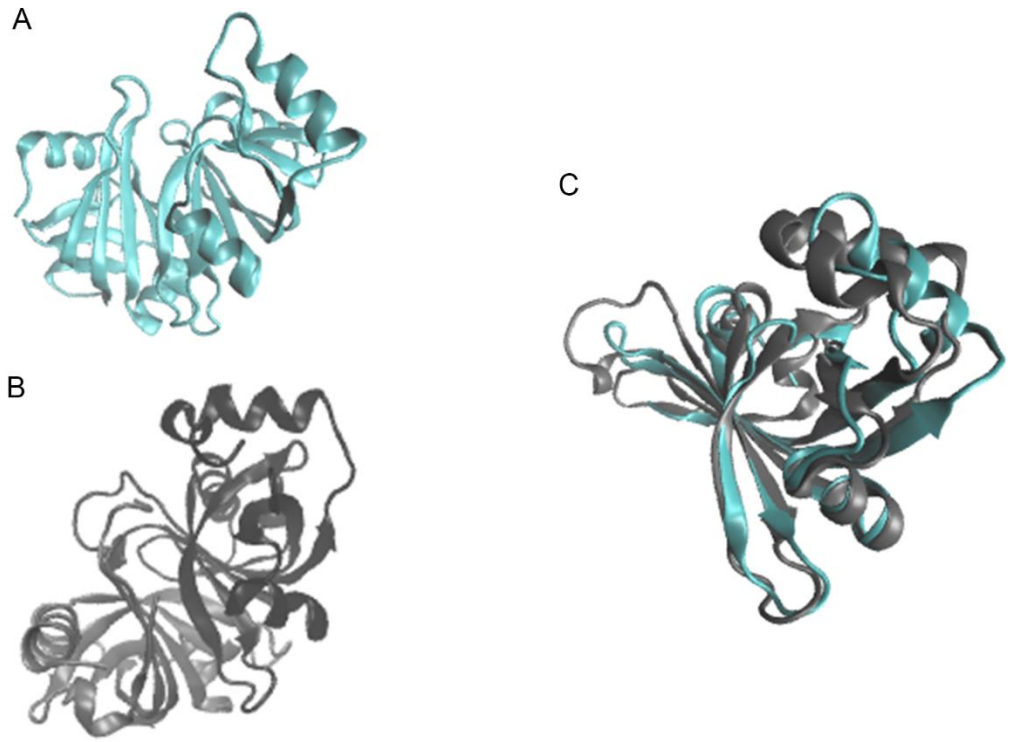

Figure 12 HupZ shares structural similarity to Pden_1323, a heme c degrading

The crystal structure of HupZ (A, 5esc), and Pden_1323 (B, 6vna). A monomer of each protein aligned (C), with an RMSD of 2.28 and a Percent Identity of 6.9%.

To further understand how the structural differences between HupZ (Fig. 13a) and Pden_1323 (Fig. 13b) allow for the degradation of c-type heme, we generated a structural alignment (Fig. 13c). Individual monomers of each protein have a 6.94% structural identity with an RMSD of 2.28. The proteins have the greatest similarity on their N terminal domain, where heme is believed to bind; however, neither protein has been crystallized with heme bound. As previously mentioned, both proteins lack the c-terminal loop containing the heme axial ligand in HugZ and ChuZ (His245) [66, 68]. They also both lack a large N terminal α/β domain that is present in other FMN-heme

degrading enzymes. The lack of both these regions probably creates a more open binding pocket, allowing the bulkier c-type heme molecule to bind [116].

3.4.5 HupZ contribute to heme metabolism in vivo

To evaluate the role of *hupZ* in heme use *in vivo,* we constructed a Δ*hupZ* mutant (M49Lyles) by insertion inactivation. We examined the mutant and the wildtype rescue strain (M49Parent) for heme use and sensitivity. Inactivation of *hupZ* had a small positive impact on growth in the regular laboratory THYB (Fig. 14a). The addition of the iron chelator dipyridyl to THYB (THYB-DP) restricted both strains growth to less than 25% compared to regular media (Fig. 14b). Supplementation with hemoglobin at a concentration range (2.5 to 20 μM) restored GAS growth in THYB-DP, indicating both strains can use hemoglobin as an iron source. Still, the hemoglobin dose-response was delayed in the M49Lyles strain compared to M49Parent. For complementation, we expressed *hupZ* in trans from GAS *recA* promoter. Comparing the complemented and control (empty vector) strains revealed again small but statically significant differences between the strains when grown on hemoglobin iron (Fig. 14c and d). Hence, the data show that *hupZ* loss reduces GAS' ability to use heme iron.

To overcome the potential redundancy in heme degrading enzymes in GAS, we tested the influence of *hupZ* expression on hemoglobin iron use by a heterologous host. HupZ was expressed from the P_{nis} promotor in *L. lactis*. Lactococal growth in GM17 was inhibited with 10 mM DP and adding hemoglobin to the iron-restricted medium restored growth, indicating *L. lactis* can use hemoglobin as an iron source (Fig. 14e). Nevertheless, *L. lactis* expressing *hupZ* grew better on hemoglobin iron (responding to lower hemoglobin concentration and reaching a higher maximal density) compared with

the negative control strain (*L. lactis* harboring an empty vector). Hence, HupZ promotes the use of heme iron in both GAS and *L. lactis*.

We next tested the sensitivity of the GAS mutant, and the wildtype rescue strains to free heme (Fig. 14F). The addition of 5 mM heme to THYB restricted the growth of the *hupZ* mutant while it had no impact on the wildtype strain. The addition of 15 mM heme inhibited the growth of both strains, but the wildtype strain grew a bit better than the *hupZ* mutant. Hence, *hupZ* helps GAS manage heme toxicity, especially in a low concentration.

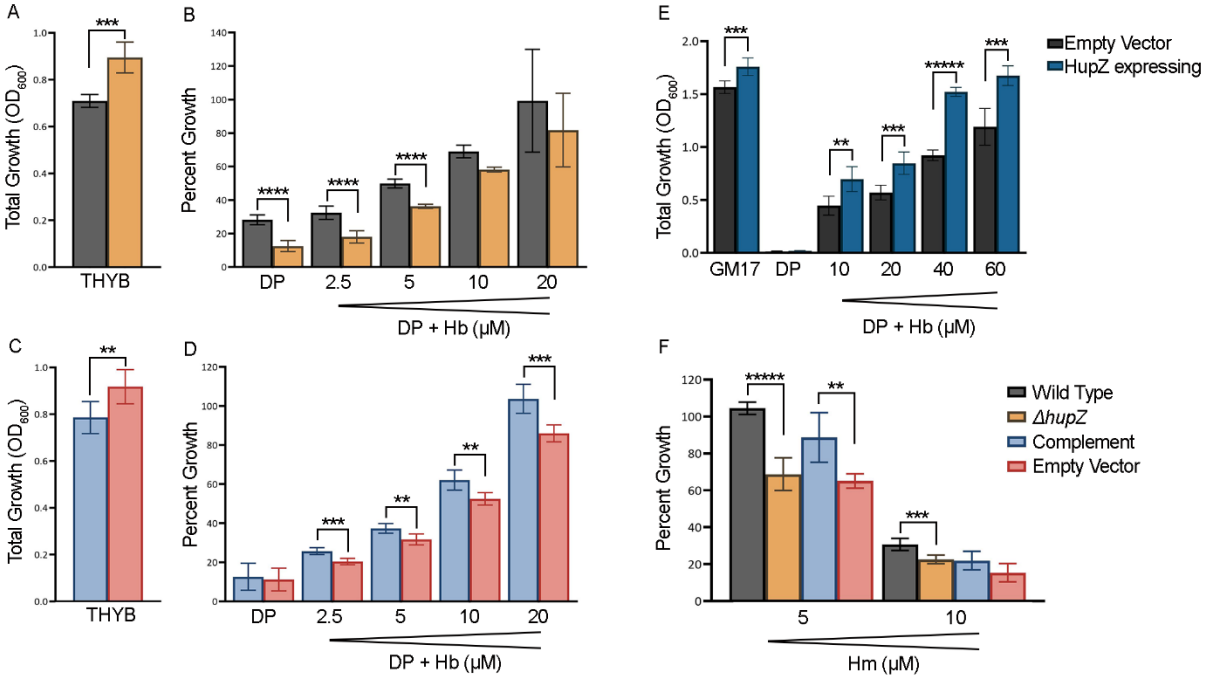

Figure 14 HupZ contributes to bacterial growth on heme-iron and aids GAS in heme tolerance

Total overnight growth of wild type (gray) and mutant (orange) in THYB **(A).** Percent growth of wild type and mutant in THYB-DP with 2.5 – 20 μM of hemoglobin (Hb) compared to normal THYB growth (**B).** Total overnight growth of complement (light blue) and empty vector (pink) in THYB **(C).** Percent growth complement and empty vector in THYB-DP with 2.5 – 20 μM of HB compared to normal THYB growth (**D).** *L. lactis* total overnight growth in GM17 **(E),** GM17-DP, or GM17-DP and a range of 10 to 60 μM of Hb, with either an empty vector (black) or expressing HupZ (dark blue). Percent growth of wild type, mutant, complement and empty vector in THYB with either 5 or 10 μM of heme (Hm) compared to normal THYB growth.

3.5 Discussion

Heme acquisition and iron release are vital for GAS infection, as they supply the pathogen with growth essential iron in the host environment. GAS lacks genes who share sequence homology to canonical heme oxygenases and hence how this pathogen process heme to release the iron is an enigma. Based on iron regulation and the co-expression with the heme receptor, *hupY,* and the *sia* heme uptake operon, we hypothesized that HupZ, a small and presumably cytoplasmic protein, is involved in heme metabolism. Crystal structure of HupZ-His_6 showed significant similarity to heme binding and degrading proteins that contain FMN-binding domains. Moreover, *in vitro* analysis revealed that a recombinant HupZ-His_6 binds and degrades heme *in vitro*. Heme-HupZ-His_6 exhibits a UV/Vis spectrum that contains a prominent Soret at 414 nm and two α and β bands in the 500 – 600 nm range indicative of heme bound with an axial heme ligand [70]. Resonance Raman spectroscopy indicated that the axial heme ligand in HupZ-His_6 was a histidine residue, but replacing the only native HupZ histidine residue with alanine did not affect the Raman spectroscopy [108]. These observations suggest it's one of the six histidine residues in the purification tag was interacting in the heme-binding. In this study, we examined HupZ's function using biochemical and genetic approaches. The data show that HupZ binds and degrades heme *in vitro* while relying on the exogenous imidazole group to coordinate the heme iron. We also demonstrated that *hupZ* expression is not essential but promotes heme use and tolerance in GAS.

Using recombinant HupZ proteins with a carboxy-terminal fusion to a Strep-tag or an amino-terminal fusion to MBP, we demonstrated that HupZ binds heme independently of the tag nature or location (Fig. 8c & 9a). Interestingly, without the His_6

tag, HupZ does not assemble into the high oligomeric state exhibited by the HupZ-His_6 variant, a state that was thought to promote heme degradation (Fig. 8b). HupZ lacks a native axial heme ligand, and furthermore, it radially uses exogenous imidazole group to coordinate heme iron as supplied by free imidazole, the His_6-tag in the His_6-MBP-HupZ fusion, and heme c. Heme coordination in His_6-MBP-HupZ was not immediate and required long incubation. This observation, together with the fact that the His_6 tag is located at the amino end of MBP, thus far from HupZ, suggest that heme coordination in His_6-MBP-HupZ probably involved some multimeric armament that allowed for the His_6 tag of one molecule to donate an imidazole group to the heme-iron bound by another molecule.

Historically, it has been presumed that the bond(s) between the heme iron and the amino acid(s) coordinating the iron is the major force holding the heme into the protein. However, experiments on globin and cytochrome mutants in which the proximal histidine was changed to glycine and the side chain replaced by an imidazole showed that the protein could still incorporate heme even without a coordinate/covalent bond attachment [117]. Additionally, mutation of the HugZ axial heme ligand, His245, to alanine, glutamine or asparagine, could all degrade heme indicated that the side chain of the residues was not required for enzymatic degradation by HugZ and may serve a role in the recognition and binding specificity of heme [66]. Hence, the protein framework might provide sufficient interactions for binding within a relatively heme-specific binding pocket. Indeed, when the axial heme ligand (His209) of the heme shuttle protein, PhuS, of *P. aeruginosa* is mutated, the *in vitro* protein can coordinate the iron with neighboring His210 or His212 instead [53].

Polyhistidine tags are one of the most widely used for protein purification. Often the tags are removed after purification by the insertion of a protease recognition sequence. However, low reaction efficiency coupled with the requirement of costly enzymes and an additional purification step means that they are commonly retained [118, 119]. Yet, the retention of these tags during experimental conditions can change ligand binding dynamics. The two-dimensional infrared vibrational echo spectroscopy of His_6-myoglobin bound to carbon monoxide showed a significant change in the short time scale dynamics compared to when the tag was removed even though there was no effect on the UV/Vis spectra [120]. The terminal placement, whether N or C, can affect the enzymatic function. For example, the carbonyl reductase S1 from *Candida magnoliae,* catalyzes δ-selective reductions with an N-terminal histidine tag but generates a mixture of β and δ products when the tag is located on the C-terminal side [121]. HupZ-His_6 is able to degrade heme, however other recombinant version can only degrade heme with the addition of imidazole or the heme c which contains a histidine residue (Fig. 11 and 12). Given histidine's propensity to affect protein dynamics and regiospecificity, along with their prominences in heme binding pockets, they may not be suitable for heme binding studies.

HupZ with heme-iron coordinated by imidazole can degrade heme in the presence of a reducing partner, as evidenced by the decrease in the Soret and the α and β band (Fig. 11). Heme degradation enzymes require reduction partners that provide the electrons necessary for degradation. CPR is the native reducing partner of the mammalian HO-1. The native partners of most bacterial heme degrading enzymes are not known. The only exceptions are the ferredoxin reductases FPR in *P. aeruginosa* and the reductases IruO and NtrA in *S. aureus,* which facilitate the reaction of HemO/PigA

and IsdG/I, respectively. [122, 123]. While heme degradation with native reducing partners results in the formation of a linear porphyrin (e.g., biliverdin) and free iron. The HupZ degradation reaction, using ferredoxin as a reducing partner, results in a product that does not have spectral properties. The formation of a chromophore that absorbed at 660 nm after acidification (Fig. 11b, insert) suggests that HupZ reaction stopped after the formation of ferric-biliverdin (or a similar molecule), which is missing a spectroscopic signature. Similar observations were made with the heme degrading enzyme PigA/HemO of *P. aeruginosa,* and HemO of *N. meningitidis,* as well as the oxidoreductive cleavage of verdohemochrome IX-α [77, 107, 124].

HupZ also degrades heme c, which contains a covalently bound proteinases chain with a histidine residue. MBP-HupZ bound heme c (MP11) with coordination of the heme iron and degraded it to a 615 nm chromophore (released by acidification). This is the first reported heme c degrading enzyme in pathogenic bacteria, but a similar enzyme was recently described in the soil microbe *P. denitrificans*. Pden_1323 also belongs to the FMN-binding class of heme binding and degrading enzymes. Like HupZ, Pden_1323 lacks the c-terminal loop that contains the axial heme ligand and the N-terminal α/β domain, creating a larger opening where the heme-binding pocket is believed to be located. The N-terminal of HugZ was shown to be unnecessary for heme degradation; in fact, a C-terminal domain truncated mutant of HugZ demonstrated an increased rate of degradation compared to full-length HugZ [66]. *P. denitrificans'* ability to degrade heme c could aid in acquiring iron from environmental hemopeptides or play a role in general cell maintenance by recycling iron from *c*-type cytochrome this bacterium utilizes for metabolic purposes. HupZ's ability to utilize heme c could provide GAS with an iron source during tissue infections. GAS triggers apoptosis of epithelial cells through

mitochondrial dysregulation [125]. GAS achieves this by stimulating the release of Cytochrome c from the mitochondria by activation of caspase-9. Once the cytochrome is released, it would be vulnerable to proteolytic degradation and could serve as a valuable source of iron during skin infections when hemoglobin is unavailable.

Pden_1323 and HupZ may be representatives of bacterial heme degrading proteins that use a partner-facilitated heme iron coordination for heme degradation. This strategy might explain why other bacteria that lack homologs to known heme degrading enzymes (e.g., *Streptococcus pneumoniae, Salmonella typhimurium,* and *Shigella dysenteriae*) can grow on heme iron. Alternatively, it is possible that the use of exogenous imidazole group for heme degradation is a curious *in vitro* phenomenon and that HupZ is primely a heme shuttling protein. *P. aeruginosa* PhuS protein, is an example of a bacterial protein that degrades heme to verdoheme *in vitro* but *in vivo* it binds heme and delivers it to the heme oxygenase PigA/HemO for degradation [126]. Surface plasmon resonance and isothermal titration calorimetry revealed that holo-PhuS and not apo-PhuS forms a complex with PigA/HemO [127]. Hydrodynamic analysis showed that on binding heme, the binding envelope becomes more hydrodynamic. It is proposed that this conformational change drives PhuS interaction with the heme oxygenase. The loss of *phuS* only mildly impacts heme toxicity and does not affect heme utilization [58, 126], but it does affect heme uptake. PhuS mutants exhibit higher levels of the heme transporter PhuR and two heme oxygenases (PigA/HemO and BphO), even when heme concentration is low, indicating that PhuS could also act as a regulator of extracellular heme flux [60].

Lastly, we showed that the loss of *hupZ* results in a small but significant decrease in the utilization of heme iron at low concentrations (Fig. 14b). In *S. aueres,* loss of

either IsdG or IsdI, or both genes does not eliminate the bacteria's ability to grow on heme iron [76]. Likewise, in *Vibrio cholerae*, the deletion of HutZ did not stop growth on heme iron, although the mutant grew slower and reached a lower final cell density than the wildtype strain [71]. The growth defect in Δ*hupZ* is less than in either of these two systems. However, HupZ degrades heme *in vivo* is also supported by the increase in hemoglobin utilization by *L. lactis* expressing *hupZ* (Fig. 14e). The limited impact on GAS growth on hemoglobin iron however, may indicate that even if *hupZ* degrades heme *in vivo* (using a partner protein or Cytochrome c fragments), GAS has alterative means to degrade heme and HupZ may serve to fine-tune free iron levels. More research is therefore needed to understand the role of HupZ in GAS heme utilization and iron metabolism.

3.6 Future Work: HupX is a potential supplier of axial ligand and electrons to HupZ for heme degradation

3.6.1 Background

Heme degrading enzymes require a redox partner to degrade heme. Cytochrome P450 reductase (CPR) is the redox partner to the mammalian heme oxygenases, HO-1/2. In studies using HO-2 (the constitutively expressed mammalian heme oxygenase), CPR was shown to form a dynamic complex with the heme oxygenase, allowing for the transfer of electrons [128]. The resulting biliverdin is further reduced to bilirubin by Biliverdin reductase and stored in the gallbladder, where it is the main component of bile. Currently, only two bacterial heme oxygenases have a proposed reduction partner. In *Pseudomonas aeruginosa*, the NADPH-dependent ferredoxin reductase (FPR) was identified as a redox partner because it is expressed under low-iron stress conditions

[122]. FPR supports the *in vitro* degradation of heme by HemO/PigA without the addition of ferredoxin. Biochemical analysis of IruO, a reductase in *Staphylococcus aureus,* identified it as a partner for IsdG/I enzymes. It was demonstrated to allow for IsdG mediated heme degradation *in vitro* without needing another redox partner [129]. Deletion of i*ruO* did not affect *S. aureus'* growth on heme iron. However, a double mutant where the iron-regulated nitroreductase, NtrA, was also inactivated could not fully utilize heme iron [123]. Also of note, IruO binds the siderophores deferoxamine B and ferrochrome A and releases iron in the presence of NADPH, indicating that it might also function as a siderophore reductase. This notion was supported by the inability of an *iruO* mutant to grow on either siderophore as the sole source of iron [129].

We identified a putative TrxB homology in a gene located five genes downstream of the *hupZ* gene in GAS. TrxB is a thioredoxin reductase that partners with thioredoxin (TrxA) to regulate the redox potential in a cell for proper protein function [130]. It is present in all forms of life and aids in oxidative stress tolerance and controls cell growth and apoptosis. In this system, TrxA modifies the disulfide bond of target proteins, while TrxB provides TrxA with the required electrons in an NADPH-dependent manner. TrxB is a dimeric flavoprotein that contains a conserved CXXC active site. The GAS genome contains two traditional *trxB* orthologs, but the putative thioredoxin reductase downstream of *hupZ* does not have this active site. This protein is highly conserved between GAS strains and other streptococcal species such as *Streptococcus dysgalactiae* and *Streptococcus equi* (92 and 93% similarity, respectively), which also contain homologs to *hupZ*. While this TrxB homology lacks the conserved CXXC site of TrxB, it does have three cysteine residues that could still be involved in disulfide linking. Here we show that putative TrxB (containing a 6x histidine tag) can provide an axial ligand

for holo-MBP-HupZ and facilitate degradation without the addition of ferredoxin. We also demonstrate that this protein can bind biliverdin *in vitro* and reduce it in the presence of NADPH. Given this data, we propose the remaining of this TrxB homolog to HupX. We hypothesize that HupZ/HupX serves as a novel heme degradation machinery, where the redox partner also supplies the axial ligand for the axial ligand the release of iron from heme.

3.6.2 Materials and Methods

3.6.2.1 Generation of pOM104

The *hupX* gene was isolated from MGAS5005 using ZE509 and ZE510 (see table 3 for primer sequences). It was cloned into the pET101 vector using directional TOPO and transformed into Top10 *E. coli*. After confirmation of the insert, it was moved into BL21 for expression

3.6.2.2 HupX expression

HupX was expressed similarly to the His_6-tagged proteins described above. Briefly and overnight was grown from glycerol stock and diluted 1:100 in fresh LB media with ampicillin. The cultures were grown at 37°C with 225 rpm until they reached an OD_{600} of 1, expression was induced with IPTG. The incubation temperature was lowed to 20°C and the rpm to 180. After 18 hours, the cells were pellet and prepped for purification, carried out on an AKTA FPLC using a HisTrap HP column. The size of the purified protein was confirmed on 13% SDS-PAGE, and a buffer exchange column was used to consolidate the protein and move it into a 20 mM sodium phosphate buffer with 500 mM NaCl (pH 7.4).

3.6.2.3Heme degradation

Degradations were carried out similar to above and in a total volume of 1 ml containing 10 μM holo-HupZ, 20 μM bovine catalase, and an NADPH regeneration system. Directly before initiating the experiment, 10 μM of HupX-His_6 was added, then 100 μM of NADPH. The UV-Vis spectra were recorded every 5 minutes for the first hour and every hour after that for a total of five hours.

3.6.2.4Biliverdin binding and reduction

10 μM HupX-His_6 was allowed to incubate with an equal amount of α-biliverdin (Sigma) for 5 minutes, and then its UV/Vis spectra were measured. 100 μM of NADPH was added to the cuvette, and the spectra were immediately read and read again after 5 minutes.

3.6.3 Results and Discussion

3.6.3.1 HupX-His_6 supplies an axial ligand and electrons needed to mediate the degradation of by HupZ

HupX-His_6 in solution with holo-HupZ shows an initial binding Soret of 412 nm but lacks any peaks in the 500 – 600 nm range where the α and β bands are when the heme iron is coordinated. For the first 20 minutes of the assay, the Soret decreases, but there is little change between 500 and 750 nm (Fig. 15a). Interestingly, at 25 minutes, the soret intensified and shifted to 421 nm, and there was the formation of α and β bands and the start of a peak at 660 nm. For the remaining 6 hours of the degradation, the soret and α and β bands decreased while the 660 nm peak increased (Fig. 15b). By the end of the reaction, only the α band can be seen (Fig.15b insert). This work demonstrates that HupX can donate electrons to HupZ for degradation. Unlike when

ferredoxin is used as a redox partner, the solution does not need to be acidified to release iron from ferric biliverdin. It also suggests that HupX may supply an axial ligand for the heme. However, since a histidine tag was used for purification, more work is needed to confirm that this is a native function of HupX and not HupZ opportunistically commandeering a residue from the purification tag.

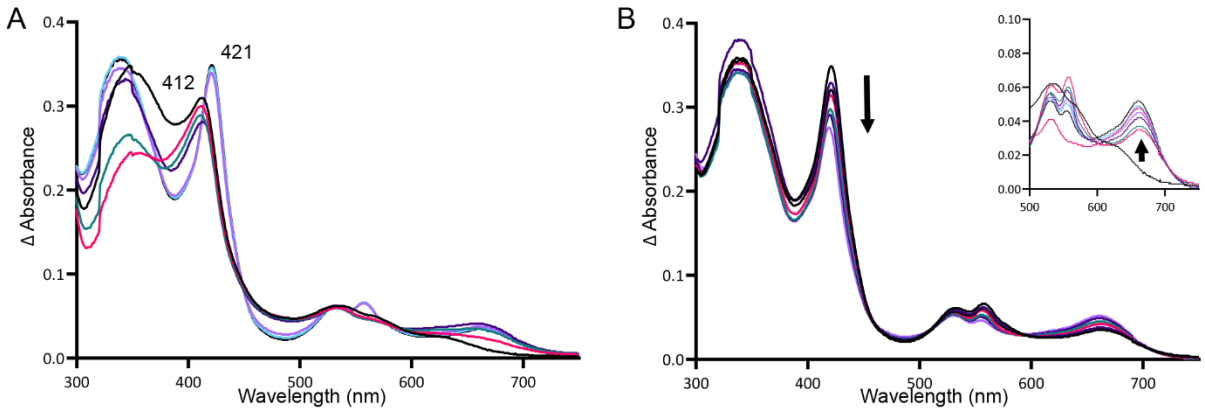

Figure 15 HupX-His6 supplies axial ligand and electrons to MBP-HupZ for degradation

3.6.3.2 HupX-His$_6$ allows for the reduction of biliverdin in the presence of NADPH

HupX- His$_6$ binds biliverdin with a 388 nm soret, with the 680 nm peak indicative of α-biliverdin (Fig. 16a). Five minutes after the addition of NADPH, the color of the solution changed from a blue-green typical of biliverdin to a yellow-green of bilirubin (Fig. 16b). Additionally, there was a dramatic reduction of the 680 nm signal, and the soret shifted to 420 nm (Fig. 16a). In all this suggest that HupX can not only donate the electrons to HupZ for heme degradation, but it could also reduce the biliverdin product to bilirubin. While *Citrobacter youngae* has been shown to convert biliverdin to bilirubin-10-sulfonate in cultures, the enzyme involved in the conversation

was not identified [131]. Therefore, HupX would be the first identified protein involved in reducing the product of heme degradation by bacteria.

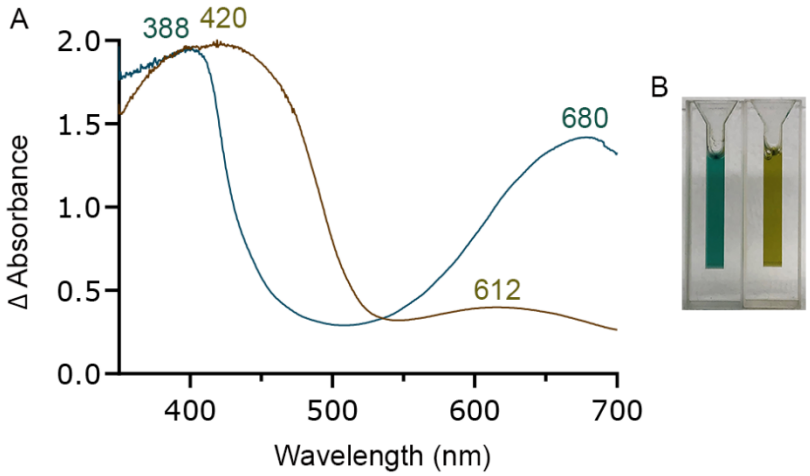

Figure 16 HupX-His6 reduces biliverdin to bilirubin

Table 2 Strains and plasmids

Strains/Plasmids	Relevant properties	Source/reference
M49Parent	NZ131 wild type rescue strain	This study
M49Lyles	NZ131 containing *hupZ::cm*^{R} mutation	This study
M49Lyles + pKV127	NZ131 containing *hupZ::cm*^{R} mutation and pKV127	This study
E. coli Top10	Cloning strain for plasmid generation	Invitrogen
E. coli BL21	Expression strain	Invitrogen
pDC123	Source of Cm^R allele	[132]
pET101	TOPO cloning vector, P_{T7}	Invitrogen
pET-His_6-MBP-TEV	N terminal 6x histidine and MBP, P_{T7}, Kan^R	Addgene #29656
pET-MBP-TEV	N-terminal MBP, P_{T7}, Amp^R	Addgene #48311
pJRS700	pVE6037 derivative, Kan^R, TM^S	[83]
pKV102	Expresses HupZ-Strep from P_{T7}	Vector Builder
pKV105	pNZ8008 derivative expressess *hupZ,* P^{nisA}, CM^R	This Study
pKV111	pUC19 derivative containing *hupZ::cm*^{R} allele, Amp^R	This study
pKV113	pKV111 derivative with a site mutation to add EcoRI site downstream of *hupZ::cm*^{R} allele	This study
pKV117	pJRS700 derivative containing *hupZ::cm*^{R} allele, Kan^R, TM^S	This Study
pKV130	pET-His_6-MBP-TEV derivative expresses HupZ, P_{T7}, Kan^R	This Study
pKV135	pET MBP TEV derivative that expresses HupZ with MBP protein from P_{T7}	This Study
pKV138	pLC007 derivative expressing *hupZ*, $Spec^R$, P_{RecA}	This study
pKV141	pLC007 derivative *hupY* deleted, $Spec^R$, P_{RecA}	This study
pLC007	Expresses *hupY*, $Spec^R$, P_{RecA}	[22]
pNZ8008	pSH71 replicon with promoter less *gusA* gene, P_{nisA}, Cm^r	[133]
pNZ9530	pAMb1 replicon expressing *nisR* and *nisK*, Ery_R, P_{RepA}	[134]
pOM104	pET101 derivative expresses HupX-His_6, Amp^R, P_{T7}	This study
pZZ2	pET101 derivative expresses HupZ-His_6, Amp^R, P_{T7}	[70]

Table 3 Primers

Prime	Target	Comment	Sequence
ZE509-S	*hupX*		5'CACCGTGAAAGATAAAGCATATG
ZE510-A	*hupX*		5'GTCAATTAAAGAGGTTGAATGCACC
ZE685-S	pNZ8008		5'CCCTTGAATTCCACTAGCGTTGCTTTACTG
ZE686-A	pNZ8008		5'GCGCGAAGCTTGGTCCTAAATACTGTTACAG
ZE728-S	*hupZ*		5'CACTCAAAATGATAACACAAGAAATGAAAGAT
ZE729-A	*hupZ*		5'GAGAAGCTTTTAAAATAAGGGTCCTAAATACT
ZE838-S	pUC19		5'GCTGAGATACGCGTAATCATGGTCA
ZE839-A	pUC19		5'ATGGGACAAGCTCGAATTCACTGGC
ZE840-S	pDC123	CM^R	5'TAGCAATGGTTGCTAACATAGCATTACGG
ZE841-A	pDC123	CM^R	5'CCAGATTGTACCTAGCGCTCTCATAT
ZE842-S	5' region of *hupZ*		5'GAGCGCTAGGTACAATCTGGTGCTAAT
ZE843-A	5' region of h*upZ*		5'ATGATTACGCGTATCTCAGCTATCTTAG
ZE844-S	3' region of *hupZ*		5'TGAATTCGAGCTTGTCCCATATTGC
ZE845-A	3' region of *hupZ*		5'CTATGTTAGCAACCATTGCTAATTGG
ZE876 -S	pKV111	Adds EcoRI to *hupZ::cm*^{R}	5'CATAGAATTCATGTGCTGAAGGCGAT
ZE876-A	pKV111	Adds EcoRI to *hupZ::cm*^{R}	5'CATAGAATTCGTTGTGTGGAATTGTGAGC
ZE978-S	*hupZ*	Adds LIC sequence	5'TACTTCCAATCCAATGCAATGATAACACAAGAAATG
ZE979-A	*hupZ*	Adds LIC sequence	5'TTATCCACTTCCAATGTTATTATTAGTTACTTTCACTGTT

4 CHAPTER 3. STRUCTURAL MODELING AND PREDICTION FOR HEME-BINDING PROTEINS

4.1 INTRODUCTION

X-rays were discovered in 1895 by Wilhelm Conrad Röntgen. Initially, scientists used X-rays to observe naturally occurring crystals. Max von Laue and associates found that X-ray irradiation of salt crystals would produce diffraction patterns that revealed the internal atomic periodicity of the crystals [135]. While X-ray diffraction does not show the atoms themselves, it shows the electron distribution, and from that, the location of atoms can be determined mathematically. The following year, 1913, the father and son team Henry and Lawrence Bragg used this knowledge to publish the structure of a diamond, sodium chloride, potassium chloride, and potassium bromide crystals [136]. Early crystallography was a process of trial-and-error as there was no standard way of deriving the results. Scientists had to try various possible atomic arrangements until they could find the structure closely resembling the diffraction pattern. In 1934 the geometrical theory of X-ray diffraction had advanced enough that Bernal and Crowfoot could demonstrate the atomic structure of pepsin [137]. The first three-dimensional protein structure published, myoglobin, was by Kendrew in 1958 [138].

A breakthrough in recombinant DNA technologies in 1970 by a group of scientists at Stanford University was a great boon for crystallography [139]. Recombinant DNA allowed for generating large amounts of target proteins *in vitro* by genetic engineering that could then be turned into crystals. The invitation of the synchrotron beam in 1898 provided the subsequent boost to the field of crystallography and the budding field of structural biology. A synchrotron beam is a form of electromagnetic radiation formed

when charged particles are accelerated perpendicular to their velocity, *i.e.,* along a curved path [140]. Typically, the particles are charged by magnetic fields, which allows them to gain very high energy levels. This energy is stored in large storage rings where the particles are orbiting with constant energy. Synchrotrons have the advantage of producing intense beams and can select a specific wavelength from a broad spectrum, including X-ray wavelengths of about 1 Å suitable for analyzing atoms in a molecule. The radiation emits in short pulses (picoseconds), allowing snapshots of intermediate steps in enzymatic turnover, intra- or inter-molecular electron transfer, or structural rearrangement. Additionally, the synchrotron beam is less damaging to the crystal than irritation via lab X-rays and allows for a hundred-fold increase in the lifetime of a crystal [141].

When a crystal is scanned with an X-rays, there is still the "phase problem" that must be solved. In analyzing the diffraction pattern of a crystal structure, different waves are superimposed on the image for each electron density in the structure. While the magnitude of the waves can be measured directly, the phase angle must be calculated, which is often referred to as the "phase problem." The Fourier transformation (also Fourier analysis) defines a function as the sum of a set of sine waves and allows for the determination of the phase from the magnitude of the wave [135]. For example, in a one-dimensional structure with three atoms, it is expected to see three areas of electron density that could be plotted as a sine wave with three peaks. For this structure, you would probably only need to decompose the signal into three sine waves, and from there, the phase can be determined. However, large protein structures contain thousands of peaks representing electron density, significantly increasing the computational burden. Calculating the Fourier transformation was sped up with a series

of refinements to the computational algorithms between the 1940s and 1965 and are referred to as the Fast Fourier transform calculations [135]. In 1979, a group in the United Kingdom set up the collaborative computation project number 4 (CCP4). A collaboration of software developers assembled a comprehensive software collection for determining biological structures from macromolecular X-ray crystallography, including the Fast Fourier transform calculations, which is still popular today [142].

The next technological advancement that rapidly improved the feasibility of structural biology came in 1978 with the generation of FRODO [143]. This system provided the first graphical representation of a crystal structure, allowing easier comparisons and comparative functional analysis between structurally similar proteins. These advances in visualizing protein structures lead to the generation of large databases of known protein structures such as the Protein Data Bank (PDB) and the Universal Protein Resource (UniProt). This resource allows direct links to common domain sequences and motives that can assist in finding the function of novel proteins.

In my studies, I have applied the principles of structural biology to elucidate the mechanisms of heme-binding in proteins. In the first chapter of this dissertation, “From Host Heme to Iron,” I made structural comparisons of heme degrading enzymes using the graphing software Pymol. In the second chapter, I created a structural alignment of HupZ with pden_1323, an enzyme of the same family of heme degradation proteins, using Visual Molecular Dynamics (VMD). This model allowed for a better understanding of how changes to the C-terminal allowed binding the larger *c*-type heme molecule. In this chapter, I will dictate how I used structural modeling to assist in studying a heme receptor and transporter, resulting in two publications. First, using comparative modeling, I developed a map of the region of monoclonal antibody to heme

capturing protein, Shr [104]. Secondly, I used iterative threading to predict the structure of the S component of a novel heme transporting energy coupling factor (ECF) transporter system [19].

4.2 NATIVE HUMAN ANTIBODY TO SHR PROMOTES MICE SURVIVAL AFTER INTRAPERITONEAL CHALLENGE WITH INVASIVE GROUP A STREPTOCOCCUS

This section discusses work of the same title published in 2021 in the Journal of Infectious Disease [104].

4.2.1 Background and summary of main findings

Shr is the first protein of a heme capture and relay system in Group A Streptococcus (Fig. 1). It directly interacts with hemoglobin to remove the heme and then passes it to the ABC transporter, SiaABC. Deletion of Shr impairs GAS growth on hemoglobin as the sole iron source, human blood and is attenuated in zebrafish and invasive mouse models [14, 102, 144]. Shr also has a proven immunological effect. Mice immunized with Shr expressing *L. lactis* were protected from GAS infection, and rabbit Shr-antiserum administrated prophylactically allows passive immunity in a mouse model [103]. We, therefore, tested if monoclonal antibodies could be generated and selected to protect mice from infection. Monoclonal antibodies are produced by a single clone of B cells and are therefore monospecific and homogeneous [145]. We collaborated with Trellis Bioscience, LLC for the generation and purification of our antibodies. B cells from human blood samples were screened against Shr fragments and control proteins using the Trellis platform. The antibody gene from clones that exhibited high affinity and specificity were then cloned into an expression vector, expressed, and

purified. My lab members examined several Shr antibodies and found that TRL186 protects mice from systemic GAS infections.

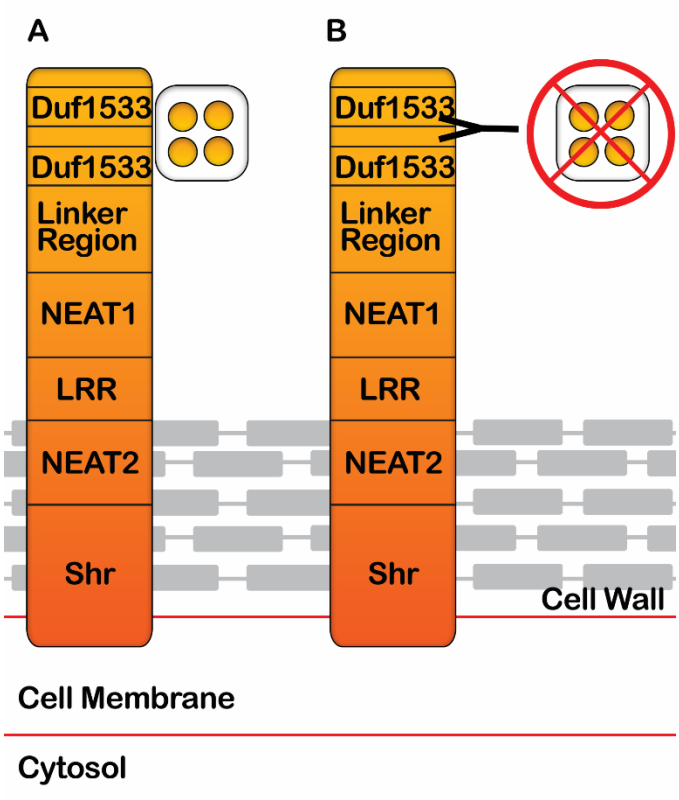

Figure 17 Shr and location of TRL186 binding cartoon

Since the addition of TRL186 to the medium impaired GAS growth on hemoglobin as the sole iron source, we inferred that TRL186 might bind at the same area of Shr that interacts with hemoglobin, thereby decreasing the cell's ability to obtain heme-iron (Fig. 17). Since hemoglobin is known to bind Shr on the N-terminal region, we generated a library of overlapping peptides in that region, and my colleague tested them for TRL186 binding [14]. Shr has two repeating DUF1533 domains in the N-terminal region, and by screening the binding affinity of the overlapping peptide

sequence, she found that the antibody was binding to the end of the first DUF1533 region over the residues IKKGDKVTFISA.

As with many transmembrane proteins, a crystal structure of Shr has not been obtained; however, researchers at the University of California, Los Angeles, were recently able to crystallize the second DUF1533 region [146]. They also confirmed that Shr used these two regions to interact with hemoglobin. I was able to predict the structure of the first DUF1533 region based on their crystal structure and map where TRL186 binds Shr using the comparative modeling software, MODELLER (Figure 18).

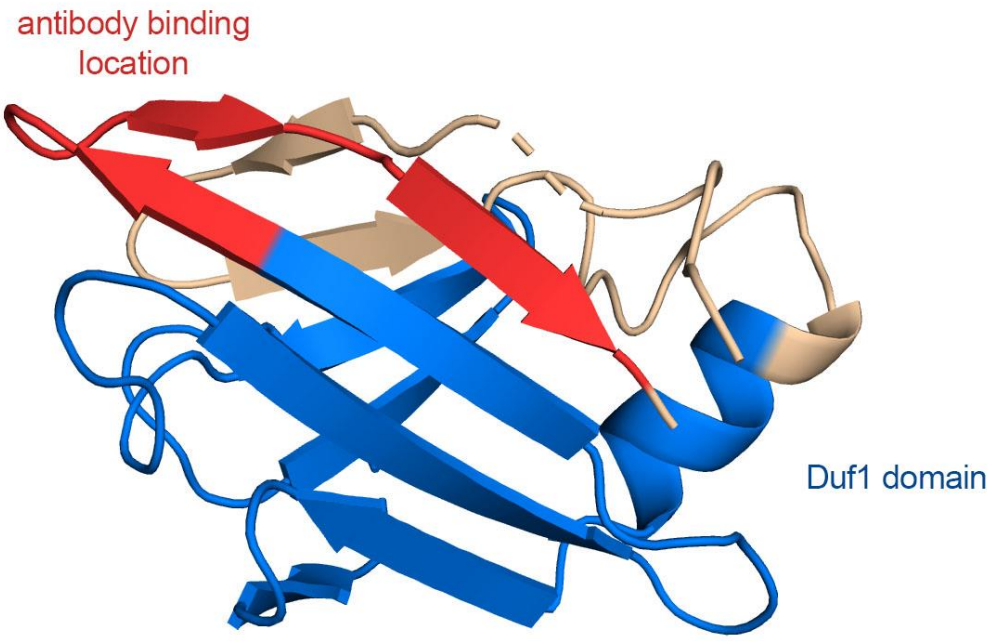

Figure 18 Shr HID1 structural prediction

4.2.2 Generating DUF 1 domain with MODELLER

MODELLER is a comparative modeling software that was released in the early 1990s [147]. Since small changes in protein sequence usually only result in minor changes to the three-dimensional structure, MODELLER can predict a protein structure from a given protein sequence using one or more proteins of known structure termed

template(s). Generally, the input for the program is an alignment between the template and the target sequence, and the output is a three-dimensional structure that contains all mainchain and sidechain non-hydrogen atoms. The distance and dihedral angle restraints are calculated based on the template structure and were obtained statistically using a database of 105 family alignments that included 416 proteins with known crystal structures [148].

First, I downloaded my template's atom file from the PDB (6dkq). Next, I generated an alignment between the two Duf1533 domains in Protein Information Resource (PIR) format (Fig. 19). The template(s) structures are listed first and are identified by containing 'structure' in the first field. The second field includes the PDB file name. The third and fourth fields identify the chain and starting residue for the program to use for the alignment, while the fifth and sixth identify the chain and final residue. For MODELLER, the remaining four fields (the protein name, source of protein, resolution, and R-factor of the crystallographic analysis) are unnecessary and can be left blank. You need to complete only the first two fields for the target structure, the first saying that it is a sequence, and the second which will be incorporated into the file name of the models.

```
>P1;6dkq
structureX:6dkq:174:B:283:B::::
SNLSLITKLSQEDGAILFPEIDRYSDNKQIKALTQQITKVTVNGTVYKDLIS-
SVKDTNGWVSNMTGLHLGTKAFKDGENTIVISSKGFEDVTITVTKKDGQIHFVSAKQ*

>P1;DUF1
sequence:DUF1:::::::::
SQLVTT-VALTQDNRLLVEEIGPYASQSAGKEYYKHIEKIIVDNDVYEK----
SLEGERTFDINYQGIKINADLIKDGKHELTIVNKKDGDILITFIKKGDKVTFISAQK*
```

Figure 19 Alignment of DUF1533 domains in PIR format

Next, I generated the python-based script to generate the model (Fig. 20). The scripts start by loading the standard MODELLER classes and setting up a verbose output to spot errors easier. Next, I set the global parameters to look for the PDB file for my template. I then tell the program the name of the alignment file (6dkq2.ali) and

define both my template and target (6dkq and DUF1, respectively). Lastly, I tell the program to make ten models and set the program to generate the structures.

```
# Comparative modeling by the automodel class
from modeller import * # Load standard Modeller classes
from modeller.automodel import * # Load the automodel class

log.verbose() # request verbose output
env = environ() # create a new MODELLER environment to build this model in

# directories for input atom files
env.io.atom_files_directory = ['.', '../atom_files']

a = automodel(env,
              alnfile = '6dkq2.ali', # alignment filename
              knowns = '6dkq', # codes of the templates
              sequence = 'DUF1') # code of the target
a.starting_model= 1 # index of the first model
a.ending_model = 10 # index of the last model

# (determines how many models to calculate)
a.make() # do the actual comparative modeling
```

Figure 20 MODELLER script to generate models

After generating ten models, I screened for the best structure by calculating the DOPE score for discrete optimized protein energy (Fig. 21). DOPE is an unnormalized number with an arbitrary scale, so it can only compare models of the same peptide or protein and not compare different proteins directly [147]. I selected the model with the lowest DOPE score and verified the geometry of adjacent residues using RAMPAGE [149]. RAMPAGE plots the torsional angles for the residues in a Ramachandran plot which tells you if any residues changes are not possible due to steric hindrance. It also specifies which specific torsional angles between adjacent amino acids are favored, allowed, or outlier regions. Using this information, I refined the model for the particular amino acids mentioned by RAMPAGE (Fig. 22). I checked the refined model with RAMPAGE to confirm that at least 98% of the amino acids had favorable bonds, and no amino acid was in an outlier region.

```
from modeller import *
from modeller.scripts import complete_pdb

log.verbose()    # request verbose output
env = environ()
env.libs.topology.read(file='$(LIB)/top_heav.lib') # read topology
env.libs.parameters.read(file='$(LIB)/par.lib') # read parameters

# read model file
mdl = complete_pdb(env, 'DUF1.B99990001.pdb')

# Assess with DOPE:
s = selection(mdl)   # all atom selection
s.assess_dope(output='ENERGY_PROFILE NO_REPORT', file='DUF1.profile',
              normalize_profile=True, smoothing_window=15)
```

Figure 21 MODELLER script to assess DOPE score

The Duf1533 domains tend to be about 60 residues in length and are found duplicated in proteins that typically also contain leucine-rich repeats (Pfam07550). The first Duf1533 domain in Shr is 63 residues, while the second domain is 66. The first Duf1533 domain has two perpendicular anti-parallel β-sheets (Fig. 18). An upstream α-helix that is part of this domain and situated between the β-sheets at their most distal region. The entire structure makes an almost triangle box. The antibody binding location is on the C-terminal side of this domain and consists of three β-strains. Based on where the antibody binding location sits relative to the Duf1533 region, we believe that TRL186 competes with hemoglobin to interact with Shr, hindering the protein's ability to remove the heme molecule for uptake.

```
# Comparative modeling by the automodel class
#
# Demonstrates how to refine only a part of the model.
#
# You may want to use the more exhaustive "loop" modeling routines instead.
#
from modeller import *
from modeller.automodel import *    # Load the automodel class

log.verbose()

# Override the 'select_atoms' routine in the 'automodel' class:
# (To build an all-hydrogen model, derive from allhmodel rather than automodel
# here.)
class MyModel(automodel):
    def select_atoms(self):return selection(self.residues['14'], self.residues['25'], self.residues['30'])

env = environ()
# directories for input atom files
env.io.atom_files_directory = ['.', '../atom_files']
# selected atoms do not feel the neighborhood
env.edat.nonbonded_sel_atoms = 2

# Be sure to use 'MyModel' rather than 'automodel' here!
a = MyModel(env,
            alnfile  = '6dkq2.ali',     # alignment filename
            knowns   = '6dkq',              # codes of the templates
            sequence = 'DUF1')              # code of the target

a.starting_model= 1                 # index of the first model
a.ending_model  = 1                 # index of the last model
                                    # (determines how many models to calculate)
a.make()                            # do comparative modeling
```

Figure 22 MODELLER script to adjust model based on RAMPAGE

4.3 A NOVEL HEME TRANSPORTER FROM THE ENERGY COUPLING FACTOR FAMILY IS VITAL FOR GROUP A STREPTOCOCCUS COLONIZATION AND INFECTIONS

This section discusses work of the same title published in 2020 in the Journal of Bacteriology [19].

4.3.1 Background and summary of main findings

Energy Coupling Factor (ECF)-transporters belong to a group of ABC transporters discovered ten years ago [150]. They have been shown to mainly transport vitamins across the cell membrane using a novel toppling mechanism instead of generating a channel like canonical ABC transporters. ECF transporters have three components, an S component that binds the ligand for transport, a T component that spans the cellular membrane, and two A components that are cytosolic ATPases and can be similar or identical. Bioinformatical analysis of the last three genes of the Sia operon (*siaFGH)* indicated that it could be an ECF transporter.

My colleague generated a mutant where she deleted these three genes and found that the mutant had impaired growth on hemoglobin as the sole source of iron, especially at lower hemoglobin concentrations. Using mass spectrometry, she confirmed that the cellular iron amounts between the mutant and the wild type were consistent but that the mutant had a lower concentration of cellular heme. This showed that SiaFGH functions as a transporter for heme and not iron. When we submitted our manuscript, no heme transporting ECF transporters had been reported. Still, in the same year, two other groups reported heme ECF transporters in *Lactobacillus sakei* and *Staphylococcus lugdunensis,* indicating that it might be a conserved function in lactic acid bacteria [20, 21]. To aid in

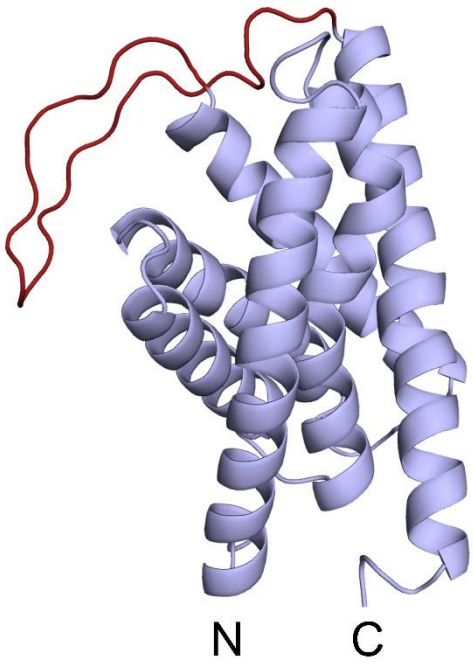

Figure 23 SiaF model predicted with iTASSER

understanding the structure and function of the S component, SiaF, I generated a model using iTASSER (Fig. 23).

4.3.2 Generating the SiaF model using iTASSER

The Iterative Threading ASSEmbly Refinement (iTASSER) program was publicly released in November 2006. It matches structure predictions with known functional templates. The meta-threading is completed by LOMETS [151]. LOMETS queries a representative, nonredundant PDB structure library to identify templates with a pair-wise sequence identity cut-off of 70%. The target sequence is divided into threading-aligned and threading-unaligned (typically single-chain loops) regions using different alignment algorithms to search for possible folds. The threading-aligned regions are excised and reassembled into the full-length model, while the threading-unaligned regions are built by *ab initio,* meaning that the simulations start at the first amino acid and tries to fit each amino acid together in sequence order.

Several models are generated, and iTASSER selects the models with the lowest free-energy conformations for the second round of assembly simulations designed to remove steric clashes and refine the global topology. A confidence score is assigned to the refined model based on three main factors [152]. The first factor comes from SPICKER, a clustering algorithm to identify near-native models from a pool of protein structure decoys that correlate external restrains' consistency. The second factor covers the inherent bond potential and root-mean-square-deviation (RMSD), and the last factor is the quality of the threading alignment. In the finished refinement, iTASSER includes the PDB for up to five proteins of predicted similarity.

The predicted SiaF model was highly similar to the S component of an ECF-transporter in *Lactobacillus brevis* (PDB 4RFS); both are α-only proteins with six

transmembrane sections arranged like a cylinder (Fig. 23). The helical cylinder appears to be rigid based on crystal structure analysis of other ECF S components [153]. EPR experiments on ThiT, a thiamine binding S-component from *Lactococcus lactis,* are consistent with the rigid core and shows that the elongated extracellular loop between the first and second α-helix changes conformation upon binding thiamine forming a gate around the substrate [154]. SiaF appears to have an extended extracellular loop between the fifth and sixth helices that could act as a gate upon substrate binding.

4.4 CONCLUSION

The applications of crystallography would be almost unrecognizable to the early pioneers of the field. The field has changed dramatically from the early 1900s, but modern advancements are still pushing the boundaries. In 2007, the European Diamond facility could only collect synchrotron data for four crystal structures per hour [141]. In contrast, ten years later, they could process more than 20 per hour. While this is undoubtedly a monumental achievement, it barely scratches the surface of potential protein structures. Other challenges to crystallography are (1) obtaining high-resolution pictures of starting states, (2) radiation damage of the structure that occurs during imaging, and (3) that measurement often occurs at cryotemperatures with high salt levels, which does not represent physiological conditions. Yet, using many of the same processes developed for processing crystallization data, we can predict a protein's structure, giving researchers clues on its function or regions of importance.

In 1994 the biannual Critical Assessment of Structure Prediction (CASP) protein-folding challenge began [155]. Entrains are giving the sequences for 100 proteins of unknown structure, and groups either use computational or experimental methods to generate structures. The computation structures are compared to the lab results and are

scored for accuracy. At the most recent CASP, the 14th iteration of the event, DeepMind, a UK-based artificial intelligence company, outpaced the competition by nearly 15% on the more complex structures, producing almost identical structures to laboratory-generated models. With the deep learning methods of their program, AlphaFold, they were able to resolve a long-standing problem in computational structural prediction, predicting the linear chain loops into three-dimensional folds [156]. While the program still has a problem predicting small repeating segments, it is an impressive step forward for structural biology. We can now compare and infer structural-functional relationships between proteins and enzymes, which have application in metallurgy, biology, earth sciences, material science, medical science, and drug discovery.

5 CONCLUDING REMARKS

Iron is an essential nutrient for most known life forms and serves a role in metabolism, DNA synthesis, and energy storage. In the human body, iron is found mostly bound to heme, which serves as an essential signaling molecule. In mammals, iron directly modulates pathways that positively regulate the circadian clock, antioxidative proteins, and glucose utilization [157]. Heme degrading enzymes also influence heme-mediate pathways by keeping the heme and the degradations products in balance. Dysregulation of this ratio can contribute to pathophysiology, particularly in the accumulation of free ferrous iron and downregulation of the pentose phosphate pathway due to increased consumption of NADPH. Biliverdin and bilirubin, the most common product of enzymatic heme degradation and reduced form, respectively, contribute to anti-inflammation and anti-apoptosis. Much less is known about the fate of the heme degradation products in bacterial systems, and what is known looks more at the microbiome-generated products than pathogenic bacteria. Intra-duodenal administration of biliverdin into rats, for example, results in bilirubin-10-sulfonate, which differs slightly from α-bilirubin that is generated by biliverdin reductase [131]. Bacterial cultures of *Citrobacter youngae*, an enteric bacterial that can cause nosocomial infections, were also shown to produce this metabolite in response to exogenous biliverdin, indicating that the bilirubin-10-sulfonate generated might be produced by bacteria in the gastrointestinal tract.

Carbon monoxide (CO) is a critical signaling molecule, and 86% of endogenous CO in humans is generated from the catabolism of heme by HO-1/2 [158]. CO is a well-known gasotransmitter that can affect locally or systemically by diffusion to remote tissues or organs. CO can modulate the microbiome and plays a vital role in the innate

immune system, especially macrophage recruitment. Mice exposed to CO resulted in changes in the enteric bacterial composition and showed increased *E. coli* 16S ribosome and the heme degrading enzyme ChuS [159]. Mice infected with *E. coli* over-expressing c*huS* had more hepatic CO than those infected with *chuS* knockout strain. Additionally, these mice also had more serum IL-12p40 than those infected with Δ*chuS*, a chemoattractant for macrophages that promotes the migration of bacterial stimulated dendritic cells. While the term gasotransmitter usually refers to CO in multicellular organisms, CO (as well as NO and H_2S) is synthesized by bacteria and has important signaling or messenger roles and some toxic effects. Hence, it is proposed that the term "small molecule signaling agent" in bacteria is more appropriate [160]. Still, CO production represents a side of the heme degradation pathway in bacteria that has yet to be elucidated.

While the heme capturing capabilities of GAS have been well described, there are still many questions about the fate of heme inside the cell. I used three new recombinant HupZ proteins to demonstrate that HupZ binds heme without an axial ligand. Provided with an exogenous histidine, reactions with holo-HupZ showed α and β bands present in the UV/Vis spectrum and are degraded in the presence of ferredoxin. What's more, I demonstrated that HupZ binds heme c and can utilize the histidine present in heme c's proteinous region for iron coordination. Heme c degradation has only been described in the sole microbe *P. denitrificans* [116]. This ability to degrade heme c could provide HupZ with an iron source during tissue infections.

Deleting the *hupZ* gene resulted in a slight decrease in growth on heme-iron, but essential functions tend to have redundancy. Work with IsdG and IsdI from *S. aureus* showed that even when the bacteria lack both heme oxygenases, growth on heme iron

was not wholly eliminated [32]. To get over the possible redundancy, I tested the ability of *L. lactis* to utilize heme. I found that when the bacteria express HupZ, its growth on iron chelated media is restored with the addition of 60 μM of hemoglobin. I also showed that HupZ protects GAS from heme toxicity at low heme concentrations. Taken together, this work establishes its role in heme metabolism and tolerance.

I also, for the first time, describe a potential redox partner for heme degradation in GAS, a putative TrxB homolog that we renamed HupX. I demonstrated that HupX can replace ferredoxin in a heme degradation reaction with HupZ and that acidification is not needed to release the iron from ferrous biliverdin. In this reaction, HupX provided HupZ with an axial heme ligand. However, the HupX construct contains a His_6-tag, so more work is needed to determine if a native HupX residue allows iron coordination. HupX-His_6 can bind and degrade bilirubin *in vitro*, yet we did not see the generation of bilirubin in our degradations. This could be due to our reaction's conditions, and future work could involve modulating the pH and salt concentration to see if bilirubin can be generated. It would also be valuable to determine if HupZ and HupX interact *in vivo* to confirm that they are partners in the cell.

HupZ was identified as a potential heme degrading enzyme due to the similarity of its crystal structure to HugZ, highlighting how crystallography can aid functional identification. Today, the applications of crystallography would be almost unrecognizable to the early pioneers of the field. The field has changed dramatically from the early 1900s, but modern advancements are still pushing the boundaries. In 2007, the European Diamond facility could only collect synchrotron data for four crystal structures per hour [141]. In contrast, ten years later, they could process more than 20 per hour. While this is undoubtedly a monumental achievement, it barely scratches the

surface of potential protein structures. Other challenges to crystallography are (1) obtaining high-resolution pictures of starting states, (2) radiation damage of the structure that occurs during imaging, and (3) that measurement often occurs at cryotemperatures with high salt levels, which does not represent physiological conditions. Yet, using many of the same processes developed for processing crystallization data, we can predict a protein's structure, giving researchers clues on its function or regions of importance.

In my studies, I assisted with the investigation of two heme-binding proteins that resulted in publications. The heme receptor, Shr, is a surface protein that has shown promise as a potential vaccine candidate [104]. We sought to identify a monoclonal antibody that would act therapeutically to GAS infection. My colleges identified TRL186 for its ability to protect mice from systemic disease and its inhibitory effect on GAS growth on hemoglobin as the only iron source. She was able to map the binding location to a domain of unknown origin (DUF1533) on the C terminal of Shr. I used the crystal structure of the repeated domain and MODELLER to map this region, giving us insight into the domain into its structure that we can test in the lab. I also modeled the structure of SiaF, a novel heme-binding ECF-transporter using iTASSER [19]. While SiaF shares structural similarity to other S components, its sequence differs from two subsequently discovered heme-binding ECF-transporters. With my structural prediction, we know that SiaF contains an elongated extracellular loop standard in this type of protein, but it is located on loop 5 instead of loop 1. Examination of this loop shows that, unlike other S components, SiaF's elongated loop has several charged residues suggesting that it may remain extracellularly during toppling. We also

identified several residues known for heme interaction that can be examed through site mutations.

Structural predictions have become a crucial first step in protein function identification. It can give insight into conserved structures that might not be visible from the sequence data, and the ability to predict structure is rapidly improving. In 1994 the biannual Critical Assessment of Structure Prediction (CASP) protein-folding challenge began [155]. Entrains are giving the sequences for 100 proteins of unknown structure, and groups either use computational or experimental methods to generate structures. The computation structures are compared to the lab results and are scored for accuracy. At the most recent CASP, the 14th iteration of the event, DeepMind, a UK-based artificial intelligence company, outpaced the competition by nearly 15% on the more complex structures, producing almost identical structures to laboratory-generated models. With the deep learning methods of their program, AlphaFold, they were able to resolve a long-standing problem in computational structural prediction, predicting the linear chain loops into three-dimensional folds [156]. While the program still has a problem predicting small repeating segments, it is an impressive step forward for structural biology. We can now compare and infer structural-functional relationships between proteins and enzymes, which have application in metallurgy, biology, earth sciences, material science, medical science, and drug discovery.

APPENDICES

Appendix A

Following is a chronological list of all the publications I have obtained during my graduate program at Georgia State University.

Lyles KV, Eichenbaum Z: **From Host Heme To Iron: The Expanding Spectrum of Heme Degrading Enzymes Used by Pathogenic Bacteria**. *Front Cell Infect Microbiol* 2018, **8**:198.

Chatterjee N, Cook LCC, Lyles KV, Nguyen HAT, Devlin DJ, Thomas LS, Eichenbaum Z: **A Novel Heme Transporter from the Energy Coupling Factor Family Is Vital for Group A Streptococcus Colonization and Infections**. *J Bacteriol* 2020, **202**(14).

Hopper CP, De La Cruz LK, Lyles KV, Wareham LK, Gilbert JA, Eichenbaum Z, Magierowski M, Poole RK, Wollborn J, Wang B: **Role of Carbon Monoxide in Host-Gut Microbiome Communication**. *Chem Rev* 2020, **120**(24):13273-13311.

Chatterjee N, Huang YS, Lyles KV, Morgan JE, Kauvar LM, Greer SF, Eichenbaum Z: **Native Human Antibody to Shr Promotes Mice Survival After Intraperitoneal Challenge With Invasive Group A Streptococcus**. *J Infect Dis* 2021, **223**(8):1367-1375.

WORKS CITED

1. Sanchez M, Sabio L, Galvez N, Capdevila M, Dominguez-Vera JM: **Iron chemistry at the service of life**. *IUBMB Life* 2017, **69**(6):382-388.
2. Haber F, Weiss, J: **The catalytic decomposition of hydrogen peroxide by iron salts.** *Proc R Soc Lond* 1934, **147**:332-351.
3. Mietzner TA, Morse SA: **The role of iron-binding proteins in the survival of pathogenic bacteria**. *Annu Rev Nutr* 1994, **14**:471-493.
4. Miller HK, Auerbuch V: **Bacterial iron-sulfur cluster sensors in mammalian pathogens**. *Metallomics* 2015, **7**(6):943-956.
5. Schwartz CJ, Djaman O, Imlay JA, Kiley PJ: **The cysteine desulfurase, IscS, has a major role in in vivo Fe-S cluster formation in Escherichia coli**. *Proc Natl Acad Sci U S A* 2000, **97**(16):9009-9014.
6. Lyles KV, Eichenbaum Z: **From Host Heme To Iron: The Expanding Spectrum of Heme Degrading Enzymes Used by Pathogenic Bacteria**. *Front Cell Infect Microbiol* 2018, **8**:198.
7. Schaer DJ, Vinchi F, Ingoglia G, Tolosano E, Buehler PW: **Haptoglobin, hemopexin, and related defense pathways-basic science, clinical perspectives, and drug development**. *Front Physiol* 2014, **5**:415.
8. Marchetti M, De Bei O, Bettati S, Campanini B, Kovachka S, Gianquinto E, Spyrakis F, Ronda L: **Iron Metabolism at the Interface between Host and Pathogen: From Nutritional Immunity to Antibacterial Development**. *Int J Mol Sci* 2020, **21**(6).
9. Parrow NL, Fleming RE, Minnick MF: **Sequestration and scavenging of iron in infection**. *Infect Immun* 2013, **81**(10):3503-3514.
10. Walker MJ, Barnett TC, McArthur JD, Cole JN, Gillen CM, Henningham A, Sriprakash KS, Sanderson-Smith ML, Nizet V: **Disease manifestations and pathogenic mechanisms of Group A Streptococcus**. *Clin Microbiol Rev* 2014, **27**(2):264-301.
11. Zuhlke LJ, Beaton A, Engel ME, Hugo-Hamman CT, Karthikeyan G, Katzenellenbogen JM, Ntusi N, Ralph AP, Saxena A, Smeesters PR *et al*: **Group A Streptococcus, Acute Rheumatic Fever and Rheumatic Heart Disease: Epidemiology and Clinical Considerations**. *Curr Treat Options Cardiovasc Med* 2017, **19**(2):15.
12. CDC: **Active Bacterial Core Surveillance Report, Emergin Infections Program Network, Group A Streptococcus, 2019**. In.; 2019.
13. Eichenbaum Z, Muller E, Morse SA, Scott JR: **Acquisition of iron from host proteins by the group A streptococcus**. *Infect Immun* 1996, **64**(12):5428-5429.
14. Ouattara M, Cunha EB, Li X, Huang YS, Dixon D, Eichenbaum Z: **Shr of group A streptococcus is a new type of composite NEAT protein involved in sequestering haem from methaemoglobin**. *Mol Microbiol* 2010, **78**(3):739-756.
15. Ellis-Guardiola K, Mahoney BJ, Clubb RT: **NEAr Transporter (NEAT) Domains: Unique Surface Displayed Heme Chaperones That Enable Gram-Positive Bacteria to Capture Heme-Iron From Hemoglobin**. *Front Microbiol* 2020, **11**:607679.
16. Ouattara M, Pennati A, Devlin DJ, Huang YS, Gadda G, Eichenbaum Z: **Kinetics of heme transfer by the Shr NEAT domains of Group A Streptococcus**. *Arch Biochem Biophys* 2013, **538**(2):71-79.
17. Liu M, Lei B: **Heme transfer from streptococcal cell surface protein Shp to HtsA of transporter HtsABC**. *Infect Immun* 2005, **73**(8):5086-5092.

18. Sun X, Ge R, Zhang D, Sun H, He QY: **Iron-containing lipoprotein SiaA in SiaABC, the primary heme transporter of Streptococcus pyogenes**. *J Biol Inorg Chem* 2010, **15**(8):1265-1273.
19. Chatterjee N, Cook LCC, Lyles KV, Nguyen HAT, Devlin DJ, Thomas LS, Eichenbaum Z: **A Novel Heme Transporter from the Energy Coupling Factor Family Is Vital for Group A Streptococcus Colonization and Infections**. *J Bacteriol* 2020, **202**(14).
20. Verplaetse E, Andre-Leroux G, Duhutrel P, Coeuret G, Chaillou S, Nielsen-Leroux C, Champomier-Verges MC: **Heme Uptake in Lactobacillus sakei Evidenced by a New Energy Coupling Factor (ECF)-Like Transport System**. *Appl Environ Microbiol* 2020, **86**(18).
21. Jochim A, Adolf L, Belikova D, Schilling NA, Setyawati I, Chin D, Meyers S, Verhamme P, Heinrichs DE, Slotboom DJ *et al*: **An ECF-type transporter scavenges heme to overcome iron-limitation in Staphylococcus lugdunensis**. *Elife* 2020, **9**.
22. Cook LCC, Chatterjee N, Li Y, Andrade J, Federle MJ, Eichenbaum Z: **Transcriptomic Analysis of Streptococcus pyogenes Colonizing the Vaginal Mucosa Identifies hupY, an MtsR-Regulated Adhesin Involved in Heme Utilization**. *mBio* 2019, **10**(3).
23. Tenhunen R, Marver HS, Schmid R: **Microsomal Heme Oxygenase: Characterization of the Enzyme**. *The Journal of Biological Chemistry* 1969, **244**(23):6388-6394.
24. Tenhunen R, Marver HS, Schmid R: **The enzymatic conversion of heme to bilirubin by microsomal heme oxygenase**. *Proc Natl Acad Sci U S A* 1968, **61**(2):748-755.
25. Ostrow JD, Jandl JH, Schmid R: **The Formation of Bilirubin from Hemoglobin In vivo**. *Journal of Clinical Investigation* 1962, **41**(8):1628-1637.
26. Schmitt M: **Utilization of Host Iron Sources by Corynebacterium diphtheriae: Identification of a Gene Whose Product is Homologous to Eukaryotic Heme Oxygenases and is Required for Acquisition of Iron from Heme and Hemoglobin**. *Journal of Bacteriology* 1997, **179**(3):838-845.
27. Wilks A, Schmitt MP: **Expression and Characterization of a Heme Oxygenase (HmuO) from Corynebacterium diphtheriae**. *The Journal of Biological Chemistry* 1998, **273**(2):837-841.
28. Kunkle CA, Schmitt MP: **Comparative analysis of hmuO function and expression in Corynebacterium species**. *J Bacteriol* 2007, **189**(9):3650-3654.
29. Cornejo J, Willows RD, Beale SI: **Phytobilin biosynthesis: cloning and expression of a gene encoding soluble ferredoxin-dependent heme oxygenase from Synechocystis sp. PCC 6803**. *The Plant Journal* 1998, **15**(1):99-107.
30. Zhu W, Wilks A, Stojiljkovic I: **Degradation of Heme in Gram-Negative Bacteria: the Product of the hemO Gene of Neisseriae is a Heme Oxygenase**. *182* 2000, **23**:6783-6790.
31. Wilks A, Heinzl G: **Heme oxygenation and the widening paradigm of heme degradation**. *Arch Biochem Biophys* 2014, **544**:87-95.
32. Skaar EP, Gaspar AH, Schneewind O: **IsdG and IsdI, heme-degrading enzymes in the cytoplasm of Staphylococcus aureus**. *J Biol Chem* 2004, **279**(1):436-443.
33. Chim N, Iniguez A, Nguyen TQ, Goulding CW: **Unusual diheme conformation of the heme degrading protein from Mycobacterium tuberculosis**. *Journal of molecular biology* 2010, **395**(3):595-608.

34. Nambu S, Matsui T, Goulding CW, Takahashi S, Ikeda-Saito M: **A new way to degrade heme: the Mycobacterium tuberculosis enzyme MhuD catalyzes heme degradation without generating CO**. *J Biol Chem* 2013, **288**(14):10101-10109.

35. Wilks A, Ikeda-Saito M: **Heme utilization by pathogenic bacteria: not all pathways lead to biliverdin**. *Acc Chem Res* 2014, **47**(8):2291-2298.

36. Avila L, Huang H-w, Damaso CO, Lu S, Moënne-Loccoz P, Rivera M: **Coupled Oxidation vs Heme Oxygenation: Insights from Axial Ligand Mutants of Mitochondrial Cytochrome b5**. *Journal of the American Chemical Society* 2003, **125**(14):4103-4110.

37. Hirotsu S, Chu GC, Unno M, Lee DS, Yoshida T, Park SY, Shiro Y, Ikeda-Saito M: **The crystal structures of the ferric and ferrous forms of the heme complex of HmuO, a heme oxygenase of Corynebacterium diphtheriae**. *J Biol Chem* 2004, **279**(12):11937-11947.

38. Unno M, Ardevol A, Rovira C, Ikeda-Saito M: **Structures of the substrate-free and product-bound forms of HmuO, a heme oxygenase from corynebacterium diphtheriae: x-ray crystallography and molecular dynamics investigation**. *J Biol Chem* 2013, **288**(48):34443-34458.

39. Unno M, Matsui T, Ikeda-Saito M: **Structure and catalytic mechanism of heme oxygenase**. *Nat Prod Rep* 2007, **24**(3):553-570.

40. Friedman J, Lad L, Li H, Wilks A, Poulos TL: **Structural basis for Novel delta-Regioselective Heme Oxygenation in the Opportunistic Pathogen Pseudomonas aeruginosa**. *Biochemistry* 2004, **43**:5239-5245.

41. Fujii H, Zhang X, Yoshida T: **Essential Amino Acid Residues Controlling the Unique Regioselectivity of Heme Oxygenase in Pseudomonas aeruginosa**. *Journal of the American Chemical Society* 2004, **126**(14):4466-4467.

42. Reniere ML, Ukpabi GN, Harry SR, Stec DF, Krull R, Wright DW, Bachmann BO, Murphy ME, Skaar EP: **The IsdG-family of haem oxygenases degrades haem to a novel chromophore**. *Mol Microbiol* 2010, **75**(6):1529-1538.

43. Matsui T, Nambu S, Ono Y, Goulding CW, Tsumoto K, Ikeda-Saito M: **Heme degradation by Staphylococcus aureus IsdG and IsdI liberates formaldehyde rather than carbon monoxide**. *Biochemistry* 2013, **52**(18):3025-3027.

44. Wu R, Skaar EP, Zhang R, Joachimiak G, Gornicki P, Schneewind O, Joachimiak A: **Staphylococcus aureus IsdG and IsdI, heme-degrading enzymes with structural similarity to monooxygenases**. *J Biol Chem* 2005, **280**(4):2840-2846.

45. Streit BR, Kant R, Tokmina-Lukaszewska M, Celis AI, Machovina MM, Skaar EP, Bothner B, DuBois JL: **Time-resolved Studies of IsdG Protein Identify Molecular Signposts along the Non-canonical Heme Oxygenase Pathway**. *J Biol Chem* 2016, **291**(2):862-871.

46. Lee WC, Reniere ML, Skaar EP, Murphy ME: **Ruffling of metalloporphyrins bound to IsdG and IsdI, two heme-degrading enzymes in Staphylococcus aureus**. *J Biol Chem* 2008, **283**(45):30957-30963.

47. Takayama SJ, Loutet SA, Mauk AG, Murphy ME: **A Ferric-Peroxo Intermediate in the Oxidation of Heme by IsdI**. *Biochemistry* 2015, **54**(16):2613-2621.

48. Graves AB, Morse RP, Chao A, Iniguez A, Goulding CW, Liptak MD: **Crystallographic and spectroscopic insights into heme degradation by Mycobacterium tuberculosis MhuD**. *Inorg Chem* 2014, **53**(12):5931-5940.

49. Duong T, Park K, Kim T, Kang SW, Hahn MJ, Hwang HY, Jang I, Oh HB, Kim KK: **Structural and functional characterization of an Isd-type haem-degradation enzyme from Listeria monocytogenes**. *Acta Crystallogr D Biol Crystallogr* 2014, **70**(Pt 3):615-626.
50. Stojiljkovic I, Hantke K: **Transport of haemin across the cytoplasmic membrane through a haemin-specific periplasmic binding-protein-dependent transport system in Yersinia enterocolitica**. *Molecular Microbiology* 1994, **13**(4):719-732.
51. Schneider S, Sharp KH, Barker PD, Paoli M: **An induced fit conformational change underlies the binding mechanism of the heme transport proteobacteria-protein HemS**. *J Biol Chem* 2006, **281**(43):32606-32610.
52. Stojiljkovic I, Hantke K: **Hemin uptake system of Yersinia enterocolitica: similarities with other TonB-dependent systems in gram-negative bacteria**. *The EMBO Journal* 1992, **11**(12):4359-4367.
53. Tripathi S, O'Neill MJ, Wilks A, Poulos TL: **Crystal structure of the Pseudomonas aeruginosa cytoplasmic heme binding protein, Apo-PhuS**. *J Inorg Biochem* 2013, **128**:131-136.
54. Schneider S, Paoli M: **Crystallization and preliminary X-ray diffraction analysis of the haem-binding protein HemS from Yersinia enterocolitica**. *Acta Crystallogr Sect F Struct Biol Cryst Commun* 2005, **61**(Pt 8):802-805.
55. Suits MD, Jaffer N, Jia Z: **Structure of the Escherichia coli O157:H7 heme oxygenase ChuS in complex with heme and enzymatic inactivation by mutation of the heme coordinating residue His-193**. *J Biol Chem* 2006, **281**(48):36776-36782.
56. Block DR, Lukat-Rodgers GS, Rodgers KR, Wilks A, Bhakta MN, Lansky IB: **Identification of Two Heme-Binding Sites in the Cytoplasmic Heme-Trafficking Protein PhuS from Pseudomonas aeruginosa and Their Relevance to Function**. *Biochemistry* 2007, **46**(50):14391-14402.
57. Suits MD, Pal GP, Nakatsu K, Matte A, Cygler M, Jia Z: **Identification of an Escherichia coli O157:H7 heme oxygenase with tandem functional repeats**. *Proc Natl Acad Sci U S A* 2005, **102**(47):16955-16960.
58. Lee MJ, Schep D, McLaughlin B, Kaufmann M, Jia Z: **Structural analysis and identification of PhuS as a heme-degrading enzyme from Pseudomonas aeruginosa**. *J Mol Biol* 2014, **426**(9):1936-1946.
59. Bhakta MN, Wilks A: **The Mechanism of Heme Transfer from the Cytoplasmic Heme Binding Protein PhuS to the δ-regioselective Heme Oxygenase of Pseudomonas aeruginosa**. *Biochemistry* 2006, **45**(38):11642-11649.
60. O'Neill MJ, Wilks A: **The P. aeruginosa heme binding protein PhuS is a heme oxygenase titratable regulator of heme uptake**. *ACS Chem Biol* 2013, **8**(8):1794-1802.
61. Deredge DJ, Huang W, Hui C, Matsumura H, Yue Z, Moenne-Loccoz P, Shen J, Wintrode PL, Wilks A: **Ligand-induced allostery in the interaction of the Pseudomonas aeruginosa heme binding protein with heme oxygenase**. *Proc Natl Acad Sci U S A* 2017, **114**(13):3421-3426.
62. O'Neill MJ, Bhakta MN, Fleming KG, Wilks A: **Induced fit on heme binding to the Pseudomonas aeruginosa cytoplasmic protein (PhuS) drives interaction with heme oxygenase (HemO)**. *Proceedings of the National Academy of Sciences* 2012, **109**(15):5639-5644.

63. Ouellet YH, Ndiaye CT, Gagne SM, Sebilo A, Suits MD, Jubinville E, Jia Z, Ivancich A, Couture M: **An alternative reaction for heme degradation catalyzed by the Escherichia coli O157:H7 ChuS protein: Release of hematinic acid, tripyrrole and Fe(III)**. *J Inorg Biochem* 2016, **154**:103-113.
64. Liu M, Boulouis HJ, Biville F: **Heme degrading protein HemS is involved in oxidative stress response of Bartonella henselae**. *PLoS One* 2012, **7**(5):e37630.
65. Onzuka M, Sekine Y, Uchida T, Ishimori K, Ozaki S-i: **HmuS from Yersinia pseudotuberculosis is a non-canonical heme-degrading enzyme to acquire iron from heme**. *Biochimica et Biophysica Acta (BBA) - General Subjects* 2017, **1861**(7):1870-1878.
66. Hu Y, Jiang F, Guo Y, Shen X, Zhang Y, Zhang R, Guo G, Mao X, Zou Q, Wang DC: **Crystal structure of HugZ, a novel heme oxygenase from Helicobacter pylori**. *J Biol Chem* 2011, **286**(2):1537-1544.
67. Liu X, Gong J, Wei T, Wang Z, Du Q, Zhu D, Huang Y, Xu S, Gu L: **Crystal structure of HutZ, a heme storage protein from Vibrio cholerae: A structural mismatch observed in the region of high sequence conservation**. *BioMed Central Structural Biology* 2012, **12**(22):1-10.
68. Zhang R, Zhang J, Guo G, Mao X, Tong W, Zhang Y, Wang DC, Hu Y, Zou Q: **Crystal structure of Campylobacter jejuni ChuZ: a split-barrel family heme oxygenase with a novel heme-binding mode**. *Biochem Biophys Res Commun* 2011, **415**(1):82-87.
69. Uchida T, Sekine Y, Matsui T, Ikeda-Saito M, Ishimori K: **A heme degradation enzyme, HutZ, from Vibrio cholerae**. *Chem Commun (Camb)* 2012, **48**(53):6741-6743.
70. Sachla AJ, Ouattara M, Romero E, Agniswamy J, Weber IT, Gadda G, Eichenbaum Z: **In vitro heme biotransformation by the HupZ enzyme from Group A streptococcus**. *Biometals* 2016, **29**(4):593-609.
71. Wyckoff EE, Schmitt M, Wilks A, Payne SM: **HutZ is required for efficient heme utilization in Vibrio cholerae**. *J Bacteriol* 2004, **186**(13):4142-4151.
72. Guo Y, Guo G, Mao X, Zhang W, Xiao J, Tong W, Liu T, Xiao B, Liu X, Feng Y *et al*: **Functional identification of HugZ, a heme oxygenase from Helicobacter pylori**. *BMC Microbiol* 2008, **8**:226.
73. Ridley KA, Rock JD, Li Y, Ketley JM: **Heme utilization in Campylobacter jejuni**. *J Bacteriol* 2006, **188**(22):7862-7875.
74. Carpenter BM, Whitmire JM, Merrell DS: **This is not your mother's repressor: the complex role of fur in pathogenesis**. *Infect Immun* 2009, **77**(7):2590-2601.
75. Troxell B, Hassan HM: **Transcriptional regulation by Ferric Uptake Regulator (Fur) in pathogenic bacteria**. *Frontiers in Cellular and Infection Microbiology* 2013, **3**:59.
76. Reniere ML, Skaar EP: **Staphylococcus aureus haem oxygenases are differentially regulated by iron and haem**. *Mol Microbiol* 2008, **69**(5):1304-1315.
77. Ratliff M, Zhu W, Deshmukh R, Wilks A, Stojiljkovic I: **Homologues of neisserial heme oxygenase in gram-negative bacteria: degradation of heme by the product of the pigA gene of Pseudomonas aeruginosa**. *J Bacteriol* 2001, **183**(21):6394-6403.
78. Wegele R, Tasler R, Zeng Y, Rivera M, Frankenberg-Dinkel N: **The heme oxygenase(s)-phytochrome system of Pseudomonas aeruginosa**. *J Biol Chem* 2004, **279**(44):45791-45802.

79. Barker KD, Barkovits K, Wilks A: **Metabolic Flux of Extracellular Heme Uptake in Pseudomonas aeruginosa Is Driven by the Iron-regulated Heme Oxygenase (HemO)**. *The Journal of Biological Chemistry* 2012, **287**(22):18342-18350.

80. Nobles CL, Maresso AW: **The theft of host heme by Gram-positive pathogenic bacteria**. *Metallomics* 2011, **3**(8):788-796.

81. Merchant AT, Spatafora GA: **A role for the DtxR family of metalloregulators in gram-positive pathogenesis**. *Molecular oral microbiology* 2014, **29**(1):1-10.

82. Schmitt M: **Transcription of the Corynebacterium diphtheriae hmuO gene is regulated by iron and heme**. *Infection and Immunity* 1997, **65**(11):4634-4641.

83. Bates CS, Toukoki C, Neely MN, Eichenbaum Z: **Characterization of MtsR, a new metal regulator in group A streptococcus, involved in iron acquisition and virulence**. *Infect Immun* 2005, **73**(9):5743-5753.

84. Hanks TS, Liu M, McClure MJ, Fukumura M, Duffy A, Lei B: **Differential Regulation of Iron- and Manganese-Specific MtsABC and Heme-Specific HtsABC Transporters by the Metalloregulator MtsR of Group A Streptococcus**. *Infection and Immunity* 2006, **74**(9):5132-5139.

85. Toukoki C, Gold KM, McIver KS, Eichenbaum Z: **MtsR is a dual regulator that controls virulence genes and metabolic functions in addition to metal homeostasis in GAS**. *Molecular microbiology* 2010, **76**(4):971-989.

86. Bibb LA, Kunkle CA, Schmitt MP: **The ChrA-ChrS and HrrA-HrrS signal transduction systems are required for activation of the hmuO promoter and repression of the hemA promoter in Corynebacterium diphtheriae**. *Infect Immun* 2007, **75**(5):2421-2431.

87. Bibb LA, Schmitt MP: **The ABC transporter HrtAB confers resistance to hemin toxicity and is regulated in a hemin-dependent manner by the ChrAS two-component system in Corynebacterium diphtheriae**. *J Bacteriol* 2010, **192**(18):4606-4617.

88. Burgos JM, Schmitt MP: **The ChrA response regulator in Corynebacterium diphtheriae controls hemin-regulated gene expression through binding to the hmuO and hrtAB promoter regions**. *J Bacteriol* 2012, **194**(7):1717-1729.

89. Reniere ML, Haley KP, Skaar EP: **The flexible loop of Staphylococcus aureus IsdG is required for its degradation in the absence of heme**. *Biochemistry* 2011, **50**(31):6730-6737.

90. LaMattina JW, Nix DB, Lanzilotta WN: **Radical new paradigm for heme degradation in Escherichia coli O157:H7**. *Proc Natl Acad Sci U S A* 2016, **113**(43):12138-12143.

91. Letoffe S, Heuck G, Delepelaire P, Lange N, Wandersman C: **Bacteria capture iron from heme by keeping tetrapyrrol skeleton intact**. *Proc Natl Acad Sci U S A* 2009, **106**(28):11719-11724.

92. Wang A, Zeng Y, Han H, Weeratunga S, Morgan BN, Moënne-Loccoz P, Schönbrunn E, Rivera M: **Biochemical and Structural Characterization of Pseudomonas aeruginosa Bfd and FPR: Ferredoxin NADP+ Reductase and Not Ferredoxin Is the Redox Partner of Heme Oxygenase under Iron-Starvation Conditions**. *Biochemistry* 2007, **46**(43):12198-12211.

93. Hannauer M, Arifin AJ, Heinrichs DE: **Involvement of reductases IruO and NtrA in iron acquisition by Staphylococcus aureus**. *Molecular Microbiology* 2015, **96**(6):1192-1210.

94. Maharshak N, Ryu HS, Fan T-J, Onyiah JC, Schulz S, Otterbein SL, Wong R, Hansen J, Otterbein LE, Carroll I *et al*: **Escherichia coli heme oxygenase modulates host innate immune responses**. *Microbiology and immunology* 2015, **59**(8):452-465.
95. Murray GL, Srikram A, Henry R, Puapairoj A, Sermswan RW, Adler B: **Leptospira interrogans requires heme oxygenase for disease pathogenesis**. *Microbes and Infection* 2009, **11**(2):311-314.
96. Watkins DA, Johnson CO, Colquhoun SM, Karthikeyan G, Beaton A, Bukhman G, Forouzanfar MH, Longenecker CT, Mayosi BM, Mensah GA *et al*: **Global, Regional, and National Burden of Rheumatic Heart Disease, 1990-2015**. *N Engl J Med* 2017, **377**(8):713-722.
97. Radcliffe JN: **On the Prevalence, Distribution, and Limitation of Scarlet Fever in England**. *Trans Epidemiol Soc Lond* 1867, **2**(Pt 2):262-277.
98. Barnett TC, Bowen AC, Carapetis JR: **The fall and rise of Group A Streptococcus diseases**. *Epidemiol Infect* 2018:1-6.
99. Davies MR, Holden MT, Coupland P, Chen JH, Venturini C, Barnett TC, Zakour NL, Tse H, Dougan G, Yuen KY *et al*: **Emergence of scarlet fever Streptococcus pyogenes emm12 clones in Hong Kong is associated with toxin acquisition and multidrug resistance**. *Nat Genet* 2015, **47**(1):84-87.
100. Johnson EE, Wessling-Resnick M: **Iron metabolism and the innate immune response to infection**. *Microbes Infect* 2012, **14**(3):207-216.
101. Bates CS, Montanez GE, Woods CR, Vincent RM, Eichenbaum Z: **Identification and characterization of a Streptococcus pyogenes operon involved in binding of hemoproteins and acquisition of iron**. *Infect Immun* 2003, **71**(3):1042-1055.
102. Fisher M, Huang YS, Li X, McIver KS, Toukoki C, Eichenbaum Z: **Shr is a broad-spectrum surface receptor that contributes to adherence and virulence in group A streptococcus**. *Infect Immun* 2008, **76**(11):5006-5015.
103. Huang YS, Fisher M, Nasrawi Z, Eichenbaum Z: **Defense from the Group A Streptococcus by active and passive vaccination with the streptococcal hemoprotein receptor**. *J Infect Dis* 2011, **203**(11):1595-1601.
104. Chatterjee N, Huang YS, Lyles KV, Morgan JE, Kauvar LM, Greer SF, Eichenbaum Z: **Native Human Antibody to Shr Promotes Mice Survival After Intraperitoneal Challenge With Invasive Group A Streptococcus**. *J Infect Dis* 2021, **223**(8):1367-1375.
105. Tenhunen R, Marver HS, Schmid R: **Microsomal heme oxygenase. Characterization of the enzyme**. *J Biol Chem* 1969, **244**(23):6388-6394.
106. Schmitt MP: **Utilization of host iron sources by Corynebacterium diphtheriae: identification of a gene whose product is homologous to eukaryotic heme oxygenases and is required for acquisition of iron from heme and hemoglobin**. *J Bacteriol* 1997, **179**(3):838-845.
107. Zhu W, Wilks A, Stojiljkovic I: **Degradation of heme in gram-negative bacteria: the product of the hemO gene of Neisseriae is a heme oxygenase**. *J Bacteriol* 2000, **182**(23):6783-6790.
108. Traore ES, Li J, Chiura T, Geng J, Sachla AJ, Yoshimoto F, Eichenbaum Z, Davis I, Mak PJ, Liu A: **Heme Binding to HupZ with a C-Terminal Tag from Group A Streptococcus**. *Molecules* 2021, **26**(3).

109. Porter NJ, Christianson DW: **Preparation of a new construct of human histone deacetylase 8 for the crystallization of enzyme-inhibitor complexes**. *Methods Enzymol* 2019, **626**:561-585.
110. Humphrey W, Dalke A, Schulten K: **VMD: visual molecular dynamics**. *J Mol Graph* 1996, **14**(1):33-38, 27-38.
111. Russell RB, Barton GJ: **Multiple Protein-Sequence Alignment from Tertiary Structure Comparison - Assignment of Global and Residue Confidence Levels**. *Proteins-Structure Function and Bioinformatics* 1992, **14**(2):309-323.
112. Kudou M, Yumioka R, Ejima D, Arakawa T, Tsumoto K: **A novel protein refolding system using lauroyl-l-glutamate as a solubilizing detergent and arginine as a folding assisting agent**. *Protein Expr Purif* 2011, **75**(1):46-54.
113. Vagenende V, Yap MG, Trout BL: **Mechanisms of protein stabilization and prevention of protein aggregation by glycerol**. *Biochemistry* 2009, **48**(46):11084-11096.
114. Giovannetti R: **The Use of Spectropotometry UV-Vis for the Study of Porphyrins**. In: *Macro to Nano Spectroscopy*. Edited by Uddin J. Croatia: InTech; 2012.
115. Wissbrock A, George AAP, Brewitz HH, Kuhl T, Imhof D: **The molecular basis of transient heme-protein interactions: analysis, concept and implementation**. *Bioscience Rep* 2019, **39**.
116. Li S, Isiorho EA, Owens VL, Donnan PH, Odili CL, Mansoorabadi SO: **A noncanonical heme oxygenase specific for the degradation of c-type heme**. *J Biol Chem* 2021, **296**:100666.
117. Schneider S, Marles-Wright J, Sharp KH, Paoli M: **Diversity and conservation of interactions for binding heme in b-type heme proteins**. *Nat Prod Rep* 2007, **24**(3):621-630.
118. Jenny RJ, Mann KG, Lundblad RL: **A critical review of the methods for cleavage of fusion proteins with thrombin and factor Xa**. *Protein Expr Purif* 2003, **31**(1):1-11.
119. Kielkopf CL, Bauer W, Urbatsch IL: **Expressing Cloned Genes for Protein Production, Purification, and Analysis**. *Cold Spring Harb Protoc* 2021, **2021**(2).
120. Thielges MC, Chung JK, Axup JY, Fayer MD: **Influence of histidine tag attachment on picosecond protein dynamics**. *Biochemistry* 2011, **50**(25):5799-5805.
121. Haas J, Hackh M, Justus V, Muller M, Ludeke S: **Addition of a polyhistidine tag alters the regioselectivity of carbonyl reductase S1 from Candida magnoliae**. *Org Biomol Chem* 2017, **15**(48):10256-10264.
122. Wang A, Zeng Y, Han H, Weeratunga S, Morgan BN, Moenne-Loccoz P, Schonbrunn E, Rivera M: **Biochemical and structural characterization of Pseudomonas aeruginosa Bfd and FPR: ferredoxin NADP+ reductase and not ferredoxin is the redox partner of heme oxygenase under iron-starvation conditions**. *Biochemistry* 2007, **46**(43):12198-12211.
123. Hannauer M, Arifin AJ, Heinrichs DE: **Involvement of reductases IruO and NtrA in iron acquisition by Staphylococcus aureus**. *Mol Microbiol* 2015, **96**(6):1192-1210.
124. Saito S, Itano HA: **Verdohemochrome IX alpha: preparation and oxidoreductive cleavage to biliverdin IX alpha**. *Proc Natl Acad Sci U S A* 1982, **79**(5):1393-1397.
125. Nakagawa I, Nakata M, Kawabata S, Hamada S: **Cytochrome c-mediated caspase-9 activation triggers apoptosis in Streptococcus pyogenes-infected epithelial cells**. *Cell Microbiol* 2001, **3**(6):395-405.

126. Bhakta MN, Wilks A: **The mechanism of heme transfer from the cytoplasmic heme binding protein PhuS to the delta-regioselective heme oxygenase of Pseudomonas aeruginosa**. *Biochemistry* 2006, **45**(38):11642-11649.
127. O'Neill MJ, Bhakta MN, Fleming KG, Wilks A: **Induced fit on heme binding to the Pseudomonas aeruginosa cytoplasmic protein (PhuS) drives interaction with heme oxygenase (HemO)**. *Proc Natl Acad Sci U S A* 2012, **109**(15):5639-5644.
128. Spencer AL, Bagai I, Becker DF, Zuiderweg ER, Ragsdale SW: **Protein/protein interactions in the mammalian heme degradation pathway: heme oxygenase-2, cytochrome P450 reductase, and biliverdin reductase**. *J Biol Chem* 2014, **289**(43):29836-29858.
129. Loutet SA, Kobylarz MJ, Chau CHT, Murphy MEP: **IruO is a reductase for heme degradation by IsdI and IsdG proteins in Staphylococcus aureus**. *J Biol Chem* 2013, **288**(36):25749-25759.
130. Arner ES, Holmgren A: **Physiological functions of thioredoxin and thioredoxin reductase**. *Eur J Biochem* 2000, **267**(20):6102-6109.
131. Shiels RG, Vidimce J, Pearson AG, Matthews B, Wagner KH, Battle AR, Sakellaris H, Bulmer AC: **Unprecedented Microbial Conversion of Biliverdin into Bilirubin-10-sulfonate**. *Sci Rep* 2019, **9**(1):2988.
132. Chaffin DO, Rubens CE: **Blue/white screening of recombinant plasmids in Gram-positive bacteria by interruption of alkaline phosphatase gene (phoZ) expression**. *Gene* 1998, **219**(1-2):91-99.
133. de Ruyter PG, Kuipers OP, de Vos WM: **Controlled gene expression systems for Lactococcus lactis with the food-grade inducer nisin**. *Appl Environ Microbiol* 1996, **62**(10):3662-3667.
134. Kleerebezem M, Beerthuyzen MM, Vaughan EE, de Vos WM, Kuipers OP: **Controlled gene expression systems for lactic acid bacteria: transferable nisin-inducible expression cassettes for Lactococcus, Leuconostoc, and Lactobacillus spp**. *Appl Environ Microbiol* 1997, **63**(11):4581-4584.
135. Su XD, Zhang H, Terwilliger TC, Liljas A, Xiao J, Dong Y: **Protein Crystallography from the Perspective of Technology Developments**. *Crystallogr Rev* 2015, **21**(1-2):122-153.
136. Authier A: **Early days of X-ray crystallography**. Oxford: Oxford University Press; 2013.
137. Bernal JD, Crowfoot D: **X-Ray Photographs of Crystalline Pepsin**. *Nature* 1934, **133**(3369):794-795.
138. Kendrew JC, Bodo G, Dintzis HM, Parrish RG, Wyckoff H, Phillips DC: **A three-dimensional model of the myoglobin molecule obtained by x-ray analysis**. *Nature* 1958, **181**(4610):662-666.
139. Cohen SN, Chang AC, Boyer HW, Helling RB: **Construction of biologically functional bacterial plasmids in vitro**. *Proc Natl Acad Sci U S A* 1973, **70**(11):3240-3244.
140. Dauter Z, Jaskolski M, Wlodawer A: **Impact of synchrotron radiation on macromolecular crystallography: a personal view**. *J Synchrotron Radiat* 2010, **17**(4):433-444.
141. Grimes JM, Hall DR, Ashton AW, Evans G, Owen RL, Wagner A, McAuley KE, von Delft F, Orville AM, Sorensen T *et al*: **Where is crystallography going?** *Acta Crystallogr D Struct Biol* 2018, **74**(Pt 2):152-166.

142. Winn MD, Ballard CC, Cowtan KD, Dodson EJ, Emsley P, Evans PR, Keegan RM, Krissinel EB, Leslie AG, McCoy A *et al*: **Overview of the CCP4 suite and current developments**. *Acta Crystallogr D Biol Crystallogr* 2011, **67**(Pt 4):235-242.
143. Jones TA: **A graphics model building and refinement system for macromolecules**. *Journal of Applied Crystallography* 1978, **11**(4):268-272.
144. Dahesh S, Nizet V, Cole JN: **Study of streptococcal hemoprotein receptor (Shr) in iron acquisition and virulence of M1T1 group A streptococcus**. *Virulence* 2012, **3**(7):566-575.
145. Castelli MS, McGonigle P, Hornby PJ: **The pharmacology and therapeutic applications of monoclonal antibodies**. *Pharmacol Res Perspect* 2019, **7**(6):e00535.
146. Macdonald R, Cascio D, Collazo MJ, Phillips M, Clubb RT: **The Streptococcus pyogenes Shr protein captures human hemoglobin using two structurally unique binding domains**. *J Biol Chem* 2018, **293**(47):18365-18377.
147. Webb B, Sali A: **Comparative Protein Structure Modeling Using MODELLER**. *Curr Protoc Bioinformatics* 2016, **54**:5 6 1-5 6 37.
148. Sali A, Overington JP: **Derivation of rules for comparative protein modeling from a database of protein structure alignments**. *Protein Sci* 1994, **3**(9):1582-1596.
149. Lovell SC, Davis IW, Arendall WB, 3rd, de Bakker PI, Word JM, Prisant MG, Richardson JS, Richardson DC: **Structure validation by Calpha geometry: phi,psi and Cbeta deviation**. *Proteins* 2003, **50**(3):437-450.
150. Santos JA, Rempel S, Mous ST, Pereira CT, Ter Beek J, de Gier JW, Guskov A, Slotboom DJ: **Functional and structural characterization of an ECF-type ABC transporter for vitamin B12**. *Elife* 2018, **7**.
151. Yang J, Yan R, Roy A, Xu D, Poisson J, Zhang Y: **The I-TASSER Suite: protein structure and function prediction**. *Nat Methods* 2015, **12**(1):7-8.
152. Zhang Y: **I-TASSER server for protein 3D structure prediction**. *BMC Bioinformatics* 2008, **9**:40.
153. Rempel S, Stanek WK, Slotboom DJ: **ECF-Type ATP-Binding Cassette Transporters**. *Annu Rev Biochem* 2019, **88**:551-576.
154. Majsnerowska M, Hanelt I, Wunnicke D, Schafer LV, Steinhoff HJ, Slotboom DJ: **Substrate-induced conformational changes in the S-component ThiT from an energy coupling factor transporter**. *Structure* 2013, **21**(5):861-867.
155. Service RF: **STRUCTURAL BIOLOGY 'The game has changed.' AI triumphs at protein folding**. *Science* 2020, **370**(6521):1144-1145.
156. Baek M, DiMaio F, Anishchenko I, Dauparas J, Ovchinnikov S, Lee GR, Wang J, Cong Q, Kinch LN, Schaeffer RD *et al*: **Accurate prediction of protein structures and interactions using a three-track neural network**. *Science* 2021, **373**(6557):871-876.
157. Duvigneau JC, Esterbauer H, Kozlov AV: **Role of Heme Oxygenase as a Modulator of Heme-Mediated Pathways**. *Antioxidants (Basel)* 2019, **8**(10).
158. Hopper CP, De La Cruz LK, Lyles KV, Wareham LK, Gilbert JA, Eichenbaum Z, Magierowski M, Poole RK, Wollborn J, Wang B: **Role of Carbon Monoxide in Host-Gut Microbiome Communication**. *Chem Rev* 2020, **120**(24):13273-13311.
159. Maharshak N, Ryu HS, Fan TJ, Onyiah JC, Schulz S, Otterbein SL, Wong R, Hansen JJ, Otterbein LE, Carroll IM *et al*: **Escherichia coli heme oxygenase modulates host innate immune responses**. *Microbiol Immunol* 2015, **59**(8):452-465.

160. Wareham LK, Southam HM, Poole RK: **Do nitric oxide, carbon monoxide and hydrogen sulfide really qualify as 'gasotransmitters' in bacteria?** *Biochem Soc Trans* 2018, **46**(5):1107-1118.